UPSCALING TREE DEMOGRAPHY TO HETEROGENOUS LANDSCAPES USING MODELS AND REMOTE SENSING

by

Cristina Barber

A dissertation

submitted in partial fulfillment

of the requirements for the degree of

Doctor of Philosophy in Ecology, Evolution and Behavior

Boise State University

August 2021

BOISE STATE UNIVERSITY GRADUATE COLLEGE

DEFENSE COMMITTEE AND FINAL READING APPROVALS

of the dissertation submitted by

Cristina Barber

Dissertation Title: Upscaling Tree Demography to Heterogeneous Landscapes Using Models and Remote Sensing

Date of Final Oral Examination: 24 June 2021

The following individuals read and discussed the dissertation submitted by student Cristina Barber, and they evaluated the student's presentation and response to questions during the final oral examination. They found that the student passed the final oral examination.

Trevor T. Caughlin, Ph.D.	Chair, Supervisory Committee
Jodi Brandt, Ph.D.	Member, Supervisory Committee
Kelly Hopping, Ph.D.	Member, Supervisory Committee
Pedro Brancalion, Ph.D.	Member, Supervisory Committee

The final reading approval of the dissertation was granted by Trevor T. Caughlin, Ph.D., Chair of the Supervisory Committee. The thesis was approved by the Graduate College.

DEDICATION

To my parents and siblings.

ACKNOWLEDGMENTS

After four years, including two marvelous summers in Panama and one terrible pandemic, here I am finishing my Ph.D. I am not going to lie. Doing a Ph.D.has a lot of challenging moments. However, I was not alone in this journey. I had my advisor, committee, colleagues, and friends that made this learning journey full of joy, exciting challenges and that encouraged a healthy work-life balance.

I would like to start by extending my most profound appreciation to my advisor Dr. Trevor Caughlin. Trevor not only provided me with extensive knowledge of quantitative and ecological expertise, but he also encouraged me to find my own voice in science. He instilled in me a deep desire to push the academic culture towards a more inclusive and open-access place. Trevor, thanks for your patience, understanding, encouraging words, and openness. Thank you also for going above and beyond to ensure that I have a good working-life balance and financial stability. I would also like to extend my deepest gratitude to my committee members, Dr. Jodi Brandt, Dr. Kelly Hopping, Pedro Brancalion, and former committee member Dr. Nancy Glenn for their constructive advice and contributions to the quality of my research. I am deeply indebted to my collaborators Dr. Sarah Graves, Dr. Stepahnie Bohlman, Dr. Greg Asner, Dr. Jefferson Hall, and Dr. Pieter Zuidema. Dr. Sarah Graves, Dr. Stepahnie Bohlman, and Dr. Greg Asner provided the species-specific map that was decisive to this analysis. Dr. Jefferson Hall extended a tremendous amount of assistance during my fieldwork. Dr. Pieter

Zuidema was instrumental during his visit to Boise into setting a good course of action for the dissertation development and helped me to obtain assistance during fieldwork.

I would like to continue by thanking the people that made my fieldwork possible. Thanks to my field assistants Enrique Ballesteros, Miguel Montenegro, Roxana García, Vicente Vaszquez and Quinten Vermissen. You all followed me through a path of long walks, Panamanian heath, and steep slopes and never gave up. Enrique, Miguel, Roxana, and Vicente, your knowledge of the terrain was critical to successfully completing the field work. I am eternally grateful for accompanying me through the tropical forest. I would also like to thank Mario Bailón for sharing his botanical knowledge with me and advising me on leading a fieldwork group. I cannot begin to express my thanks to the Fundación Pro Eco Azuero. Starting with its former director Ruth Metzel and its current director Sandra Vásquez and continuing with Edward García and Milagros Castillo. Thanks for all the invaluable logistic support for the fieldwork and all the work you do to restore Azuero.

Many thanks to the Biology department and Human-Environmental Systems faculty of Boise State for your policy of open doors and great valuation of your students. I cannot leave Boise State without mentioning Dr. Jodi Brandt, who is always willing to provide career advice, building community, and made me feel safer during the pandemic. Special thanks also to Dr. Jennifer Forbey for giving me the tools to empower my own language as a valuable tool for science communication. I would also like to thanks my labmates Andrii Zaiats, Juanmi Requena, Merry Davidson, Peter Olsoy, Sandra Velazco, and Cara Applestein for being such a great community and for sharing all their knowledge with me. Thanks Andrii for always make me feel supported despite my

biggest academic fears and thanks Juanmi for being a little piece of home in the lab and always being ready to share your huge knowledge.

I would also like to recognize all the support and encouragement from my friends during this Ph.D. First of all thanks to Mikel Joaristi, Iker Vazquez, Irati Maritxalar, Amaia Lojo, Iñaki Sagarna, Olatz Buesa and Usue de Velasco for taking me in and being my family in Boise. I am also very grateful to my friends and colleges in the Biology department, the Human-Environmental systems, and Geoscience. Special thanks to my board mates in the Ecological Research Association (ERA) for helping to build community. Special thanks also to my climbing friends Rebecca Donaldson, Brian Busby, and Austin Davis for making it easier coming back from Spain after the pandemic and make true my dream of leading outside. I would like to continue by thanking my people back in Madrid. Thanks to Monica Fernandez, Alvaro Gonzalez, Sonia Sequera, Marina Rincón, and Millan Jara for always being excited for me being back, putting up with how little we see each other, and always believing in my capacity to finish this.

Lastly, I would like to appreciate the huge role that my family has played along my whole career. Me gustaría agradecer a mis padres todo el esfuerzo que pusieron, incluso en contra de la voluntad de mi yo adolescente, para que aprendiera a hablar inglés. También me gustaría daros las gracias por aceptar con buena cara mis decisiones laborales a pesar de que nos mantienen lejos durante muchos meses al año. También me gustaría darles las gracias a mis hermanos por ser mis cómplices a lo largo de estos años y especialmente por cubrir mi ausencia en casa durante estos años. Gracias a todos por hacer que nuestra casa sea un refugio, y por vuestro cariño incondicional.

ABSTRACT

Tree demography is foundational to ecology and conservation, from mass tree die-offs to forest recovery. Plot-level studies of tree demography, including field measurements of tagged individuals, have been fundamental for developing ecological theory and forest management strategies. However, the limited spatial extent of field plots impedes generalizing plot-level models for spatial predictions across heterogeneous landscapes. Novel high-spatial resolution remote sensing imagery has opened the possibility for measuring tree demographic rates with continuous spatial coverage at landscape to regional extents. Remote sensing derived measurements could address pressing research questions, including disentangling causes of high variation in natural regeneration across secondary forest landscapes. Despite the promise of high-spatial resolution imagery for ecology, applying these data to ecological questions will require novel modeling approaches that can account for large amounts of spatial data that often include hierarchical structure. In this thesis, I apply high-resolution remote sensing to upscale tree demography at landscape scales, and provide guidelines for ecologists seeking to parametrize spatially explicit models for neighbor interactions by combining field data, high-resolution remote sensing, and Bayesian quantitative methods. Chapter 1 demonstrates how high-spatial resolution remote sensing can help improve predictions of tree recruitment at the landscape scale. This chapter is the first step towards new support tools that inform restoration projects about where and which species will regenerate naturally in agricultural landscapes. Chapter 2 addresses how to optimize neighbor

interaction models using the Hamiltonian Monte Carlo algorithm. I demonstrate how ragged matrices could solve data storage inefficiencies associated with the neighbor interaction models' pairwise structure. I also provide code for a model parametrization that solves a sampling pathology associated with high correlation in hierarchical structures and an overview of metrics to assess when this hierarchical structure pathology is present. Chapter 3 explores the influence of biophysical and anthropogenic drivers on tree mortality in agricultural landscapes using high-resolution remote sensing data. The results suggest that accessibility and land management are core factors that could be managed to prevent the mortality of agricultural trees. Educational initiatives and new policies that address anthropogenic factors could be the answer to reduce agricultural tree loss. Overall, this thesis brings together Bayesian statistical methods with novel high-resolution remote sensing to overcome the spatial limitation of field measurements and produce spatial predictions and inference on drivers of tree demography across heterogeneous landscapes.

TABLE OF CONTENTS

LIST OF TABLES

LIST OF FIGURES

LIST OF ABBREVIATIONS

CI	Credibility intervals
CNDD	Conspecific negative density dependence
DBH	Diameter at breast height
DEM	Digital elevation model
ESS	Effective sample size
FLR	Forest landscape restoration
GAO	Global Airborne Observatory
GIS	Geographical information system
HMC	Hamiltonian Monte Carlo
MAE	Mean absolute error
NDVI	Normalized Difference Vegetation Index
PDF	Probability density function
STRI	Smithsonian Tropical Research Institute
SVM	Support vector machine
UAS	Unoccupied aerial systems

CHAPTER ONE: SCALING UP PREDICTIONS OF TREE SPECIES RECRUITMENT IN A TROPICAL LANDSCAPE

Abstract

Predicting forest recovery at landscape scales will aid forest restoration efforts. The first step in successful forest recovery is tree recruitment. Forecasts of tree recruit abundance, derived from the landscape-scale distribution of seed sources (i.e., adult trees), could assist efforts to identify sites with high potential for natural regeneration. However, previous work has revealed wide variation in the effect of seed sources on seedling abundance, from positive to no effect. We quantified the relationship between adult tree seed sources and tree recruits, and predicted where natural recruitment would occur in a fragmented tropical agricultural landscape. We integrated species-specific tree crown maps generated from hyperspectral imagery and property boundaries data on land ownership with field data on the spatial distribution of tree recruits from five species. We then developed hierarchical Bayesian models to predict landscape-scale recruit abundance. Our models revealed that species-specific maps of tree crowns improved recruit abundance predictions. The conspecific crown area had a much stronger impact on recruitment abundance (8.00% increase in recruit abundance when conspecific tree density increases from zero to one tree; 95% CI: 0.80 to 11.57%) than the heterospecific crown area (0.03% increase with the addition of a single heterospecific tree, 95% CI: -0.60 to 0.68%). Land ownership was also an important predictor of recruit abundance: the best performing model had varying effects of the conspecific and heterospecific crown

area on recruit abundance, depending on property identity. We demonstrate how novel remote sensing approaches and cadastral data can be used to generate high-resolution and landscape-level maps of tree recruit abundance. Spatial models parameterized with ecological, socioeconomic, and remote sensing data are poised to assist decision support for forest landscape restoration.

Introduction

Natural regeneration in tropical landscapes is a low-cost natural climate solution that can sequester carbon while supporting other ecosystem services (Robin L. Chazdon and Uriarte 2016; Lennox et al. 2018; Matos et al. 2020; Cook-Patton et al. 2020). Operationalizing natural regeneration as a strategy in forest landscape restoration (FLR) plans will require identifying locations where native tree cover will return without active restoration (Norden et al. 2015; R. L. Chazdon and Guariguata 2018). However, natural regeneration in tropical landscapes is unpredictable, with high variability in successional trajectories among sites (Norden et al. 2015). Understanding the demographic mechanisms that drive landscape-scale forest recovery could reduce uncertainty in secondary forest succession forecasts (Menge and Chazdon 2016; T. Trevor Caughlin, Peña-Domene, and Martínez-Garza 2019).

Tree recruitment is a demographic rate required for forest recovery but is poorly understood at landscape scales. A minimum number of seeds must arrive to initiate forest recovery (Caughlin et al. 2016a). Low recruitment, including seed dispersal, germination, and seedling survival, can be a critical impediment for reforestation (Holl et al. 2000). Nevertheless, attempts to relate seed sources (e.g., forest patches) to tree recruitment in reforesting landscapes have shown mixed results. For example, some studies have found

that recruit abundance increases with closer proximity to forest fragments (Parrotta 1993; Heather P. Griscom, Griscom, and Ashton 2009; Crk et al. 2009; Robiglio and Sinclair 2011; Elliott, Blakesley, and Hardwick 2013; Crouzeilles and Curran 2016; Breugel et al. 2019), while others have found weak or undetectable effects of surrounding forest cover on recruit abundance (Duncan and Duncan 2000; Lopes et al. 2012; Zahawi et al. 2013; Holl et al. 2017). Resolving why some studies find strong impacts of landscape seed sources on recruitment while others do not, will advance our ability to forecast natural regeneration over large areas.

A challenge of quantifying the relationship between seed sources and recruitment rates is that seed dispersal occurs at large spatial scales (>km), but recruitment success varies spatially at fine scales (m). The spatial patterns of dispersal and recruitment are modified by differences in dispersal syndromes and functional traits among species and the relative abundance of reproductive trees in the landscape. Attempts to understand recruitment patterns by lumping multiple tree species into a single metric (e.g., distance-to-forest-edge; Robiglio and Sinclair 2011, Crouzeilles and Curran 2016, Holl et al. 2017) do not take species-specific dispersal syndromes and abundances into account. Therefore these attempts may erroneously predict high recruitment potential for species absent as reproductive trees in the landscape. Alternately, a high abundance of conspecific trees (trees of the same species) could negatively affect recruitment due to conspecific negative density dependence (CNDD; Comita et al. 2010, Johnson et al. 2012, Uriarte et al. 2018). We hypothesize that predictions of tree recruitment in tropical agricultural landscapes will improve when based on maps containing all reproductive trees identified to the species (C.A. Harvey, Tucker, and Estrada 2004; Graves et al.

2016; Tarbox, Fiestas, and Caughlin 2018).

Another potential factor explaining the high uncertainty in forest recovery trajectories is human land use. Land management choices can result in different disturbance regimes (e.g., burning, clearing) that influence forest recovery (Mesquita et al. 2001). Landowner preferences also influence species abundance and ecological dynamics that shape recruitment (Heather P. Griscom, Griscom, and Ashton 2009; Metzel and Montagnini 2014). For example, when deciding whether or not to enable natural regeneration on their properties, some farmers may favor rare species' natural regeneration rather than common species (Lengkeek 2003). Thus, land management is likely to alter tree recruitment patterns in ways that are species-specific and vary across the landscape.

High-resolution spatial information on the position and identity of trees on land management may help to improve predictions of tree recruitment. In particular, aerial lidar and hyperspectral imagery can be used to map individual adult tree crowns and species across multiple land ownership units (F. J. Fischer, Maréchaux, and Chave 2019). Segmented tree crowns from lidar data can be paired with hyperspectral imagery to identify individual adult trees to species (Graves et al. 2016). Species-specific tree crown maps derived from airborne high spatial and spectral resolution imagery have demonstrated the potential to address ecological questions requiring a landscape perspective (Schimel et al. 2015), such as community assembly across elevation gradients (Durán et al. 2019).

Our objective is to predict the abundance of tree recruits at broad spatial scales in a diverse tropical agricultural landscape. We combined 1) species-specific mapped tree

crowns derived from fused hyperspectral and lidar imagery, 2) field data on recruit abundance, and 3) property boundary data to quantify how abundance and spatial distribution of tree recruits are related to seed sources and land management, and to predict landscape-level recruit abundance. Our work is directly relevant to landscape-scale reforestation activities because it improves our ability to identify areas where native tree recruitment will occur with minimal intervention. We answer the following questions:

1) Can species-specific tree crown maps from hyperspectral and lidar imagery improve our ability to predict the abundance of tree species recruits?
2) Does the effect of the total neighboring tree crown area on recruit abundance vary between tree species?
3) Does land ownership influences tree recruitment abundance?

Given answers to questions (1-3), we then demonstrate how spatial models for tree recruit abundance could provide decision-support for where natural regeneration is likely to occur.

Materials and Methods

Study Site

Our study area is located in the Azuero Peninsula of southwestern Panama (Figure 1.1). The average rainfall is 1,700 mm yr^{-1}, and the dry season is from December to March. The soils are derived from volcanic, plutonic, and sedimentary rocks (Buchs et al. 2010). The Azuero Peninsula was historically dominated by dry tropical forest but was cleared for timber and ranching during the 20^{th} century, resulting in less than 2% remnant forest cover (H.P. Griscom et al. 2011). Recently, as off-farm economic activities have

led to declines in agricultural activity, tree cover has increased across the region (Sloan 2015) in the form of forest patches, isolated pasture trees, riparian forest corridors, and live fences (H.P. Griscom et al. 2011). However, areas with tree cover increases are spatially-dispersed and counterbalanced by areas with tree cover loss (Tarbox, Fiestas, and Caughlin 2018). Stakeholders in the Azuero increasingly express concern over forest scarcity, leading to community-driven efforts to restore tree cover to degraded lands (Metzel and Montagnini 2014). Local interest in restoration parallels national-scale initiatives, such as Panama's "Alliance for one million", which seeks to restore tree cover to one million hectares of degraded land. Identifying areas suitable for natural regeneration will aid these large-scale reforestation initiatives.

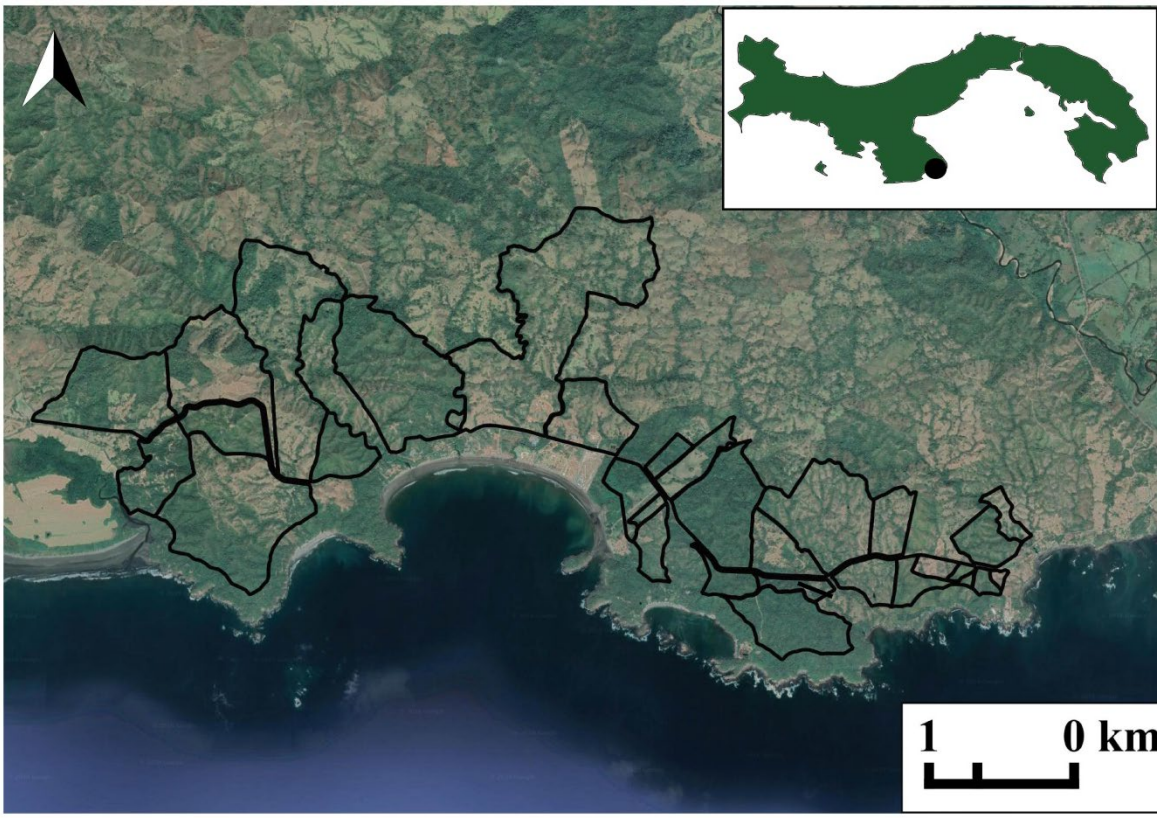

Figure 1.1 Study area in Southwestern Panama. The black lines represent the properties included in this study. Green colors indicate mostly forest vegetation cover, and tan colors indicate non-forested land covers. The black dot in the upper-right corner displays the location of the study site in Panama. Map data: Google, Airbus, Maxar Technologies.

Tree Species Selection

To relate the abundance of tree recruits to adult trees in the surrounding landscape, we used a map of adult tree species derived from aerial lidar and hyperspectral data (Graves et al. 2016). These aerial data were collected by the Global Airborne Observatory (GAO; formerly the Carnegie Airborne Observatory) in January 2012 (Asner et al. 2012). The dual-laser waveform lidar scanned data were used to develop a canopy height model with a pixel size of ~1.13 m that enabled individual tree crown segmentation (Dalponte and Coomes 2016), resulting in 298,971 crowns across 23,000 ha. The hyperspectral imagery (380–2510 nm; 5 nm bandwidth) was then used in a

support vector machine (SVM) model to classify segmented crowns to tree species, with a training data set of 1,112 field-identified tree crowns (see Graves et al. 2016 for additional details). For our study, we selected five focal species based on two criteria: (1) the SVM could classify the tree species with high predictive accuracy (F-score >70%) and (2) the presence of recruits in landscape-scale plots within our study area (Hall and Ashton 2016). The five species include *Byrsonima crassifolia, Calycophyllum candidissimum, Cedrela orodata, Guazuma ulmifolia*, and *Enterolobium cyclocarpum.* Together, these five species represent a range of phylogeny, functional traits, and human use (Appendix A, Table A1). Although the focal study species belong to different successional stages, all five species survive and grow well in full sunlight during their first years (Hall and Ashton 2016).

Environmental and Social Covariates

In addition to the mapped tree crowns, we developed two additional covariates as predictors of tree recruit abundance at landscape scales: elevation and land ownership. Because topography influences secondary succession (Breugel et al. 2019), we incorporated it as a predictor variable in our models, using a digital elevation model with 1.13 m spatial resolution, developed from the aerial lidar over our study area (Asner et al. 2012). Preliminary model selection suggested that elevation outperformed slope, aspect, or topographic roughness indices for predicting tree recruit abundance, so we used elevation to represent topography in our models.

The majority of land in the Azuero Peninsula is privately owned, and property boundaries in the region help explain spatial heterogeneity in land cover change (H.P. Griscom et al. 2011). In addition, private land properties represent a unit commonly used

in restoration interventions (Oliveira Fiorini et al. 2020). To account for land ownership in our models, we used a cadastral dataset developed by Panama's National Authority for the Administration of Lands and provided by the Fundación Pro Eco Azuero. As a predictor variable, we used the identity of the parcel in which recruit abundance was measured (Appendix A, Figure A1).

Field Data on Tree Recruit Abundance

We measured tree recruit abundance in July 2018 by counting individuals of our focal species in transects stratified across the landscape. We defined tree recruits as individuals at least 0.5 m in height but < 1 cm in diameter at breast height (DBH). We measured tree recruit abundance in transects of 100 m x 5 m, separated into 25 m^2 quadrats. The 100 m length of transects helped ensure that each transect could include a range of surrounding tree crown densities. To span a range of land ownership, we stratified transect placement across 30 properties (Figure 1.2), placing between one and three transects within each property. When possible, we placed one transect per property into each of the three major habitats in the study area: riparian corridors, active pasture, and secondary forest. We used habitats to stratify within the different tree covers across the landscape. In total, our sampling scheme resulted in 1,100 quadrats representing 2.75 ha.

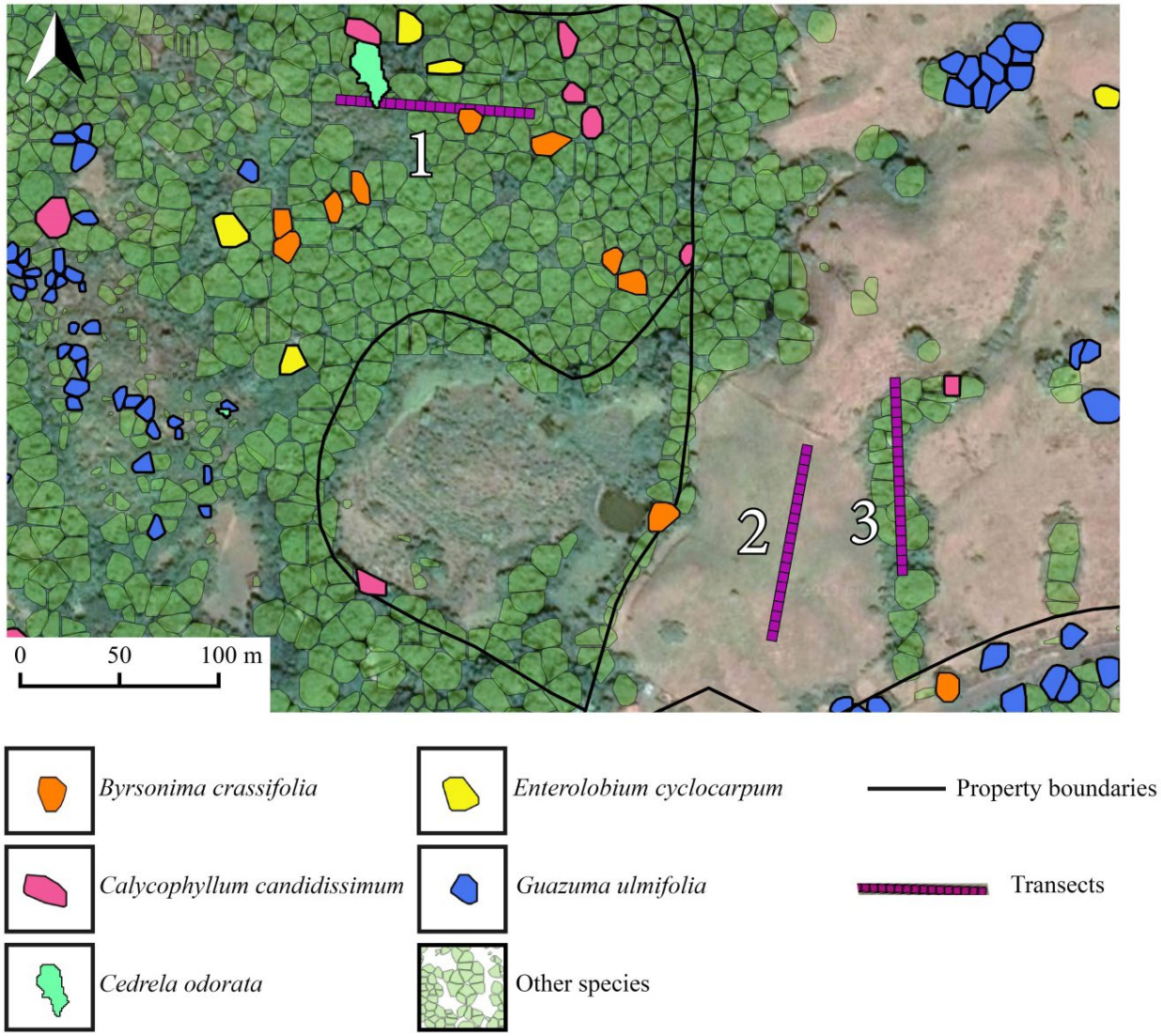

Figure 1.2 Placement of transects in the study area in a typical parcel. Transects in the field are allocated in (1) secondary forest, (2) active pasture, and (3) riparian forest. Colored polygons represent the five target species in the study and are a subset of mapped individual tree crowns from Graves et al. (2016). Map data: Google, Airbus, Maxar Technologies.

Linking Mapped Tree Crowns to Tree Recruit Abundance

To develop models that account for the relationship between tree crowns and recruit abundance, we measured total tree crown area in neighboring landscapes around quadrats. We separated the tree crown area into the conspecific crown area for each of our focal species, representing tree crowns of the same species as recruits, and

heterospecific crown area, representing tree crowns of all other species. We then summed the tree crown area within 100 m of the center of each 25 m^2 quadrat. We chose a threshold of 100 m based on previous literature that suggests only a small percentage of tree seeds disperse >100 m (Nathan and Muller-Landau 2000). To improve model convergence, we standardized covariates by centering around the mean and dividing by two standard deviations (Gelman 2008).

Model Development

Our primary modeling goal was to evaluate how neighboring tree crowns impact tree recruit abundance. To accomplish this goal, we developed models of increasing complexity to test spatial covariates' impact on model predictions.

Tree recruit abundance in heterogeneous landscapes exemplifies overdispersed count data, which is typically modeled with a negative binomial distribution. An alternate choice for count data with a large number of zeros is a zero-inflated model (Appendix A, Zero-inflated model, Eq. 1A; Lachlan et al. 2019). Our fine-scale study design (25 m^2 quadrats) and the rarity of recruitment in agricultural landscapes resulted in data rich in zeros. Therefore, we developed a zero-inflated model that included a binomial distribution to represent whether recruitment occurred or not, and a negative binomial distribution representing the likelihood of recruit abundance, conditional on recruitment (Appendix A, Zero Inflated model).

We began by assessing intercept-only models representing different distributional assumptions for recruit abundance. The next step was to incorporate elevation as a covariate to account for spatial variability. We added elevation before any other covariates because relative to data on land ownership and mapped tree crowns,

topographic data is widely available at global scales (Brown, Sarabandi, and Pierce 2005). We then added random effects representing land ownership and recruit species identity to the elevation-only model. These random effects enabled the baseline value for recruit abundance to vary by property membership or by recruit tree species (random intercept) and the relationship between elevation and recruit abundance to vary depending on property membership or recruit tree species (random slopes). In addition to models with either property membership or recruit tree species as a random effect, we tested models with both property membership and recruit tree species as random intercepts and slopes.

Building off models that incorporated elevation, property membership, and recruit species identity, we added heterospecific and conspecific tree crown area as additional covariates. Visual examination of the relationship between conspecific tree crown area and recruit abundance suggested a hump-shaped relationship (Appendix A, Figure A2), and incorporating a quadratic term for the effect of conspecific tree crowns resulted in significant improvements in model fit. Thus, we included a quadratic term for conspecific tree crown area in negative binomial models for abundance. In contrast, including a quadratic term for heterospecific tree crowns in models for abundance did not improve model fit and resulted in convergence problems, so we modeled heterospecific tree crowns using only linear terms.

Next, we expanded models for tree crown area by including random effect terms that enabled the slope of the tree crown area to vary by recruit species identity and property membership. These random effects imply that recruit species identity and/or property membership mediate the relationship between tree crown area and recruit

abundance. In sum, our most complex model included heterospecific and conspecific tree crown area and elevation as variables dependent on recruit species identity and property membership.

Model Fitting

We used a Bayesian modeling framework with Hamiltonian Monte Carlo sampling to analyze our data. Our models were run in the Stan programming language using the brms package in R v. 3.6.3 (Bürkner 2017). We ran twelve chains for 8000 iterations with a warmup of 6000 iterations, resulting in 24000 posterior draws per model. We assessed the chain mixing and convergence of the parameters using the Gelman-Rubin statistic (*R-hat* < 1.1; (Gelman and Hennig 2017) and through visual examination of chains using trace plots.

Model Selection

We assessed the predictive accuracy of our models for recruit abundance with out-of-sample data. Our out-of-sample assessment was based on a k-fold approach that iteratively split quadrat data into 90% training data and 10% test data withheld from model fitting. We repeated this procedure ten times, with no test data repetition between folds (Boyce et al. 2002). We then assessed model performance using mean absolute error (MAE) calculated for each of the ten folds test datasets. MAE can be interpreted on the data's original scale as the difference between observed and predicted recruit counts in quadrats.

Results

We located and identified 481 recruits, representing 53 recruits of *Bysrsonima crassifolia,* 110 recruits of *Calycophyllum candissium*, 206 recruits of *Cedrela odorata*,

90 recruits of *Guazuma ulmifolia,* and 22 recruits of *Enterolobium cyclocarpum* (Figure 1.3). We included a total of 23,875 adult tree crowns from the species-specific tree crown map with an average crown area of 93 m^2 (more details about tree crowns in Appendix A, Table A2).

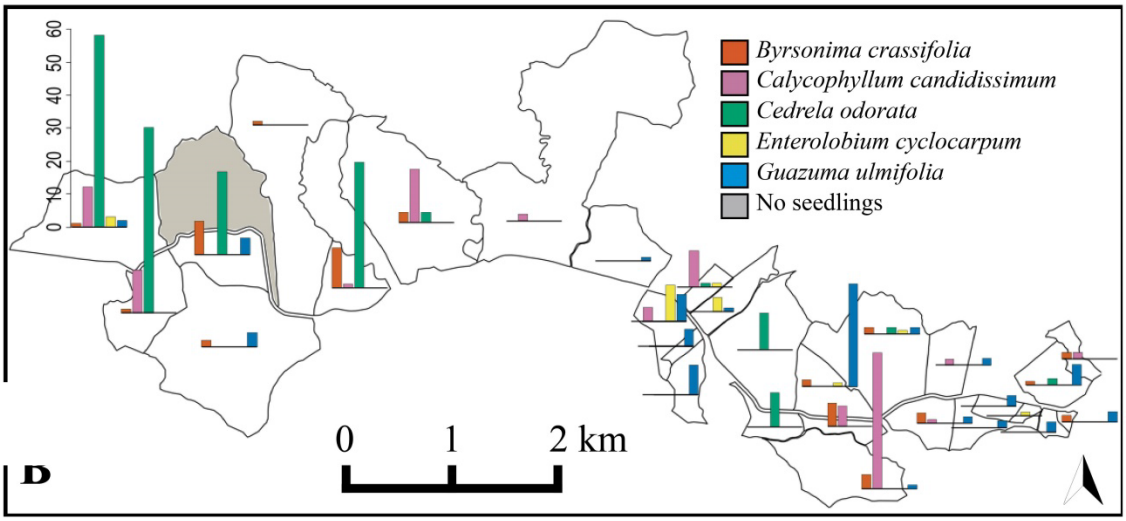

Figure 1.3 Landscape-scale abundance of tree species recruits in 2018, Panama. Black lines represent landowner property boundaries, and histograms display seedling abundance by species on each of the properties.

Species-Specific Tree Crown Maps' Potential to Predict Tree Species Recruit Abundance

The best model to predict recruits of all five species included in the mapped conspecific and heterospecific total tree crown area as a predictor variable with effects varying by property identity (Appendix Table A3). However, when looking at the model error by recruits' species, the best model for recruit abundance varied between species (Appendix A, Table A3). For four out of five species (*Byrsonima crassifolia*, *Cedrela odorata, Calycophyllum candidissimum,* and *Enterolobium cyclocarpum*), including conspecific and heterospecific tree crown area as covariates provided better predictions than models without these covariates. Allowing variability between properties and recruit

species also improved the predictions of tree species recruit abundance by a 2% (Appendix A, Table A3).

Effect of Total Tree Crown Area by Tree Species

Conspecific and heterospecific trees did not contribute equally to recruit abundance (Figure 1.4). Recruit abundance was more strongly related to conspecific tree crown area than to heterospecific tree crown area. Hereafter, recruit abundance refers to the recruit abundance predicted by the full zero-inflated model, the number of recruits refers to the negative binomial phase of the model, and the probability of recruitment refers to the binomial phase of the model. For an average focal tree species in an average property, adding one conspecific average-sized tree crown (93 m^2) results in a predicted increase of 8.00% (95% CI: 0.80 to 11.56%) in the number of recruits. In contrast, adding one heterospecific average-sized tree crown (93 m^2) in an average property results in a predicted increase of only 0.03%, with high uncertainty over whether the heterospecific tree crown area has a positive or negative impact on the number of recruits (95% CI: -0. 60 to 0.68%). Compared to heterospecific tree crown area, conspecific tree crown area also had a stronger impact on recruitment probability. For an average tree species in an average landowner property, adding one conspecific tree crown was predicted to increase the probability of recruitment by 0.05 (95% CI: -0.04 to 0.14), while adding one heterospecific tree crown had a near-zero impact on the probability of recruit abundance (95% CI: -2.26×10^{-3} to 3.57×10^{-3}).

We found evidence for CNDD with a decrease in the predicted number of recruits in plots with high conspecific tree crown area (Figure 1.4). Our models produced a negative estimate for conspecific tree crown area's quadratic effect on the count of tree

recruits (-0.99; 95%CI: -1.63 to -0.37). For a low total area of conspecific tree crowns, the conspecific tree crown area's linear term dominates, resulting in an increased number of recruits. For a high total area of conspecific tree crowns, the quadratic term dominates, resulting in fewer recruits. For example, at a high density of 60 average-sized conspecific trees, recruitment abundance is 0.01 (95%CI: 0.00 to 2.8), while at a low density of 23 conspecific trees, recruitment abundance is 0.38 (95%CI: 0.01 to 1.93).

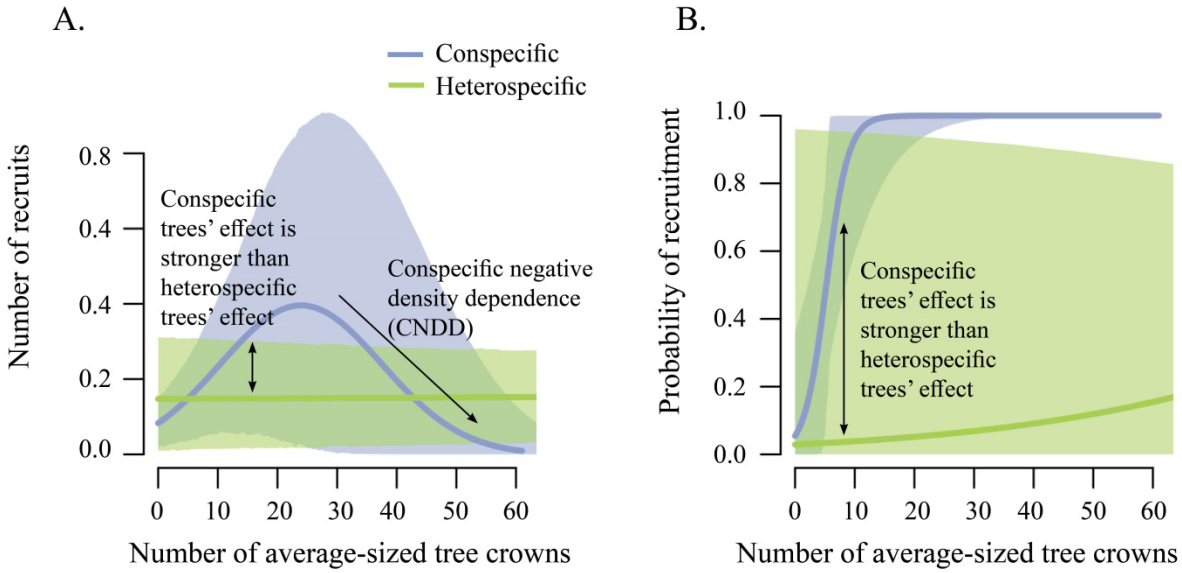

Figure 1.4 Conspecific tree crown area has a stronger positive effect on recruit abundance than the heterospecific tree crown area. These curves were created using the model structure of "Individual tree crowns, Species & Property" (Appendix A, Table A3). Panel A shows the effect of increasing the number of conspecific and heterospecific tree crowns on the number of recruits of an average species in an average property, corresponding to the negative binomial model. Panel B shows the effect of increasing the number of conspecific and heterospecific tree crowns on the probability of recruiting an average species in an average property, corresponding to the binomial model. The shaded area in both panels represents 80% credibility intervals.

Models predicted a robust positive relationship between conspecific total tree crown area and the number of recruits for all species. Effects of increasing conspecific tree crowns from zero to one led to a range of increases in recruit abundance from 7.00%

(95%CI: -2.00 % to 15.00 %) for *Enterolobium cyclocarpum* recruit abundance to 8.80% (95%CI: 1.40 % to 16.00 %) increase for *Cedrela odorata*. Across species, the effects of the heterospecific crown area on the number of recruits were generally smaller and more uncertain than the effects of conspecific total tree crown area and varied across species from positive to negative (Figure 1.5). The effects of heterospecific total tree crown area on recruitment also varied across species from positive to negative. In the binomial phase, models predicted a weak and positive relationship between conspecific total tree crown area and the probability of recruitment for all species ranging from increases in 0.19 (95%CI: -0.06 to 0.31) to 5.04×10^{-4}(95%CI: -0.01 to 0.041) when conspecific tree crowns in the surrounding landscape increase from zero to one. Across species, the effects of heterospecific crown area on recruitment probability varied from positive to negative (Figure 1.5).

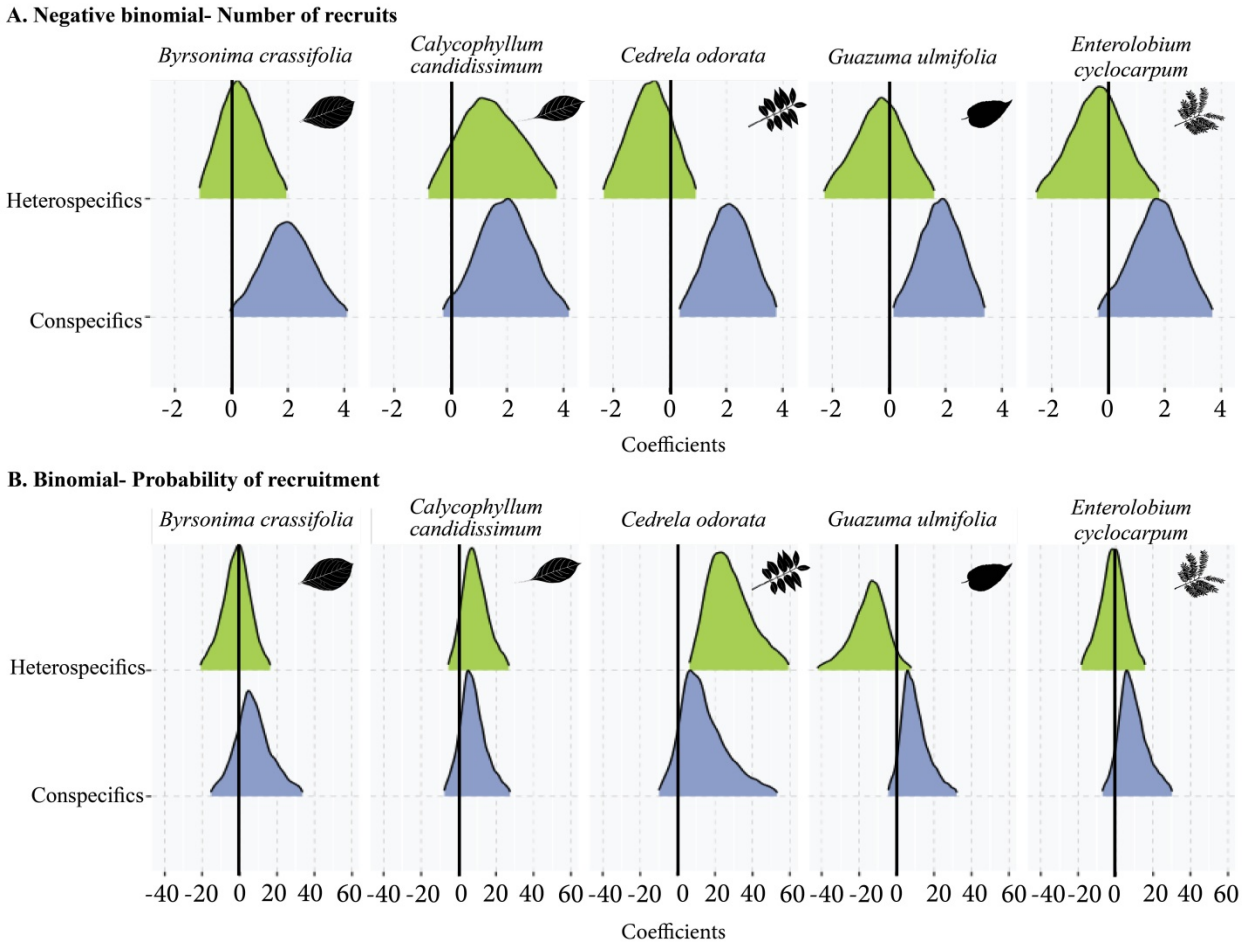

Figure 1.5 Conspecific total tree crown area and heterospecific tree crown area have different effects on the number of recruits and the probability of recruitment across all species. Panel A shows the posterior density distribution of conspecific and heterospecific crown area on the number of recruits on the log-linear scale, corresponding to the negative binomial model. Panel B shows the posterior density distribution of conspecific and heterospecific trees on the probability of recruitment on the logit scale, corresponding to the binomial model. The effects shown represent the total effects of total tree crown area on recruit abundance with 95% CI, including the community-level (fixed) effects and the species-level (random) effects.

Land Ownership Influence on Tree Recruitment Dynamics

Property membership can alter relationships between total tree crown area and recruit abundance (Appendix A, Figure A3). Depending on the property, adding one conspecific tree crown of average size can lead anywhere from a decrease in recruit abundance of 1.75% (95%CI: -16.25% to 14.16%) to an increase of 13.43% (95%CI:

2.43% to 25.75%). Dependence of relationships between total tree crown area and recruit abundance on property membership was also evident in probability of recruitment, albeit with less variation than in the number of recruits. Relative to other covariates, elevation had a weak effect on recruit abundance (Appendix A, Figure A4).

Recruitment Abundance Predictions' Potential to Provide Decision Support

We illustrate how our modeling framework could be applied to forecast natural regeneration in two properties of our study area. We applied our best-fitting model (Model "Individual tree crowns & Property" in Appendix A, Table A3) to forecast recruit abundance as a continuous surface across property one and property four. Considering a threshold for natural regeneration as >1 recruit per 25 m2, differences within and between properties are apparent (Figure 1.6). In property one, the presence of conspecific tree crowns of *Byrsonima crassifolia* results in predicted natural regeneration of this species in 10.05% of the property area (95% CI: 0.00 to 13.59%). On the other hand, *Calycophyllum candidissimum* is predicted to have low natural regeneration in this property (3.51% of the property area; 95% CI: 0.00 to 6.38%), primarily due to negative density dependence and adverse effects of property identity on the baseline recruit abundance for this species. In property four, these species-specific predictions show high natural regeneration for both species, where 21.83% (95% CI: 0.00 to 36.44%) of property area meets our threshold for natural regeneration of *Byrsonima crassifolia,* and 20.70% (95% CI: 0.00 to 28.50%) of the area of this property meets our threshold for natural regeneration for *Calycophyllum candidissimum.* Altogether, these examples demonstrate how our models enable species-and property-specific predictions of tree species recruit abundance in a heterogeneous landscape.

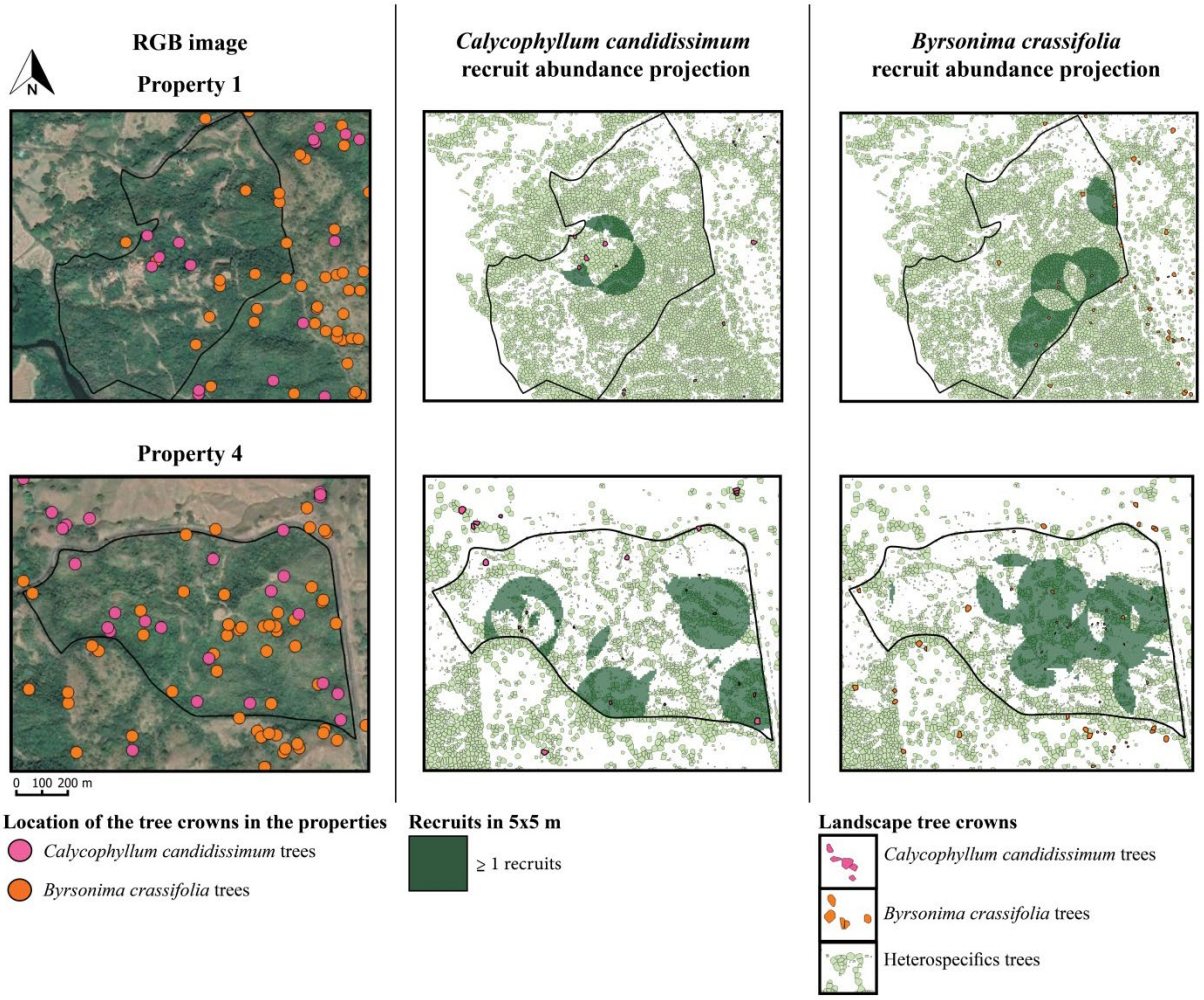

Figure 1.6 Potential application of models for reforestation decision support. Parcel identity in Appendix A, Figure A2.

Discussion

Large-scale restoration projects could benefit from ecosystem services provided by low-cost natural regeneration if we can predict where native species will recruit (Robin L. Chazdon and Guariguata 2016). We applied a species-specific map of tree crown area to predict tree recruit abundance in an agricultural landscape. Accounting for the species identity of neighboring tree crowns improved predictions of tree recruit abundance. However, the effect of the conspecific and heterospecific tree crown area was conditional on land ownership. Predicting tree recruit abundance in tropical landscapes

will require accounting for the identity of trees by separating conspecific trees from heterospecific trees. Altogether, our results enable predictions of tree species recruit abundance across landscapes at the resolution of individual trees and the extent of land management units. High spatial resolution predictions of tree recruitment potential will enable species and property-specific decision-making and facilitate the integration of natural regeneration into forest landscape restoration plans.

Predicting Tree Recruitment from Species-Specific Tree Crown Maps

We have demonstrated the potential of species-specific tree crown maps from hyperspectral and lidar data to improve our ability to predict the abundance of tree species recruits. Our best model for all species included species variability by differentiating conspecific from heterospecific neighboring tree crowns. This approach also allowed including CNDD, which provides another example of a species-specific process key to predictive capacity in our models. An additional benefit of high spatial resolution data on tree crown abundance in heterogeneous landscapes is the ability to account for trees outside forests, including dispersed pasture trees and live fence trees, that may not be included in coarse forest cover metrics (T. Trevor Caughlin et al. 2016; Tarbox, Fiestas, and Caughlin 2018).

Improving species classification algorithms' accuracy will aid our capacity to predict ecological processes, including tree species recruitment. As more accurate methods for tree crown segmentation and species classification are developed (e.g.: Dalponte et al. 2019), we anticipate that the predictive capacity of ecological patterns from tree crown maps will improve. For example, convolutional neural networks have demonstrated potential species classification accuracies over 90% (Bin Zhang, Zhao, and

Zhang 2020). A related challenge will be propagating uncertainty from tree crown segmentation and species classification based on remotely sensed data through ecological predictions (Maddox et al. 2019).

The Relevance of Species Identity for Recruitment

We found that the effect of conspecific tree crowns on recruit abundance is stronger than that of heterospecific trees. This is consistent with patterns observed in other tropical landscapes (Comita et al. 2010) and indicates that differentiating conspecific from heterospecific is essential to understand patterns in natural regeneration. Previous tree recruitment studies in tropical landscapes have aggregated conspecific and heterospecific tree crown area into non-species-specific forest cover (Zahawi et al. 2013; Holl et al. 2017). Our results suggest that the varying impacts (from weak to strong effects) of forest cover on seedling recruitment from previous studies may have partially resulted from the lack of species identity data on reproductive trees in existing forests.

Landscape-scale CNDD provides an example of an ecological process where differentiating between same and different species is essential for accurate prediction. We also found evidence for CNDD in our study, with decreased recruit abundance when conspecific total tree crown area was high. In natural landscapes, CNDD is prevalent across many tropical tree species and is likely driven by host-specific natural enemies (Comita and Stump 2020). We suggest that CNDD may also play a role in agricultural landscapes, including our study area, an agropastoral region subject to hundreds of years of cattle ranching and continued management.

In contrast to the effects of conspecific total tree crown area, which were fairly consistent across all species, effects of heterospecific total tree crown area varied widely

between species. Differences in heterospecific tree crown area effects between species are suggestive of intraspecific differences in life history. For example, *Calycophyllum canddissimum* had a strong positive relationship with heterospecific total tree crown area, potentially resulting from this species' relatively high abundance during mid-late succession. Alternately, recruit abundance of *Guazuma ulmifolia*, a light-demanding early successional species (Kalacska et al. 2004; Hall and Ashton 2016), exhibited a more negative relationship with heterospecific total tree crown area. While a higher sample size of tree species with variable functional traits will be necessary to test these relationships rigorously, landscape-level, species-specific tree crown maps provide a rich dataset to improve our understanding of how species functional traits and dispersal syndromes impact forest succession.

Land Ownership Influence on Tree Recruitment

Cadastral data on land ownership was an important data source for models' predictive capacity. In our study area, where the vast majority of the land is privately owned, cadastral data represents differences in land management history with far-reaching consequences for ecological processes (T. Trevor Caughlin et al. 2016; Mariana Valencia Mestre 2017). This spatial variability could result from differences in landowners' decision-making (Lengkeek 2003; Heather P. Griscom, Griscom, and Ashton 2009) or underlying biophysical differences between properties (e.g. soil fertility; Hall et al. 2011). A limitation in this study is that we cannot extrapolate recruitment predictions beyond the sampled properties. Finding drivers of property recruitment variability that can be measured using sensing could enable to create predictive models in larger areas than this study. For example, dectecting grass species using hyperspectral data could

provide (Schmidt and Skidmore 2001) information of the presence in properties of invasive grasses used in cattle ranching with negative effects on natural regeneration (Heather P. Griscom, Griscom, and Ashton 2009). In the context of an ongoing forest transition in the Azuero Peninsula driven by regional socioeconomic changes (Sloan 2015), understanding the human drivers of spatial heterogeneity at farm scales remains a critical research need.

Recruitment Abundance Predictions Potential to Provide Decision Support

Overall, predicting tree species recruitment at the scale of individual trees and properties will improve decision support for reforestation projects (Robin L. Chazdon and Guariguata 2016). Using models similar to the one we have developed here, restoration managers could identify target areas with high natural regeneration as low cost opportunities for forest recovery (Robin L. Chazdon and Guariguata 2016), at the scale of landowner properties where restoration interventions take place (Oliveira Fiorini et al. 2020). Given that different tree species provide different ecosystem services, and farmer preference for particular species can vary, forecasts of individual species recruitment will boost the value of natural regeneration maps. Our work is the first step towards a decision support tool that could improve species and site selection by providing information on which tree species are likely to recruit naturally in a given farm.

CHAPTER TWO: BAYESIAN MODELS FOR SPATIALLY-EXPLICIT INTERACTIONS BETWEEN NEIGHBORING PLANTS

Abstract

Interactions between neighboring plants drive population and community dynamics in terrestrial ecosystems, and understanding these interactions has critical implications for both fundamental and applied ecology. Interaction strength depends on the distance between neighboring plants, necessitating spatial approaches to model neighbor interactions. Newly-developing Bayesian methods, such as the Hamiltonian Monte Carlo algorithm, offer the flexibility and speed to address many of the challenges associated with fitting spatially-explicit models for interaction strength between plants. We present a guide for parameterizing models for neighbor interactions in the Stan programming language and demonstrate how Bayesian computation can assist ecological inference for plant-plant interactions. Modeling plant neighbor interactions present several challenges for ecological inference. First, the pairwise data structure of neighbor interaction matrices often leads to large matrices that demand high computational power in statistical models. Second, non-linear functions for distance decay often present the most biologically realistic choice for interaction strength and require modeling tools beyond a linear or generalized linear model framework. Finally, hierarchical structure in neighbor interaction data is the norm, including repeated measurements within field plots, species, and individuals. Complex datasets, including hierarchical terms (e.g., "random effects"), can result in model convergence problems such as correlations between

variance and group-level effect terms. We explore modeling choices and solutions for these challenges with examples representing spatial data on three different plant demographic rates: growth, germination, and recruitment. An overarching result from our work is that ragged matrices, which reduce the size of pairwise interaction matrices, can result in higher efficiency across data types. We also demonstrate how contemporary metrics for model convergence, including divergent transitions and effective sample size (ESS), can diagnose problems that result from complex non-linear structures. Finally, we highlight different model structures for hierarchical terms in neighbor interaction models, including centered and non-centered parameterizations. We provide reproducible examples in the Stan programming language to enable a broad range of ecologists to apply our methods for fitting neighborhood interactions, including solutions to common problems with model fit. Individual-based models, including spatially-explicit models for plant neighbor interactions, are becoming increasingly central to many ecological questions. Our work illustrates how Bayesian computation can provide flexibility, speed, and diagnostic capacity for fitting plant neighbor models to large, complex datasets. The methods we demonstrate are applicable to any dataset that includes a measured plant demographic rate and locations of individual plants, from forest inventory plots to remotely sensed imagery. Further developments in statistical models for neighbor interactions are likely to improve our understanding of plant population and community ecology across systems and scales.

Introduction

Interactions between neighboring plants impact how plants grow, survive, and reproduce. Although these interactions occur at the scale of individual plants, the

consequences of neighbor interactions shape population and community structure across terrestrial ecosystems. Plants tend to do worse in single-species neighborhoods than in many-species neighborhoods (Sortibrán, Verdú, and Valiente-Banuet 2014), an individual-level dynamic that helps explain how plant biodiversity is maintained across ecosystems, from montane deserts (Adler, Ellner, and Levine 2010) to tropical rainforests (Comita and Stump 2020). Plants can also facilitate the growth and survival of their neighbors, particularly in disturbed or stressful environments where "nurse plants" promote faster ecosystem recovery (Adler, Ellner, and Levine 2010). Managing plant neighborhoods, from thinning dense stands of trees (Cescatti and Piutti 1998; Lechuga et al. 2017) to planting species that will facilitate their neighbors (Gómez-Aparicio 2009), is a cornerstone of forestry, restoration, and agriculture. The importance of neighbor interactions across basic and applied ecology points to the need for statistical approaches that can quantify how plant neighborhoods impact plant demography. Such analyses must account for space, as plants interact more with closer neighbors than with neighbors further away (Figure 2.1).

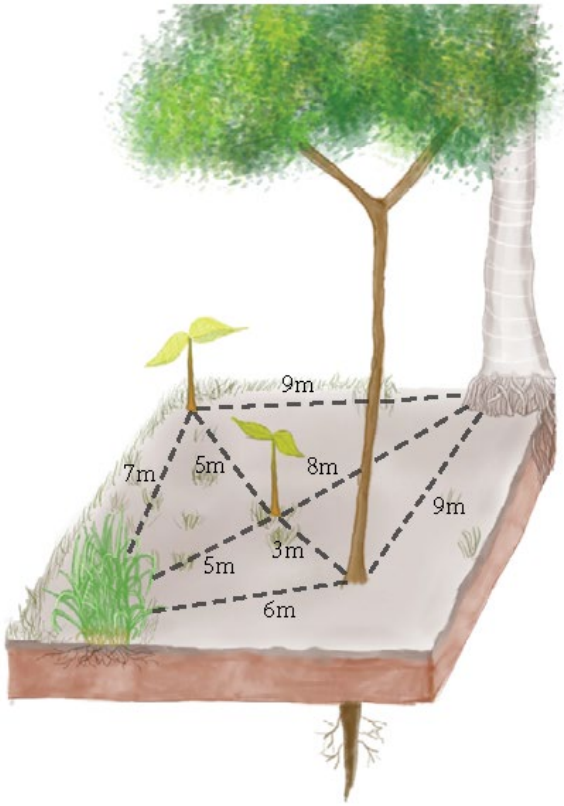

Figure 2.1. Spatial structure of a plant neighborhood. The seedling in the center of the plot experiences a range of neighbor interactions, depending on the neighbor's species identity, size, and physical distance.

As an approximation to spatially-explicit models, many studies have used plant density in a fixed radius (Buckley et al. 2001; Goldberg et al. 2001; LaManna et al. 2017). Aggregating plant neighborhoods into a single density metric as input to statistical models requires assuming fixed relationships between distance and interaction strength. Relative to plant densities, spatially-explicit models enable a more realistic representation of individual plant traits (Zambrano et al. 2020) and the relationship between neighbor distance and interaction strength (Keil et al. 2021). However, fitting spatially-explicit plant neighbor interactions requires accounting for the distance between each pair of potential neighbors, which can be computationally expensive. Typical sample sizes of >100

individual plants in ecological studies result in high-dimensional pairwise matrices that require high amounts of computer memory and processing power to analyze.

A common simplification is to assume that the interaction between neighbors far from each other is zero, creating an effective neighborhood radius (Stoll and Weiner 2000; Muller-Landau et al. 2004). Effective neighborhood radii result in matrices with many zero elements, as most plant neighbors are typically outside of the effective neighborhood radius. Matrices rich in zeros are found in a wide range of disciplines, from graphics manipulation to acoustics (Dokmanic et al. 2015), and are known as sparse matrices. While there are existing methods to optimize computation on sparse matrices (Olson et al. 2016; Mohr et al. 2017; Turek and Huth 2018; Rawal, Fang, and Chien 2019), these methods have not yet achieved wide use in ecology.

Another challenge to fitting individual-based models for neighbor interactions is that interaction strength is almost always non-linear, including strong interactions between close neighbors and sharp declines in interaction strength when neighbors are further apart. Unlike linear models with a standard functional form, there are a wide range of possible non-linear functions (Bolker 2008). Non-linear models are also more prone to identifiability problems, meaning it is difficult to define a single solution for the equation (Pickard 1987; Ogle 2009). The challenges of fitting non-linear models point to the need for flexible methods for model parameterization, including diagnostic metrics to assess model fit.

In addition to non-linearity, hierarchical structures that violate assumptions of independence between individual observations can complicate statistical models for plant neighbor interactions. Hierarchical structures are ubiquitous in ecological data, including

individuals representing different genotypes (Zaiats et al. 2020) and individuals nested within different sites (Schneider, Law, and Illian 2006; T. T. Caughlin et al. 2015). Bayesian methods present a powerful tool for fitting spatially-explicit plant interactions models with well-developed protocols for assessing convergence and avoiding local maxima due to non-linearity and hierarchical structure (Vehtari, Gelman, et al. 2020; Gelman et al. 2020). Nevertheless, guidance for fitting Bayesian models in the context of challenges associated with typically large and sparse datasets for neighbor interactions remains scarce. For example, a common sampling pathology associated with hierarchical models occurs when correlations between the variance and estimates of group-level ("random") effects are high, limiting the ability of the sample to efficiently explore the probability surface. Solutions to this pathology (e.g. Betancourt and Girolami 2015) have not yet been explored in the context of non-linear models for neighbor interactions.

In this paper, we provide a roadmap for how Bayesian methodology can fit non-linear and spatially explicit models for neighbor interactions. Our work builds off a recent advance in Bayesian inference, the Hamiltonian Monte Carlo (HMC) algorithm, which has improved sampling efficiency for many problems relative to older algorithms (Monnahan, Thorson, and Branch 2017). The Stan software package provides an interface to HMC, including model assessment tools, with high value for fitting neighbor interaction models (Stan Development Team 2019a). The flexibility of the Stan programming language provides new opportunities to apply Bayesian methods to large datasets, including optimization of sparse matrices. In addition, uncertainty and model assessment metrics provided in the Bayesian framework allow a more intuitive implementation of hierarchical structures (e.g., random effects; Monnahan et al. 2017,

Ogle and Barber 2020) in non-linear models with non-normal error structures. Using multiple examples of plant demographic rates, including growth, germination, and recruitment, we demonstrate optimization strategies for sparse matrices and alternate parameterizations for hierarchical structure in neighbor interaction models. By providing Stan code to fit a range of spatially-explicit neighbor interaction models, our overarching goal is to enable broader use of these powerful models in ecology.

Materials And Methods

We begin with a general model for a Bayesian neighbor interaction model:

$$[\theta_1, \theta_0, z|\mathrm{y}] \alpha [\mathrm{y}|z, \theta_0][z|\theta_1][\theta_0][\theta_1]$$

Equation 1

In Eq. 1, y represents the observed data (e.g., growth, survival, or recruitment), z represents the latent neighbor interaction process, $\boldsymbol{\theta_0}$ is a vector of parameters that represent the physical and biological effect sizes of the attributes of a plant's location, and $\boldsymbol{\theta_1}$ is a matrix of parameters representing the effect sizes of the neighbors' attributes (e.g.: DBH, location and species). $[\theta_1, \theta_0, z|\mathrm{y}]$ is the conditional probability density function (PDF) of $\boldsymbol{\theta_1}, \boldsymbol{\theta_0}, z$ given y, $[\mathrm{y}|z, \theta_0]$ is the conditional PDF of y given $z, \boldsymbol{\theta_0}$, $[z|\theta_1]$ is the conditional PDF of z given $\boldsymbol{\theta_1}$. Lastly, $[\theta_0]$ and $[\theta_1]$ are the marginal distributions of $\boldsymbol{\theta_0}$ and $\boldsymbol{\theta_1}$ respectively. The relationship between the data and parameters in Equation 1 can be described with a kernel (e.g.: Eq2 from Canham and Uriarte 2006). Note that this kernel is deterministic and represents the pattern of the ecological process in the absence of any randomness or error (Bolker 2008).

$$y(p_i) = g(p_i) \sum_{j=1}^{n} f\left(x_{i,j}\right)$$

Equation 2

where $y(p_i)$ is the plant *i* vital rates (y) at a given location p_i, $g(p_i)$ is a function representing the effect of the physical and biological attributes (θ_0) at point p_i, $x_{i,j}$ is a matrix of the attributes of plant j relative to the plant *i*, and f(x) is a function describing the effect of individual j on $y(p_i)$, also referred as the interaction kernel. Equation 3 represents an example of an interaction kernel:

$$f\left(distance_{i,j}\right) = \sum_{j=1} \frac{1}{a_2\ distance_{i,j}}$$

Equation 3

where $\text{distance}_{i,j}$ is a pairwise matrix that contains the distance from plant *j* to plant *I* and a_I is a parameter representing the relationship between $\text{distance}_{i,j}$ and $f\left(\text{distance}_{i,j}\right)$. These pairwise matrices can become large with increasing sample size and hence become very computationally intensive. One solution is to assume that neighbors beyond a distance threshold, or effective neighborhood radius, do not interact (Ribbens, Silander, and Pacala 1994). When we set the effective neighborhood radius, we redefine values beyond the radius to zero and transform the pairwise matrix into a sparse matrix.

Optimization of Sparse Matrices Using Ragged Matrices in a Neighbor Interaction Model.

Sparse matrices could be optimized by transforming the sparse matrix into a ragged matrix (Chalauri, Laluashvili, and Gelashvili 2018). A ragged matrix has a different number of elements in each row, limiting the use of linear algebra operations on matrices but reducing computer processing time. In Stan, the built-in function "segment()" creates a ragged matrix by storing non-zero elements and their position in the pairwise matrix in a vector of non-zero observations plus two index vectors that indicate the position of non-zero elements within the matrix (Figure 2.2).

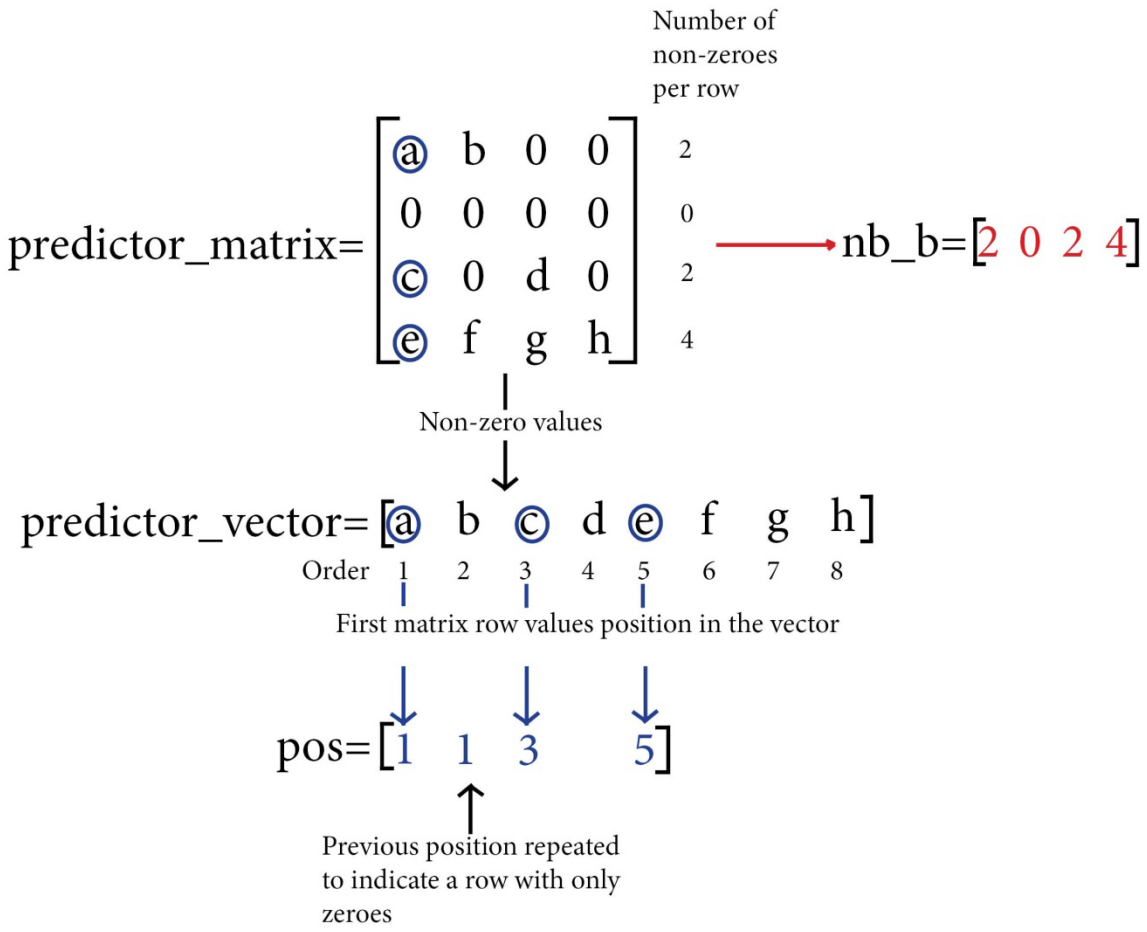

Figure 2.2 Segment function requires the creation of a vector with no zeroes, an index of the non- zero values on each matrix row and an index of the position in the vector of the first values of the matrix rows.

Example 1: Plant Growth

We simulated a spatially explicit data set representing plant growth to demonstrate how ragged matrices can improve computation time for neighbor models. We model the growth of stationary plants as a function of their intrinsic growth (i.e., growth in isolation) and their local neighborhood characteristics (i.e., neighbor size and proximity; Eq. 4). To evaluate how choosing an effective neighborhood radius could introduce bias in parameter estimation, we fit six different models with effective neighborhood radii of 5m, 10m, 15m, and 20m. The "true" effective radius of this

simulated data is 10 m. With real data, the decision for radius size should be based on biological knowledge, for example, root zone area (Zaiats et al. 2020). Alternately, the effective neighborhood radius can be chosen by testing the predictive performance of different sized radii (Pacala and Silander 1985; 1987).

The equation below represents our generative model for neighbor-dependent growth.

$$size_{t_{1,}i} \sim normal(\mu_i, \sigma^2)$$

$$\mu_i = \alpha + \beta size_{t_0,i} + a_3 \sum_{j=1}^{n} \frac{size_{t0,i,j}^{a_1}}{\exp(distance_{i,j}^2 a_2)}$$

Equation 4

In equation 4, $size_{t_0,i}$ and $size_{t_1,i}$ are the sizes of plant i at time t=0 and 1, respectively, $distance_{i,j}$ is the distance between *i* and neighbor plant *j*, and $size_{t_0,j}$ represents the size at time t=0 of plant *j*. α is the intercept, β is the effect of $size_{t_0,i}$, and parameters *a1*, *a2* , and *a3* are the effects of the neighbors' size and distance. To estimate parameters from simulated data, we used weakly informative priors, with *α, β, a1, a2*, and *a3* following a normal(0,5) distribution and sigma following an exponential(1) distribution.

We fit models in Stan using both a sparse matrix and a ragged matrix approach. These approaches share a large amount of code, with two main differences between the sparse and ragged matrices. For the code using the sparse matrix, the data block in Stan has two sparse matrices containing the distances and sizes of the plants within the effective neighborhood radius of 10 m. We define N as the number of individual plants.

```
     int N;      // number of individuals

     vector [N] sizemat[N];  //matrix containing the sizes
of the neighbor plants

     vector [N] distmat[N];  // matrix containing the dista
nces of the neighbor plants
```

In contrast, the code using the ragged matrix contains in the data block the three vectors required to use the `segment()` function (Figure. 2.2) for size and distance. The non-zero values from both matrices are stored the vectors `size_vector` and `dist_vector`. Then we create the two index vectors indicating where the non-zero values were located in the matrices. The two index vectors are the same for distance and size since the plants that become zero after applying the effective neighborhood radius are identical in both matrices. We also define obs as the number of non-zero values in the sparse matrices.

```
      int obs;    // number of non-zero values in the spars
e matrices

     vector [obs] size_vector;  //vector containing the non
-zero sizes of the neighbor plants

     vector [obs] dist_vector;  //vector containing the non
-zero distances of the neighbor plants
```

```
     int pos[N];  // index vector indicating the order in t
he size_vector and distance_vector of the first row numbers
from the size and distance matrices

     int n_nb[N]; // index vector indicating number of non-
zero values in the size and distance matrices
```

In the transformed parameter block, a nested for-loop defines an interactions kernel (Stan Development Team 2019b; Full code in Appendix B, Code for chapter 2, Simulation sparse matrix code).

```
     for(i in 1:N){

     for(j in 1:N){

             smat[i,j]=sizemat[i,j]^a1;

      dmat[i,j]=distmat[i,j]^2*a2;}}

     for(n in 1:N){

             kernel[n]=sum(smat[n]./exp(dmat[n]));}
```

In contrast, in the ragged matrix code, non-zero elements used to create the neighbor kernel are referenced using vectors from the segment function (Full code in Appendix B, Code for chapter2, Simulation ragged matrix code). Similar to the sparse matrix formulation, these calculations take place in transformed parameters block in Stan:

```
     for (i in 1:obs){
      size_vec[i]=size_observations[i]^a1;
      dist_vec[i]=dist_observations[i]^2*a2;}
     for (n in 1:N){
      kernel[n]=sum(segment(size_vec, pos[n], n_nb[n]))./ex
p(segment(dist_vec, pos[n], n_nb[n]));}
```

Example 2: Plant Recruitment

To further explore applying the ragged matrix as an optimization strategy in neighbor interaction models, we parametrized a model using real data on the seedling abundance of invasive strangler fig trees, *Ficus macrocarpa,* in Southwest Florida. We analyze Caughlin et al. (2012) data, which includes the total number of strangler fig seedlings in fifty-two 30 x 30 m plots along a 250-km transect. Distances to adult fig trees within an effective neighborhood radius of 300 m were recorded. We model seedling recruitment using a negative binomial distribution, with a mean (μ) and an over dispersion parameter (φ):

$$recruitment_i \sim negative\ binomial(\mu_i, \varphi)$$

$$\mu_i = a + b\sum_{j=1}^{n} \frac{1}{c + distance_{i,j}} CP_i$$

Equation. 5

where *a* is the global intercept and *b* describes the strength of the interactions kernel, which decays as a function of *c* and the distance from plot *i* to adult fig tree *j* for n total adult trees per plot. Similar to other strangler figs, F. microcarpa begins its life cycle by germinating in the canopy of a host tree. The number of potential host trees in the 30 x 30 m plots, CP, is multiplied by the kernel as an offset, assuming that more host trees create more opportunities for fig tree seedlings to recruit.

The original study exponentiated *a , b* and *c* to keep the parameters positive. To replicate the previous results, fit with maximum likelihood estimation in Caughlin et al. (2012), we ensure non-negative values for the mean of the negative binomial distribution by constraining parameters *a , b* and *c* to positive values. However, we note that the log-link is the canonical link-function for the negative binomial distribution and probably a better way to ensure positive values for future studies (Full code in Appendix B, Code for chapter2, Real data sparse matrix code).

To fit our Bayesian models, we used a normal distribution with a mean of 0 and a standard deviation of 100 as a weakly informed prior for parameters a , b and c, and an exponential distribution with a rate of 0.5 for φ. In this example, there are seedling plots that do not have any adult strangler fig trees nearby, resulting in zeroes in the n_nb vector (second row of predictor matrix in Figure 2.2) that we replace with the global intercept using an `ifelse` statement (Full code in Appendix B, Code for chapter2, Real data ragged matrix code).

We estimate the model fitting efficiency between sparse matrices and ragged matrices by dividing the elapsed time to run 1000 iterations by the effective sample size (ESS). Iterations are the repeated sampling of the probability surface to look for

minimum log-likelihood, in which the output of each step is used as the input for the next iteration. ESS is an estimate of how much the autocorrelation within the chains increases uncertainty in estimates. Higher ESS indicates lower autocorrelation and decreased uncertainty in parameter estimates (Stan Development Team 2019b). We also checked whether estimated parameter intervals recover the parameters used to generate the data by looking at the posterior distributions. Lastly, we checked common diagnostic metrics to evaluate convergence, such as the $\widehat{R}$, ESS, divergences, energy and Bayesian fraction of missing information. We considered convergence when the $\widehat{R}$ was lower than 1.1, all the chains mixed without any divergences, and the ESS was over 10%, which means that we had enough effective samples so the energy transition density, and the marginal energy distribution were similar (Vehtari, Gelman, et al. 2020; Gelman et al. 2020).

Centered and non-centered parametrization for random effects in neighbor interaction models.

Example 3: Plant Seeds Germination

To demonstrate how hierarchical models for plant neighbor interactions can be fit in a Bayesian context, we analyzed a dataset on seedling germination that includes multiple individuals nested within field plots in central Thailand. Plant neighborhoods include seedling and adult trees, all of the same species as marked seeds placed on the forest floor in 1 m^2 plots. The marked seeds comprised a seed addition experiment spanning a 5 km gradient of tree abundance in a tropical forest. In this study, the effective neighborhood radius was set at 10 m. The study's primary objective was to quantify how the density of seedling and adult tree neighbors impacted the probability of seed germination. More information on the study can be found in Caughlin et al. (2015). We

model the germination probability of seeds as proportional data using the binomial distribution and a centered parametrization for the random effects (ω; Eq. 6).

$$germination \sim binomial(n, p)$$

$$logit(p_{i,k}) = \mu + bCon.Seedlings_i + a\sum_{j=1}^{n}\frac{size_{i,j}}{distance_{i,j}^{g}} + \omega_{k[i]}$$

$$\omega_k \sim nomal(0, \sigma)$$

$$a \sim normal(0,1)$$

$$\sigma \sim normal(0,1)$$

Equation 6

where the input to the binomial distribution includes the total number of seeds added to each plot (n) and the probability of successful germination events (p). Size is a pairwise matrix containing the size of the adult trees (j) that affect germination of plant i, and distance is the pairwise matrix containing the distance between the adult neighbor j and germinating plant i . μ is the baseline germination, b is the decrease in seed survival as a function of neighbor density, $Con.Seedlings_i$ is the amount of conspecific seedlings to represent the crowding effect, a is the parameter that represents the effect of neighbor size and distance on recruitment, g is the distance decay of the effect of neighbor size and distance, and ω is the random effect of plot k, to account for non-independence between seeds in the same plot.

A common sampling pathology associated with hierarchical models that include group-level ("random") effects, such as the plot-level intercepts to account for seeds

within the same field plot in Eq 6., is correlations between the variance and estimates of random effects. These correlations limit the ability of samplers to explore probability surfaces thoroughly as they can cause a "funnel" shape in the probability density that is hard to explore by the sampler and can result in poor model convergence (Neal 2011). Recent work with Hamiltonian Monte Carlo sampling has led to an improved understanding of fitting hierarchical models, including methods to address correlation problems in hierarchical structures (Betancourt and Girolami 2013). One solution is to reparametrize the model, creating a linear model structure to decouple variance from random effect estimates (Eq.7; McElreath 2017). This solution is often referred to as the "non-centered parameterization," in contrast to the "centered parameterization" in which the levels of the random effects have a common prior, in this case with mean 0 and standard deviation σ.

$$\omega_{k[i]} = c + \sigma z_{k[i]}$$

$$z_j \sim normal(0,1)$$

$$c \sim normal(0,1)$$

$$\sigma \sim normal(0,1)$$

Equation 7

In equation 7, the *germination* distribution and the $logit(p_{i,k})$ are the same as in equation 6 and then we re-write the random effects centered parametrization $\omega_k \sim \text{nomal}(0, \sigma)$ as a deterministic sum of the mean and scaled group variances, $\omega_{k[i]} = c + \sigma z_{k[i]}$ (McElreath 2020). Namely, we replace the original variance, σ, with a product of variance and site-specific scaling parameter, z, sampled from a unit normal prior.

These unit normal prior causes z to be orthogonal and hence reduces correlation between the variance and estimates of random effects. In Stan, these changes are easily implemented and require only minor changes to the model.

For the centered parametrization we create the interactions kernel in the transformed parameters block using the following code (Full code in Appendix B, Code for chapter2, Real data centered parametrization code):

```
      for (n in 1:N){
      if (am[n]==0){g[n]=mu+ b*Cseedlings[n]+omega[plots[n]];}
      else{
        g[n] = mu + b*Cseedlings[n] + a* sum(segment(size_observations,p
os[n], nb_b[n]) ./exp(ger*log(segment(dist_observations, pos[n],nb_b[n]
)))) + e[plots[n]];
        }
      }
```

while for the non-centered parametrization we add a piece of code before the interactions kernel in which we parametrize the random effects in a linear model structure (Full code in Appendix B, Code for chapter2, Real data non-centered parametrization code):

```
      for (n in 1:M){
        omega[n]= mu_omega+ slope_omega[n]*scale_omega;}
      for (n in 1:N){
      if (am[n]==0){g[n]=mu+ b*Cseedlings[n]+omega[plots[n]];}
```

```
      else{

        g[n] = mu + b*Cseedlings[n] + a* sum(segment(size_observations,p
os[n], nb_b[n]) ./exp(ger*log(segment(dist_observations, pos[n],nb_b[n]
)))) + e[plots[n]];

        }

      }
```

where `omega` is the random effect, `mu_omega` is the intercept, `slope_omega[n]` is the variance and `scale_omega` is the scaling parameter. `g` is the probability of successful germination events, and `Cseedlings` is the count of conspecific seedlings within field plots.

To compare the centered and non-centered parametrization we checked efficiency by dividing the elapsed time to run 1000 iterations by the ESS. We also compared posterior distributions between parametrizations and checked common diagnostic metrics to evaluate convergence, including $\widehat{R}$, divergent transitions, and ESS. We also graphically explored how well the model sampled the correlated area by plotting the correlation between the variance and estimates of random effects for the centered parameterization and between the random effect estimates and one of the parameters estimated in the linear model structure for the non-centered parameterization. These convergence metrics and plots provide insight into whether correlations between the variance and group-level effects occur in the centered parameterization. We also compared the output from both parametrizations by evaluating model uncertainty and fit to the original data, calculating the mean absolute error (MAE) between the predictions and the original data.

Results

Comparison Between Sparse Matrix and Ragged Matrix Performance

Example 1: Plant Growth

For the model using simulated data on growth, the results showed that the ragged matrix is more efficient than the sparse for almost all effective neighborhood radii. However, for the generative effective radius at 10m, both strategies were equally efficient. Nevertheless, using ragged matrices to fit neighbor interaction remains advantageous because the greater efficiency of ragged matrices enables faster exploration of models with different neighbor effect radii (Figure 2.3).

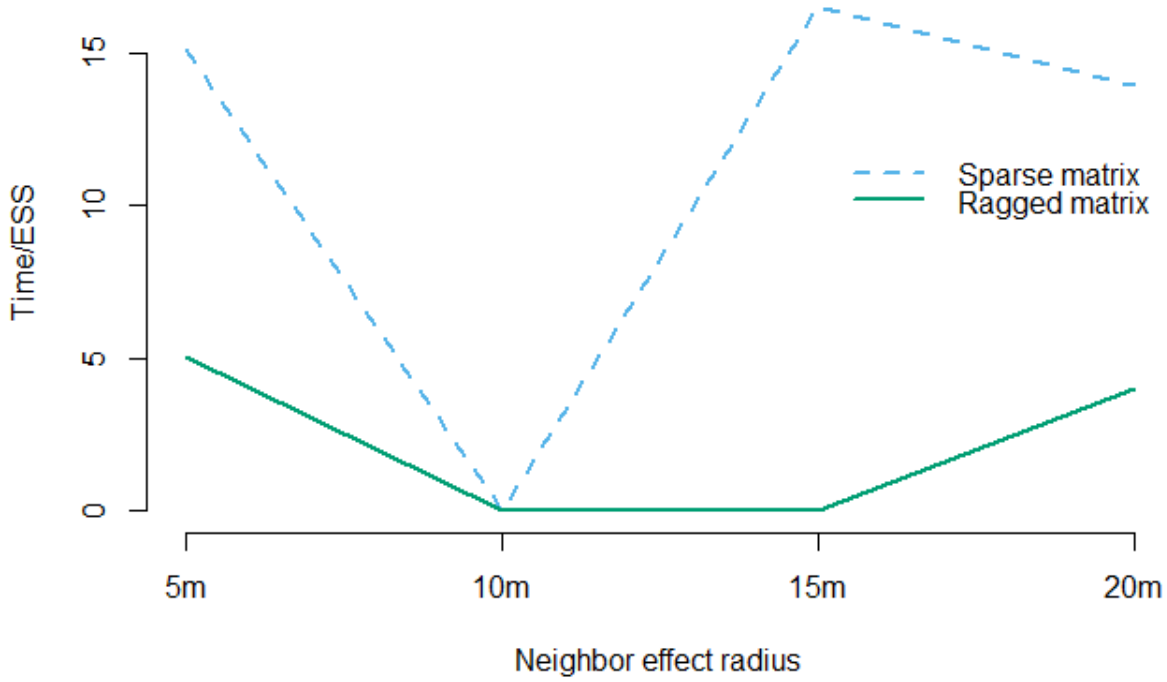

Figure 2.3 For the models fit using the simulated growth data, the ragged matrix is more efficient than the sparse matrix for models of all neighbor effects, except 10 m. Note that 10 m was the "true" effective neighborhood radius used to simulate data. The dashed blue line shows the change in efficiency using the sparse matrix under different effective neighborhood radii. The solid green line shows the change in efficiency using the ragged matrix under different effective neighborhood radii. Smaller values of Time/ESS represent increased efficiency and higher values represent decreased efficiency.

The ragged matrix and the sparse matrix approaches could recover the true parameters with an effective neighborhood radius of 10 m. However, the ragged matrix provided consistently tighter credibility intervals than the sparse matrix at an effective neighbor radius different than the "true" radius.

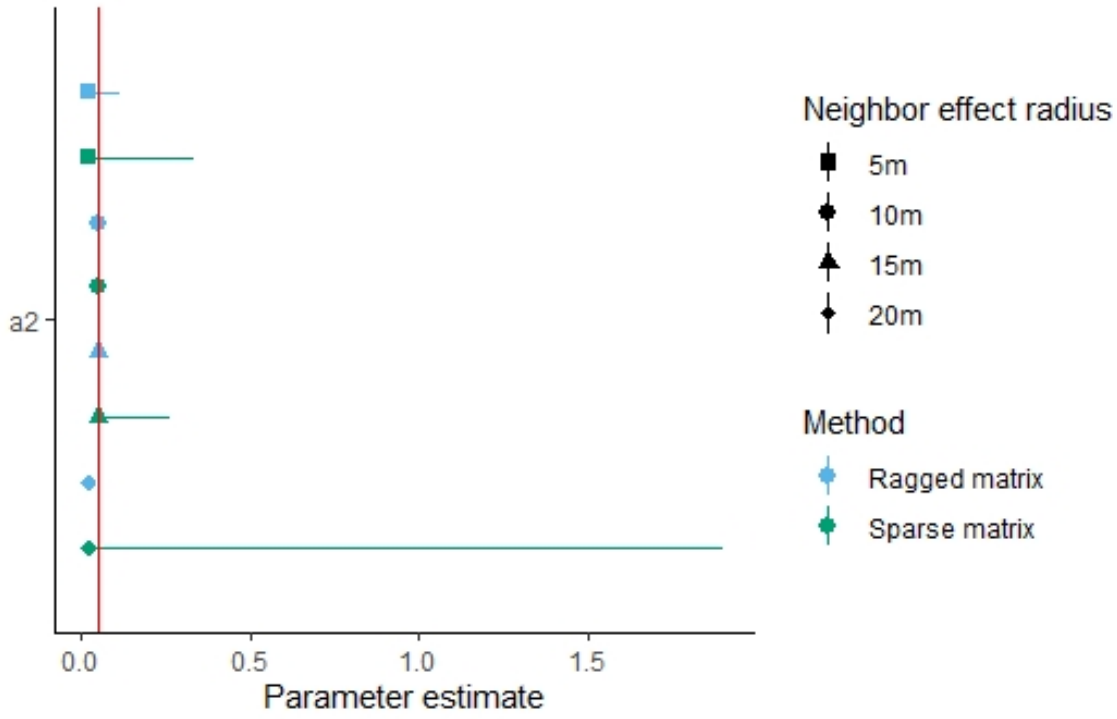

Figure 2.4 The effective neighborhood radius selection is essential to obtain unbiased estimates. The bias was similar for all the parameters and effective neighborhood radii, so in this graph, we just show one of the parameters. The chosen parameter estimates are for a2, which estimates distance decay in the interaction strength between growth and distance. The green shapes are the estimates of the segment function parameters. The blue shapes are the matrix parameter estimates. Each of the shapes corresponds to a different effective neighborhood radius. The red line is the true parameter used in the simulation. 95% Credibility Intervals (CI) showed in the figure. Note that the CIs for the 10 and 15 m radii are not visible.

At the 10m and 15m radius using both the sparse and the ragged matrices there were no divergent transitions in 8000 iterations. For the sparse matrix at 10 m radius and for the ragged matrix at 10 and 15 m radii, the $\hat{R}$ for all the parameters was lower than 1.1 and the ESS was over 10%, indicating convergence (Appendix B, Tables B1-B3). Models fit with other radii showed divergences, low ESS, and high $\widehat{R}$, which indicated poor convergence for the models using both the sparse and the ragged matrices (Appendix B, Tables B4-B8).

Example 2: Plant Recruitment

For the models using the strangler fig trees recruitment data from Caughlin et al. (2012), model efficiency was greater for the model fit with the ragged matrix. The model fit with the ragged matrix was 3.6 times more efficient than the model fit with the sparse matrix, with an efficiency of 3.01e-08 Time / ESS (s) for the sparse matrix relative to an efficiency of 8.42e-09 Time / ESS (s) for the ragged matrix. However, parameter estimates were similar for both model parameterizations (Appendix B, Figure. B1), and produced estimates qualitatively similar to the frequentist maximum likelihood estimation presented in the original analysis (Figure 2.5). Both of the Bayesian models converged well (Appendix B, Tables B9, and B10).

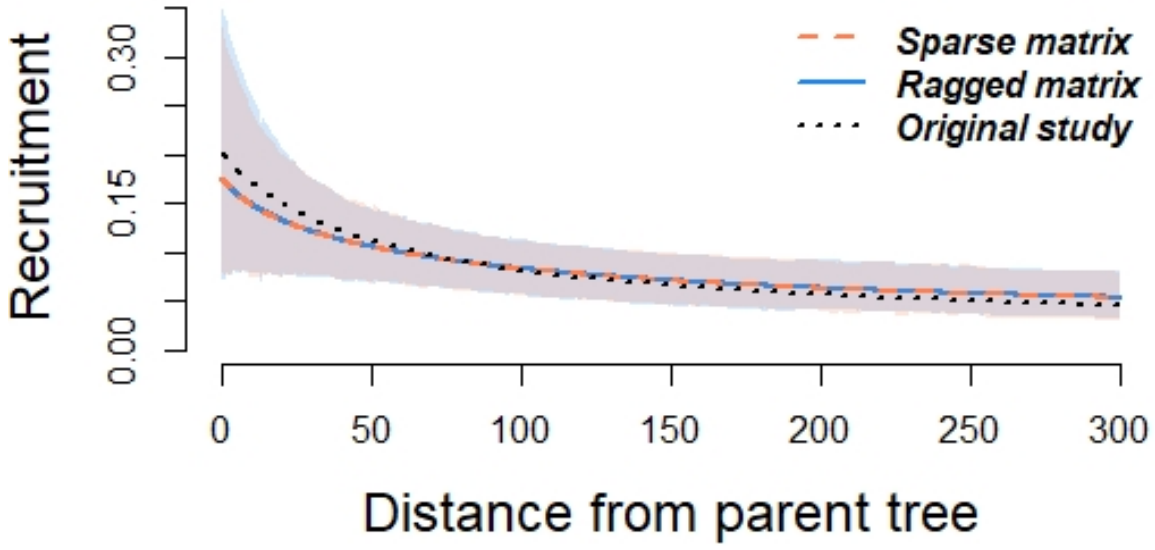

Figure 2.5 The ragged matrix and the sparse matrix approaches obtained similar estimates of the relationship between recruitment and the distance from a single parent tree. Curves show the relationship between recruitment and distance from parent tree parametrized using the sparse matrix, the segment function, and the frequentist maximum likelihood model fit using the lme4 package (Bates et al. 2015) from in the original study. The shaded areas around the curves are the 95% Credibility Intervals (CI).The CI for the sparse and the ragged matrix overlap mostly. In the areas where they do not overlap the sparse matrix CI is the shaded area in orange and the ragged matrix is the shaded area in blue.

Comparison Between Centered and Non-Centered Parametrization Performance

Example 3: Plant Seeds Germination

For the models using the seedling recruitment data from Caughlin et al. (2015) the centered parametrization had an efficiency of 1.02e-05 Time / ESS (s), while the non-centered parametrization sampled nearly 114 times more efficiently, with 8.92e-08 Time / ESS (s). Both parametrizations showed no divergences, the ESS was over 10%, the $\widehat{R}$ was lower than 1.1 and the chains mixed well. For this data set, we found minimal evidence for convergence problems due to correlations between group-level parameters

and variance terms (Appendix B, Tables A11 and A12). However, when visually comparing the exploration of the probability surface of the centered and non-centered parametrization we can observe how the non-centered parametrization was able to explore the "funnel" shape caused by the hierarchical structures correlation (Figure 2.6).

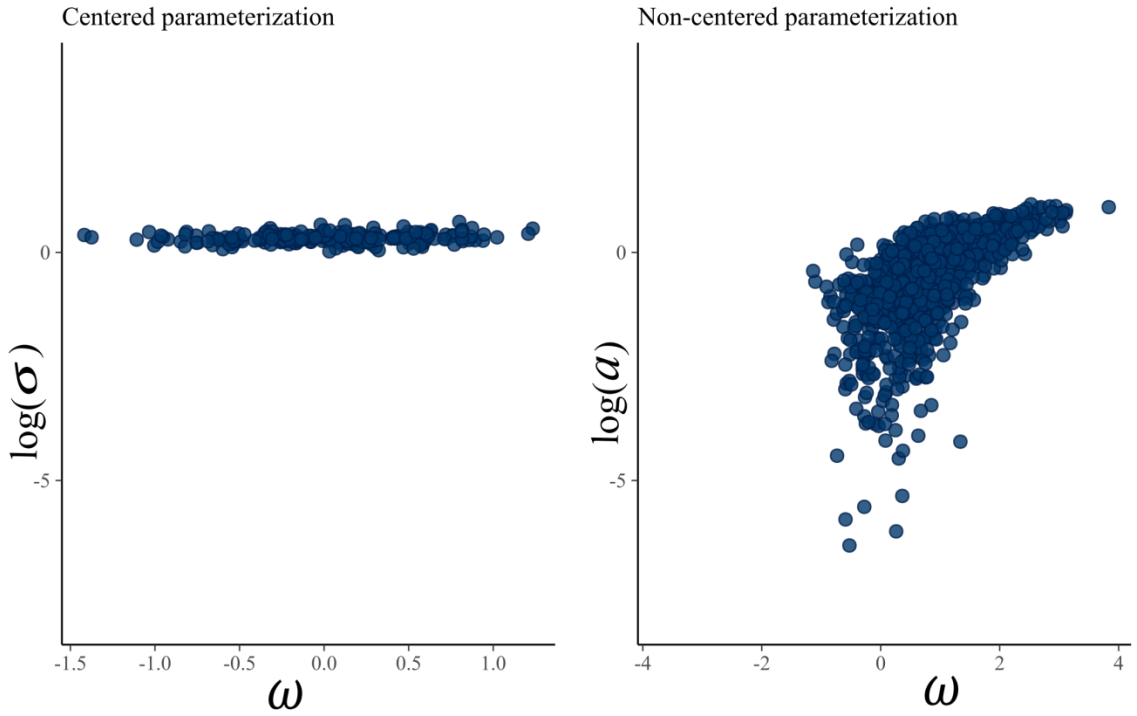

Figure 2.6 The non-centered parametrization was able to explore the "funnel" distribution caused by the hierarchical structures correlations, while the centered parametrization never explored further than the neck of the "funnel" and was not able to sample in the tail of the distribution. ω is the first plot random effect coefficient, σ is the variance of the plot random effects in the centered parametrization and the a is the intercept of the linear structure for the random effects in the non-centered parametrization.

The parameter estimates were similar for the centered and non-centered parametrizations, with wider 95% CI for parameters μ and *ger* for the non-centered parametrization (Figure 2.7). The error between the observed and predicted germination was similar for both parametrizations and slightly underestimates germination (Appendix B, Figure B2). Mean Absolute Error also indicated comparable results between the two

parameterizations, with a value of 1.196 (95% CI: 0.002 to 4.453) for the centered parametrization and 1.194 (95% CI: 0.000 to 4.376) for the non-centered parametrization.

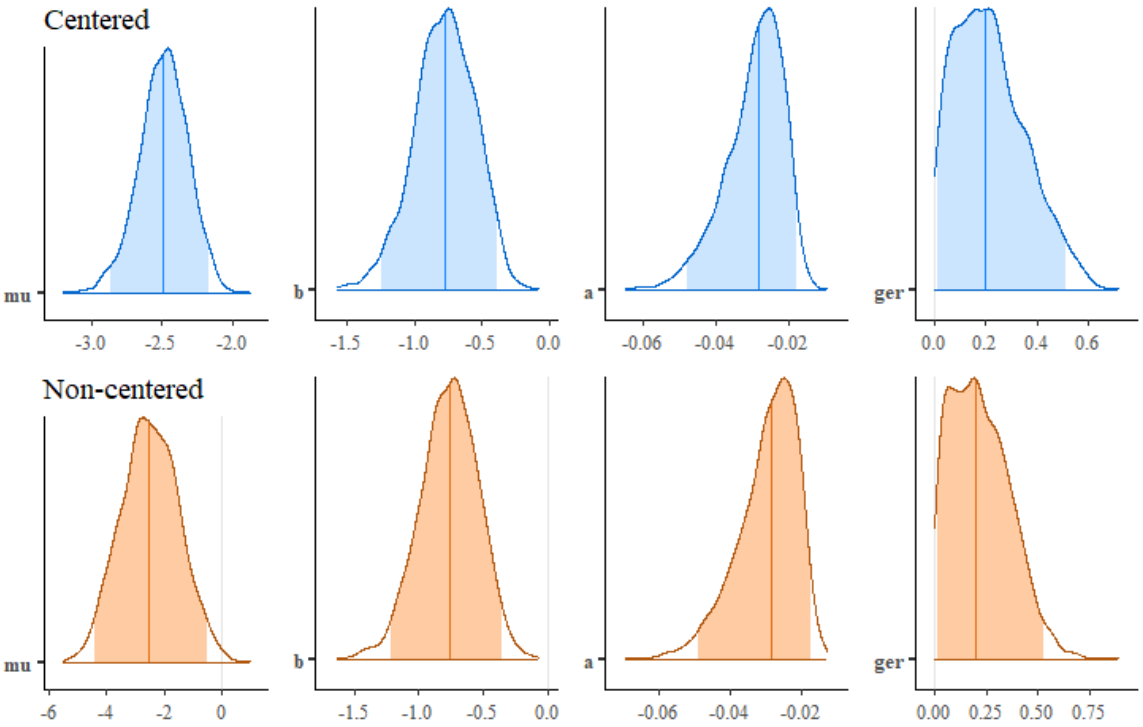

Figure 2.7 Posterior distribution of the fixed effect estimated parameters of the model describing germination rate with distance from adult trees using a centered and non-centered parametrization. The estimated parameters are similar for both parametrizations; however the non-centered parametrization has wider 95%CI for parameters μ and ger compared with the centered parametrization. The 95% CI are the shaded areas in the posterior distribution.

Discussion

We have demonstrated how to leverage contemporary Bayesian methods to estimate neighbor interactions from spatial data on plant demography. The pairwise data structure of matrices representing neighbor interactions often leads to large datasets that present computational challenges. An overarching result from our work is that ragged matrices greatly increase computational efficiency, relative to matrices that include elements for each pair of plants in the study. We also demonstrated how Bayesian models

can include hierarchical structures in models of neighbor interactions, including hierarchical structure to account for pseudoreplication between individuals of the same species or in the same plot (Schneider, Law, and Illian 2006). Correlations between random effect parameters are inherent to many hierarchical models, and our work illustrates potential solutions for convergence issues when fitting hierarchical models with non-linear terms for neighbor interactions. Altogether, we expect that fitting neighbor models with contemporary Bayesian software packages, such as the Stan programming language, will open up new opportunities for ecological inference and prediction on large, complex datasets that include the location of individual plants.

Sparse vs. Ragged Matrices in Stan

Spatially explicit neighbor interactions matrices are frequently simplified using an effective neighbor radius that sets interaction strength of neighbors beyond the radius to zero (Stoll and Weiner 2000; Muller-Landau et al. 2004). This simplifying assumption creates a sparse matrix structure, with many zeros for non-interacting plant neighbors, that can be computationally inefficient. The solution of using ragged matrices to optimize computation efficiency in neighbor interaction models increased sampling efficiency relative to using the entire sparse matrix for a range of neighborhood effect radii, with the exception of the true neighborhood radius. However, the effective neighborhood radius is almost never known *a priori,* so we generally recommend the ragged matrix approach for faster exploration and selection of different effective neighborhood radii. Built-in functions in the Stan programming language enable sparse representations of a matrix that improve storage efficiency but are limited in improving the sampling speed (Stan Development Team 2019b). Our result show that ragged matrices could significantly

improve computational speed in addition to storage requirements. We expect that the generality of our method has broad applicability for spatial problems in ecology that rely on pairwise matrices, from landscape graph-theoretic connectivity (Urban and Keitt 2001) to pairwise relatedness analysis between individuals (Hardy 2003).

Parameter estimation was similar for the ragged and the sparse matrix and depended on the size of effective neighborhood radius. A model fit using simulated data representing plant growth revealed that the most accurate parameter estimates corresponded to the "true" effective neighborhood radius, with minimal decreases in accuracy for a bigger radius and larger decreases in accuracy for radii smaller than the "true" radius. This result is similar to previous frequentist models for plant neighborhood dynamics Canham and Uriarte (2006), where larger radii provide estimates with lower biases than smaller radii. Overall, we would recommend erring on the side of including a larger effective neighborhood radius rather than having a too-small radius regardless of whether the model is parameterized with a ragged or a sparse matrix approach. An alternate approach could include estimating the neighbor effect radius simultaneously with parameters from the neighbor model. Such an approach would enable propagation of uncertainty from plants left out of the model to model output (Uriarte et al. 2004). The flexibility of the Stan programming language presents an ideal platform to test and refine future iterations of models for spatial neighbor interactions.

Hierarchical Modeling

Our results suggest a potential tradeoff between uncertainty in random effects and sampling efficiency, with narrower uncertainty intervals for the centered parameterization but higher sampling efficiency for the non-centered parameterization. Although the

centered parametrization converged and the metrics did not show any sampling problem that indicated correlation problems, we observed problems exploring the correlated area of the hierarchical structures. In models that present stronger correlation problems in the hierarchical structures we would expect non-reliable parameters estimates and convergence problems instead of the narrower uncertainty that we obtained in this example (Neal 2011; Betancourt and Girolami 2013). The advantages of one parametrization over another are highly case-specific and depend on the properties of the dataset.

The metrics provided by Stan can be essential to decide which kind of parametrization would be the adequate one. In this study we assessed the centered and non-centered parametrization of random effects by checking parameters estimations, model convergence, CI, random effects posterior correlation, efficiency and model fit to the original data (Gelman et al. 2020). Further research across a range of data structures and study systems will be necessary to develop concrete recommendations for which parameterization should be used (Gorinova, Moore, and Hoffman 2020). As the range of potential hierarchical data structures for neighbor interactions increases, including temporal (Valenta et al. 2020), spatial (Pu, Umaña, and Jin 2020), and phylogenetic autocorrelation (Zambrano et al. 2017; Zaiats et al. 2020), developing efficient ways to fit these models should be a research priority. Automatic parametrization algorithms that build efficient sampling schemes from the data are a promising research avenue in applied statistics that could be used to parametrize neighbor interaction models (Gorinova, Moore, and Hoffman 2020).

Research Perspectives

An ever-growing body of literature seeks to understand population, community, and ecosystem dynamics though individual based models (Deangelis et al. 2020; Hardy 2003; Seidl et al. 2012; Romero-Mujalli, Jeltsch, and Tiedemann 2019). Statistical models that can represent the location of individuals in space are critical to achieving the promise of individual-based models in ecology. (Canham and Uriarte 2006; Bo Zhang and DeAngelis 2020). Fortunately, the number of datasets that include data on plant locations is growing as well. Any dataset where the x and y coordinates of plant individuals are recorded has potential to serve as the basis for a neighborhood interaction models. As data sharing becomes the cultural norm, we anticipate that an increasing number of existing experimental and observational datasets could be used to fit neighbor interaction models (Soranno et al. 2015). Some examples of existing databases with spatial coordinates of individual plants include common garden experiments (Zaiats et al. 2020; Madsen et al. 2020) and forest inventories on permanent plots (Lieberman and Lieberman 2007; Gillerot et al. 2021).

The increasing volume of remote sensing data at the resolution of individual plant canopies also presents novel opportunities to fit neighbor interaction models. Remote sensing data that are capable of identifying plant canopies, via computer vision and machine learning, includes aerial lidar, unoccupied aerial systems (UAS), and high resolution satellite imagery (T. T. Caughlin et al. 2016; Graves et al. 2016; Adak et al. 2020; Shen et al. 2020). High resolution remotely sensed data could offer unprecedented opportunities to parameterize individual-based models for vegetation, including continuous spatial coverage of neighbor interactions across environmental gradients at

landscape to regional extents such as soil moisture, topography, and soil fertility (Kemppinen et al. 2018; Misra et al. 2018; Sankey et al. 2021). However, we expect that increased uncertainty in identifying individual plants from air or space may require statistical models to disentangle measurement from process error (T. Trevor Caughlin et al. 2020).

In summary, we have demonstrated how contemporary Bayesian algorithms, such as Hamiltonian Monte Carlo sampling implemented in the Stan programming language, provide a flexible and efficient way to fit plant neighborhood models. We also provided guidelines for ecologists to parametrize neighbor interaction models under a Bayesian framework using Hamiltonian Monte Carlo. We hope that these guidelines together with new advances on models parametrizations, and the increasing availability of spatially explicit data will help to advance the study of population, community, and ecosystem dynamics though spatially explicit individual based models.

CHAPTER THREE: ANTHROPOGENIC AND BIOPHYSICAL DRIVERS OF TREE MORTALITY ACROSS A TROPICAL AGRICULTURAL LANDSCAPE

Abstract

Trees in agricultural landscapes provide a range of ecosystem services and are critical for maintaining agricultural productivity, storing carbon, and conserving biodiversity. Declines in tree abundance represent a severe threat to the ecological integrity of agricultural landscapes. Nevertheless, data on rates and drivers of anthropogenic and natural individual tree mortality in these landscapes remain scarce, as the low density of agricultural trees over large areas presents challenges for field measurements as well as medium-resolution satellite imagery. To overcome these challenges, we combined a map of tree species at the individual canopy level, produced using high-resolution hyperspectral and lidar imagery, with field validation data and a high-resolution image acquired seven years later. Our methods resulted in predictions of tree crown mortality for 61,918 individuals of five tree species across 23,000 ha of a tropical agricultural landscape. The large spatial extent of our study area enabled us to develop and test spatial hypotheses relating tree mortality to anthropogenic, biophysical, and tree-level factors, including topographic variation, individual tree size, surrounding tree density, property size, and distance to roads. We found that trees located in small properties far from roads had a lower mortality probability than trees in large properties close to roads and that isolated trees had a higher mortality probability than trees surrounded by other trees. In contrast, we found that tree height and tree crown area had

minimal effect on tree mortality. Lastly, we found that higher elevations have lower mortality rates and that site exposure has almost no effect on tree mortality. This study suggests that anthropogenic factors related to accessibility and property size play an important role in determining the fate of agricultural trees. Policies and educational initiatives that target these anthropogenic factors and consider the socio-economic context could reduce the mortality of agricultural trees.

Introduction

The abundance of trees in agricultural landscapes is decreasing (P. Gibbons et al. 2008), impacting the agricultural ecosystem functionality. Agricultural trees, especially isolated trees, are carbon sinks, improve landscape connectivity and soil structure, act as biodiversity reservoirs, and catalyze forest succession (Philip Gibbons and Boak 2000; Celia A. Harvey et al. 2000; 2006; María Jimena Esquivel and Calle Díaz 2002; Manning, Fischer, and Lindenmayer 2006; Zomer et al. 2016). Due to their ecological importance, agricultural trees are likely to both prevent and increase resilience to climate change (Manning, Gibbons, and Lindenmayer 2009; Vignola et al. 2015). In addition, agricultural trees provide a range of ecosystem services to landowners (C A Harvey and Haber 1999; Murgueitio et al. 2011; Maria Valencia Mestre 2017). For example, agricultural trees can alleviate the effects of drought and flooding and provide shade for cattle. Retaining these benefits will mean preventing tree mortality caused by ecological and anthropogenic dynamics in agricultural landscapes. Research suggests that once the driving factors of mortality are known, management activities could reduce tree mortality, especially if the drivers have an anthropogenic source (Outcalt and Wade 2004, Breece et al. 2008, Bradford and Bell 2017).

The drivers of tropical tree mortality in agricultural landscapes have been studied at local scales in the field (Williams-Linera 1990; Rudel and Horowitz 1996; Mesquita, Delamônica, and Laurance 1999; Angelo et al. 2004) and at landscape-scales using remote sensing (Barona et al. 2010; Plieninger 2012; Houghton 2012; Plieninger et al. 2015; Chadid et al. 2015; Sy et al. 2015; Schwartz, Budsock, and Uriarte 2019; R. Fischer, Giessen, and Günter 2020; Gustafson, Raven, and Ehrlich 2020). However, local scale studies cannot be generalized to heterogeneous landscapes such as agricultural land. Most landscape-scale studies are at the pixel level, which does not capture the individual trees' mortality drivers and excludes isolated trees from the analysis. Individual tree-level studies are essential to understand how individual tree characteristics, such as size or species, affect tree mortality (Boudreau et al. 2005; Nguyen et al. 2016; Gora and Esquivel-Muelbert 2021). Field data, such as tagged trees in forest inventory plots, are a primary method for measuring individual tree mortality. However, field data are limited to a small spatial extent, which is problematic for achieving sufficient sample sizes to analyze mortality events in landscapes with low tree density. Assessing the drivers of tree mortality at individual tree-level across extents that can capture heterogeneity in agricultural landscapes remains a challenge. Nevertheless, several studies warn that agricultural tree cover is decreasing (Ozolins, Brack, and Freudenberger 2001; P. Gibbons et al. 2008; Plieninger et al. 2015).

Anthropogenic factors occurring across scales can have a strong influence on tree mortality in agricultural landscapes. Historical land management practices linked to policies (Brandt et al. 2017) and cultural factors (Geist and Lambin 2001) can have long-lasting legacy effects on ecological processes (L. A. Brudvig et al. 2021). Land-use

transitions linked to market shifts (Rudel et al. 2009; Heagney, Falster, and Kovač 2021), such as agricultural de-intensification and development for tourism, are also potential drivers of tree cover change in many landscapes (Gössling 2002; Sluiter and de Jong 2007; Grau and Aide 2008; Cramer, Hobbs, and Standish 2008; Brandt et al. 2019; Hoang et al. 2020). At an individual tree scale, farmer decision-making remains a strong determinant of ecological processes (Busck 2002; Lengkeek 2003; M. Jimena Esquivel et al. 2008; Sánchez-Romero et al. 2021). We might find differences in tree demography between properties as individual landowners will manage their land to promote the abundance of certain species in their properties (Garen et al. 2011; Assogbadjo et al. 2012; Metzel and Montagnini 2014). Spatial covariates, including proximity to roads (Freitas, Hawbaker, and Metzger 2010; Plieninger et al. 2015), surrounding forest cover (Plieninger 2012), and farm size (M. C. Valencia Mestre, Ferguson, and Vandermeer 2018), represent the numerous effects of anthropogenic factors at different scales and can be used in predictive models for tree cover change (Tarbox, Fiestas, and Caughlin 2018). Because anthropogenic factors are essential in shaping agricultural landscapes and can often be managed more easily than large-scale biophysical factors (Garen et al. 2009; Casas and Viñuela 2010; Slusser, Calle, and Garen 2015a), identifying the anthropogenic factors driving tree mortality on the agricultural landscape could lead to policies and management strategies to prevent tree cover loss.

In addition to human drivers of tree cover change, individual tree characteristics are likely to influence tree mortality in agricultural landscapes. For example, larger trees have competitive advantages over smaller trees, such as the capacity to reach deeper water tables and intercept more light (Binkley et al. 2013). However, large trees are also

more susceptible to hydric stress, wind damage, and carbon starvation (Laurance et al. 2000; Bennett et al. 2015; McDowell et al. 2018; Schwartz, Budsock, and Uriarte 2019), especially isolated trees (Williams-Linera 1990). In addition, trees that reach harvesting sizes are more likely to be logged (Nguyen et al. 2016; Gora and Esquivel-Muelbert 2021). Understanding how tree size relates to mortality rates can improve management strategies to maintain tree population size. For example, low mortality of large individuals often means that population growth rates are more sensitive to the loss of large trees than the loss of small trees (Zuidema 2000).

Finally, topography is an essential driver of tree mortality across heterogeneous landscapes. Topographic differences can buffer the effects of drought-induced tree mortality (Guarín and Taylor 2005; Bonal et al. 2016) and how exposed to wind trees are (Laurance and Curran 2008). For example, slope affects water drainage and runoff, and aspect affects solar radiation (Guarín and Taylor 2005; Zuleta et al. 2017; Esteban et al. 2021). Topography can also affect the accessibility and suitability of agricultural activities of an area. Deforestation in flatter low elevations is usually lower than at higher elevations (Camargo et al. 2005; Silva et al. 2007; Mon et al. 2012; Plieninger et al. 2015).

Disentangling the relative importance of cross-scale drivers of tree mortality, including individual tree characteristics, human land management, and topography, will be critical to strategies that conserve tree cover in agricultural landscapes. Biophysical and anthropogenic dynamics interact at different spatial scales (Gardner et al. 2009; T. Trevor Caughlin et al. 2019). As a result, these landscapes have a high level of heterogeneity, and biophysical variables can have unexpected outcomes. For example,

while trees surrounded by forest might suffer higher mortality due to competition (Comita et al. 2010), isolated trees in agricultural land can have higher mortality because agricultural lands are prone to land-use change to more profitable uses (Plieninger et al. 2015). Potential trade-offs between human and biophysical drivers of tree mortality point to the need for studies of tree cover loss at the resolution of individual trees but with a large enough extent to represent multiple sources of landscape heterogeneity, from land-use history to topographic variation.

High spatial-resolution remote sensing offers the opportunity to collect individual tree mortality data over large areas (Paz-Kagan et al. 2017; Campbell et al. 2020) and can be coupled with data representing the spatially heterogeneous dynamics between nature and humans (Torres-Romero and Olalla-Tárraga 2015; T. Trevor Caughlin et al. 2019; Requena-Mullor et al. 2019). For example, cadastral data can represent land management units (Barber et al. In review), and road maps can represent the accessibility of the area (Tarbox, Fiestas, and Caughlin 2018). Another reason to use high-resolution remote sensing is the low mortality rates of adult trees (McMahon, Arellano, and Davies 2019; Arellano, Zuleta, and Davies 2021). In many studies, adult tree mortality approximates a rate of <0.90 per year, which means that even with data on >100 trees, only one tree on average would die during an annual study period (Dahlgren 2011; Thomas et al. 2013; Eitzel et al. 2015). Increasing the sample size to obtain sufficient data to quantify mortality requires sampling impractically large areas for fieldwork in landscapes where tree cover is sparse (e.g., agricultural land). We propose using high-spatial-resolution remote sensing to quantify how large-scale biophysical and anthropogenic factors drive individual tree mortality in agricultural landscapes.

This paper evaluates the anthropogenic and biophysical factors driving individual tree mortality across 23,000 ha of an agricultural landscape. We used high-resolution remote sensing data, which allowed us to obtain information at a resolution capable of capturing individual tree characteristics and larger-scale drivers of mortality. We analyzed a series of possible mortality drivers such as (1) anthropogenic factors including property size, distance to roads, and surrounding tree cover, (2) tree traits including tree height and crown area, and (3) topographic variables including elevation and solar exposure. The overarching goal of our work is to apply novel remotely sensed data to inform the conservation of agricultural trees in a pastoral region of Southwestern Panama, broadly similar to many landscapes across Latin America.

Materials And Methods

Study Site

This study takes place in the municipality of Pedasi, in the Peninsula of Azuero, Panama, and encompasses 23,000 ha (Figure 3.1). The area is characterized by a dry season from December to March, with most of the average rainfall of 1,700 mm yr^{-1} falling from April-November. Before the 20^{th} century, dry tropical forests dominated this landscape; however, human activities such as cattle ranching have reduced the extent of the dry forest to ~2% of its historical extent (H.P. Griscom et al. 2011). The landscape comprises active pastures, riparian corridors, an increasing number of touristic areas, and naturally regenerating areas (Metzel and Montagnini 2014). Low land productivity and land speculation for tourism is resulting in agricultural de-intensification but is also prompting farmers to seek the restoration of ecosystem functions, including tree planting for silvopastoral systems (H.P. Griscom et al. 2011; Slusser, Calle, and Garen 2015b).

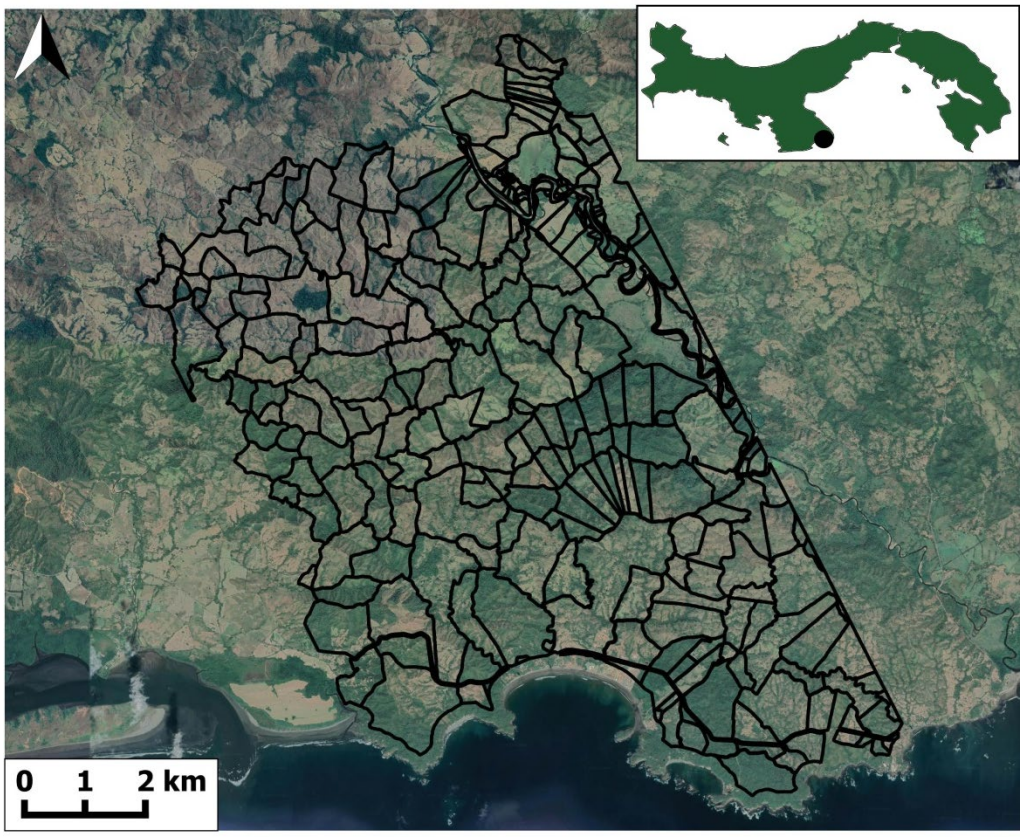

Figure 3.2 Study area in Southwestern Panama. The black lines represent the 388 properties included in this study. Green colors indicate mainly forest vegetation cover, and tan colors indicate non-forested land cover. The black dot in the upper-right corner displays the location of the study site in Panama. Map data: Google, Airbus, Maxar Technologies.

Tree Species Selection

To identify adult trees present in the landscape in 2012, we used a map of adult tree species, including 298,971 crowns of 21 species across 23,000 ha (Graves et al. 2016). This map was created using lidar and hyperspectral aerial data collected by the Global Airborne Observatory (GAO; formerly the Carnegie Airborne Observatory) in January 2012 (Asner et al. 2012). First, the authors used a canopy height model with a pixel size of ~1.13 m to produce an individual tree crown segmentation (Dalponte and Coomes 2016). Then the tree crowns were classified by species using hyperspectral data (380–2510 nm; 5 nm bandwidth) and a support vector machine algorithm (see Graves et

al. 2016 for further details). We selected five species that the support vector machine could classify with high predictive accuracy (F-score >70%) and representative of a range of phylogeny, functional traits, and human use (Appendix A, Table A1). The species were *Byrsonima crassifolia, Calycophyllum candidissimum, Cedrela orodata, Guazuma ulmifolia*, and *Enterolobium cyclocarpum.*

Quantifying Tree Mortality Using High-Resolution Remote Sensing Imagery and Field Data

Out of the 61,589 mapped tree crowns belonging to our five focal species from Graves et al. (2016), we classified the state of 5,885 trees randomly selected across the whole 23,000 ha that this study encompasses. First, we identified trees present in the field in 2012 using the map of trees derived from hyperspectral and lidar data from Graves et al. (2016). Then we overlaid the mapped outlines of the trees on imagery from 2019 obtained from Google Earth Pro and visually classified the state of the five focal species trees in 2019 as dead or alive (Figure 3.2). This mortality classification using high-resolution remote sensing enabled collecting large amounts of data relevant for tree demography. However, remote sensing data also introduces new sources of error relative to field data. From an aerial perspective, trees may be covered by other vegetation, break, or be obfuscated by atmospheric distortion or phenological changes unrelated to mortality. These multiple sources of error complicate the detection of tree mortality. To overcome measurement error in classifying trees as dead or alive from aerial imagery, we use a model-based approach to account for imperfect detection. Models accounting for detectability are widely used in wildlife ecology (i.e., occupancy models and capture-recapture; McCrea and Morgan 2014, Broms et al. 2016), and their use in plant ecology

using remote sensing is increasing (Kellner and Hubbell 2018; T. Trevor Caughlin et al. 2020). Modeling tree mortality conditional on detection allowed us to model both the mortality process and classification errors simultaneously.

In this study, we had two levels of detection error, false classification of live trees as dead and dead trees as alive. Following a similar approach to Miller et al. (2011), we used field validation data to improve detection estimates in models with two categories of detection error. Our field data includes mortality events for a subsample of 329 trees. The unambiguous field data, where trees were censused in-person by trained ecologists, enabled an independent quantification of the probability of tree mortality and its detection.

To obtain the field data on tree status in 2012 and 2019, we visited 329 trees across the 23,000 ha of this study. We located the trees with a GPS unit (Bad Elf) with accuracy <5 m. We confirmed the death of trees by identifying the remains in the field and excluded trees that had fallen but exhibited regrowth. Pasture trees removed from the pasture by farmers, including the tree stump, were classified as dead since there were no trees around that could be confused with the target tree. After the field data collection, the 329 trees measured on the field were also classified using remote sensing by an ecologist that did not participate in the field data collection to create a detection history.

Figure 3.3 Mapped trees from 2012 over imagery from 2019. The circular shapes represent the contour of the tree crowns in 2012. The red shapes are the trees whose state was ground-truthed and measured using remote sensing to characterize possible detectability problems, and the yellow shapes are trees whose state was classified using only remote sensing. The red tree crown on the left corresponds to a tree's death between 2012 and 2019, and the rest of the tree crowns correspond to surviving trees between 2012 and 2019. Map data: Google, Airbus, Maxar Technologies.

Environmental and Social Covariates for the Mortality Model

Based on existing literature, we compiled a list of anthropogenic factors, tree traits, and topographic variables that might be affecting the mortality of agricultural trees. Differences in land management strategies could have an impact on tree mortality in agricultural landscapes. For example, land owners of large areas tend to intensify land use (M. C. Valencia Mestre, Ferguson, and Vandermeer 2018). To characterize land management variability in the landscape, we obtained the identities of the properties and property sizes from a cadastral dataset developed by Panama's National Authority for the

Administration of Lands and provided by the Fundación Pro Eco Azuero from 2010. Accessibility and land-use change are two other anthropogenic factors that could affect tree mortality. Distance to roads is a good estimator of accessibility and risk of land-use change associated with development (Freitas, Hawbaker, and Metzger 2010; Plieninger et al. 2015). We calculated distance from trees to roads using the Euclidean distance and a road's map from 2011 created by the Smithsonian Tropical Research Institute and provided by the Fundación Pro Eco Azuero (Milton Solano 2011).

We expected larger trees to have higher mortality because of of hydraulic failure, carbon starvation, and logging (Bennett et al. 2015; Gora and Esquivel-Muelbert 2021). To represent individual tree size in our models, we extracted tree height and tree crown area from the map of trees from Graves et al. (2016). We also expected different mortality rates between species because of species traits (Iida et al. 2014) and because of different species timber value (Degen et al. 2006), so we extracted species identity from the map of trees from Graves et al. (2016). Tree densities within 30m could positively affect mortality through increased competition (Comita et al. 2010). On the other hand, isolated trees in agricultural land might be logged due to land-use change (Freitas, Hawbaker, and Metzger 2010; Plieninger 2012) and are more exposed to wind and drought (Williams-Linera 1990). We estimated tree density as the sum of tree crowns from all the trees within a 30 m radius from the map of trees from Graves et al. (2016). This study considers an isolated tree a tree with no tree cover within a 30 m radius.

We expected areas at lower elevations to have higher mortality because they are more suitable and easy to access for cattle ranching than higher elevations (Camargo et al. 2005; Silva et al. 2007; Mon et al. 2012; Plieninger et al. 2015). We also hypothesized

solar to impact mortality negatively since areas with higher solar exposure are located in steeper slopes that are more difficult to access (Silva et al. 2007) or a positive impact on mortality, since trees on areas with higher solar exposure are more likely to suffer from drought (Schwartz, Budsock, and Uriarte 2019). We obtained topography variables from a digital elevation model (DEM) with a 1.13 m spatial resolution developed from the aerial lidar over our study area (Asner et al. 2012). We extracted elevation, aspect, and slope from the DEM. We then calculated solar exposure using the aspect and slope (Balice et al. 2000, Johnson and Miller 2006; Eq.8). Solar exposure is an integrative metric that represents heat stress vegetation experiences on steep, south-facing slopes.

$$Solar\ exposure = slope \cdot \cos(\frac{aspect - 180}{180})$$

Equation 8

Covariates for the Detection Probability Model

Based on the literature and our observations while remotely measuring mortality, we created a set of variables that could be influencing the detection probability of tree mortality. We expected that a higher canopy cover would increase the chance of misclassification (Vahidi et al. 2018). To represent canopy cover, we extracted the Normalized Difference Vegetation Index (NDVI) in 2019 around 50 m of the trees from Landsat imagery in Google Earth Engine to obtain a measurement of tree density that might influence detection probability on the images. NDVI is closely related to forest structural metrics in this ecosystem, including tree canopy cover (Caughlin et al. 2016). We expected that taller trees and trees with bigger tree crowns would be more visible and harder to misclassify (Cho et al. 2012), and included tree height and crown area in our detection model. Lastly, we expected trees on higher elevations and flatter slopes to have

better visibility than trees in lower elevations and steeper slopes (Waser, Ginzler, and Rehush 2017). Hence, we included elevation and slope extracted from the digital elevation model (DEM) from the aerial lidar over our study area (Asner et al. 2012) in the detection probability model.

Model Development

Altogether, our data include 5,885 trees with remotely measured mortality, 329 trees with field and remotely measured mortality, and 55,375 mapped tree crowns that remained unclassified. The remotely measured mortality potentially includes trees accurately classified as alive, trees accurately classified as dead, trees falsely classified as alive, and trees falsely classified as dead. To account for imperfect detection, we used a Bayesian state-space model with two categories of detection error (Miller et al. 2011, Chambert et al. 2015; Figure 3.3).

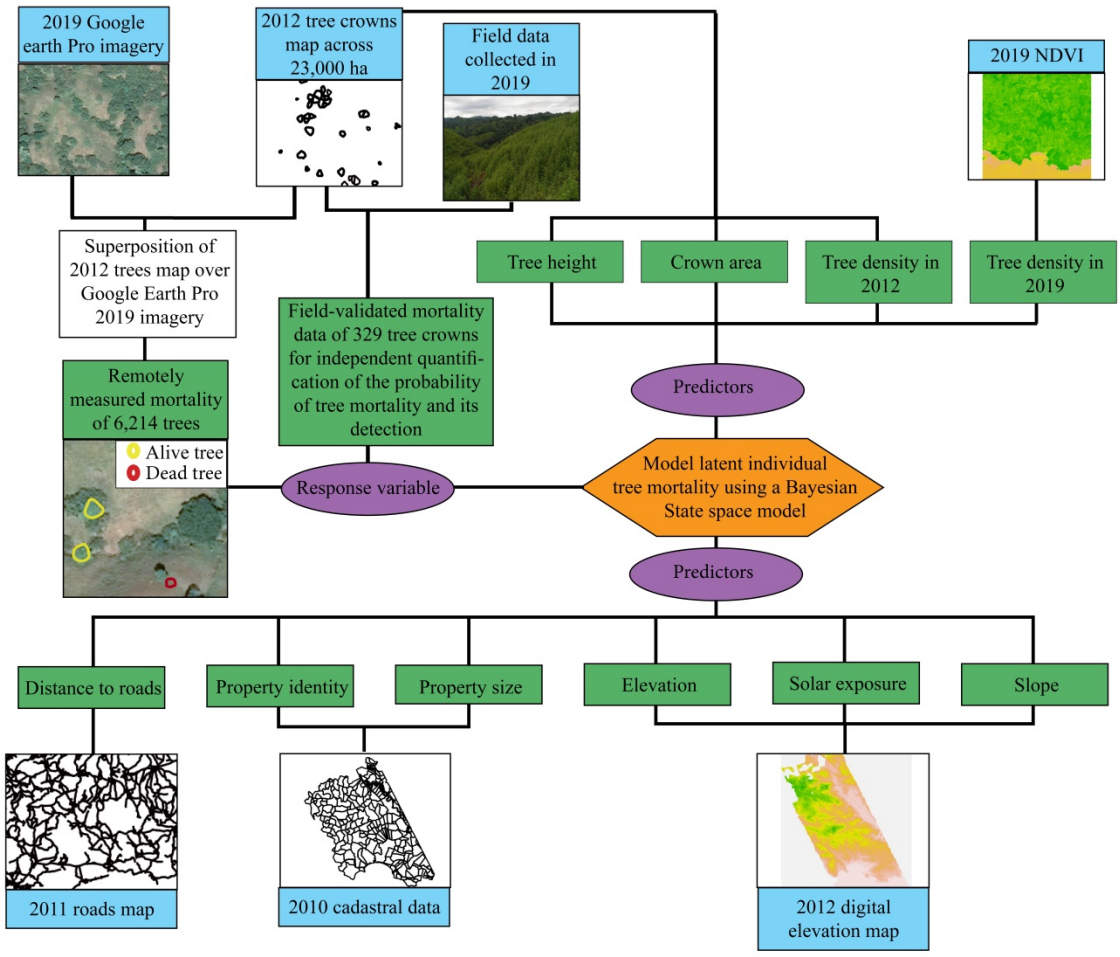

Figure 4.3 Workflow for developing the state-space model. Blue parallelograms indicate input data, green parallelograms indicate derived products, ellipses indicate the type of variable and hexagons indicate processes. 2019 Google Earth Pro: Google, Airbus, Maxar Technologies, 2012 tree crowns map: Graves et al. 2019, 2019 NDVI: Landsat imagery in Google Earth Engine, 2011 roads map: Smithsonian Tropical Research Institute and provided by the Fundación Pro Eco Azuero (Milton Solano 2011), 2010 cadastral data: Panama's National Authority for the Administration of Lands and provided by the Fundación Pro Eco Azuero from 2010, 2012 digital elevation map: Asner et al. 2012

We created a detection history for remotely sensed trees using zeroes and ones, in which we sampled each tree twice using two different methods (fieldwork measurement and remote sensing classification). We used zero when the tree was classified as dead and one when the tree was classified as alive. For example, a tree that was found to be alive in the field but dead on the remote sensing classification has a detection history of y=[1,0],

and a tree that was found to be alive in the field and in the remote sensing classification has a detection history of y=[1,1].

In our model, z_i represents the true state of the i^{th} tree (z_i=1 if the tree is alive and z_i=0 if the tree is dead). ψ is the probability of a tree being alive, and 1- ψ is the probability of a tree being dead. p_{11} is the probability of a tree being truly alive, and p_{10} is the probability of a tree being falsely alive. We can represent our model's probability in a diagram (Figure 3.4) given this data structure.

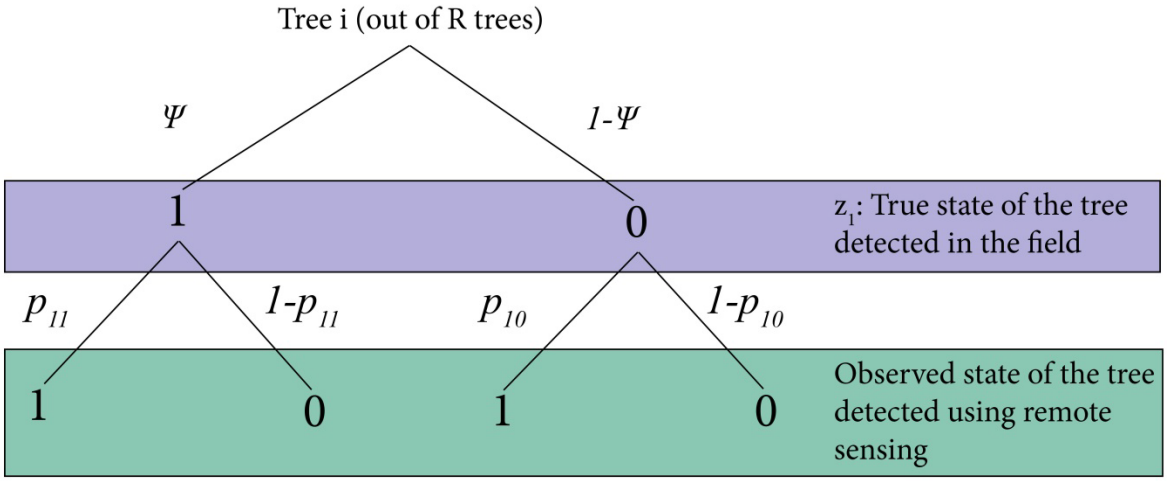

Figure 3.4 Tree diagram showing the different probabilities in our model. ψ = probability of a tree being alive, 1- ψ = probability of a tree being dead, p11 = probability of a tree being truly alive, 1- p11= probability of a tree being falsely dead, p10 = probability of a tree being falsely alive, 1-p10= probability of a tree being truly dead.

Assuming independence between the sampled trees and between sampling methods, we can write the likelihood of mortality, given the data following Royle and Link's capture-recapture equation (2006), including two detection levels (p_{10} and p_{11}; Equation 9).

$$L(p_{11}, p_{10}, \psi, |y)\alpha \prod_{i=1}^{R} \{[p_{11}^{y_i}(1-p_{11})^{T-y_i}]\psi + [p_{10}^{y_i}(1-p_{10})^{T-y_i}](1-\psi)\}$$

Equation 9

Where R is the number of classified trees, T is the survey, and y is the detection history. In our case, we did two surveys, one in the field and the other using remote sensing imagery.

The objective of this model is inference on drivers of tree mortality (z_i) in the landscape, so we included all the hypothesized variables in the mortality model. Predictor variables are tree height, crown size, solar exposure, elevation, tree density in 2012 within 30m, distance to roads, and property size as fixed effects and two random effect intercepts, one varying by species and the other varying by parcel. We evaluated the strength of the effects of the variables included in the model using the probability of direction (Dumandan et al. 2021). The probability of direction is derived from the parameters number of posterior samples greater or less than zero. For many statistical models, probability of direction has similar behavior to frequentist p-values. However, unlike a frequentist p-value, the probability of direction can be directly interpreted as the probability of positive or negative effects. We tested for correlation between tree height and tree crown area to ensure no interference between them in the model, and results showed no correlation (correlation= 0.175; 95% CI: 0.167 to 0.183). We modeled z, the true state, and the probability of detection following a Bernoulli distribution. The model structure is the following:

$z_i = Bernoulli(\psi)$

$$\psi = \beta_0 + \propto_{sp} + \propto_{prop} + \beta_1 \cdot height + \beta_2 \cdot crown\ area + \beta_3 \cdot site\ exposure + \beta_4 \cdot elevation + \beta_5 \cdot forest\ cover\ 2012 + \beta_7 \cdot distance\ to\ roads + \beta_8 \cdot parcel\ size$$

Equation 10

Where β are the fixed effect coefficients and α are the random effects coefficients. We conducted model selection to identify which variables best predicted the probability of detection. We used looic approximation from the package loo in R (Vehtari, Gabry, et al. 2020) for the model selection (Model selection information in Appendix C). The structure of the model is as follows:

$$(y_{it}|z_i) \sim Bernoulli(M)$$

Equation 11

Where $M = z_i p_{11} + (1-z_i) p_{10}$ for observational state using remote sensing of y=1 and, $M = z_i(1-p_{11}) + (1-z_i)(1-p_{10})$ for observational states using remote sensing of y=0 (Eq.12).

$$p_{11} = \beta_0 + \beta_1 \cdot crown\ area + \beta_2 \cdot tree\ density\ in\ 2019$$

$$p_{10} = \beta_0 + \beta_1 \cdot height + \beta_2 \cdot elevation + \beta_3 \cdot tree\ density\ in\ 2019$$

Equation 12

For all the trees within the 23,000 ha, we could not classify a total of 55,375 trees. We treated those trees as missing values for the response variable. The final step was estimating those values within the Hamiltonian Monte Carlo framework using a generative model (Nakagawa 2015). When a given observation is missing, we simulated it using the modeled detection and survival probability given the topography, socioeconomic factors, and tree characteristics. By simulating the missing observations, we allow the model to account for the uncertainty linked with having missing values

across the landscapes, and we ensure that our conclusions are valid across the landscape, including over the entire database of >60,000 mapped tree crowns (Kellner and Hubbell 2017; 2018; T. Trevor Caughlin et al. 2020).

Results

The repeat field census of tree status revealed that out of 329 trees measured in 2012, 56 had died in 2019. The classification using remote sensing revealed that, out of 6,214 trees, 567 had died in 2019. We validated the remote sensing classification using the 329 field-validated trees and found that 88.45% of trees were accurately classified while 11.55% of trees were misclassified (Table 3.1). The highest classification error was mistakenly classifying dead trees as alive, with an error rate of 37.5%.

Table 3.1 Confusion matrix showing the user accuracy and the producer accuracy of the classification using remote sensing. The data used for validations is the mortality data collected in the field.

		Field data		
		Alive	**Dead**	**User accuracy**
Remote sensing classification	**Alive**	256	21	92.41%
	Dead	17	35	32.69%
	Producer accuracy	93.77%	37.50%	88.45%

Mortality Model

Tree density had the strongest effect on mortality, with isolated trees having higher mortality than trees surrounded by other trees. Tree density had a negative effect ($P_{direction}(\theta_{1,\text{tree density}} \leq 0) = 0.97\%$) on tree mortality with a decrease of 0.21 (CI95%: 0.00

to 0.48) from a tree surrounded by 0% tree density in 2012 within a 30 m radius to a tree surrounded by 100% tree density in 2012 within 30 m radius. The second strongest driver of tree mortality was elevation, which was the only topographic variable that strongly affected mortality. Trees at higher elevations had a lower probability of mortality than trees at lower elevations. Elevation had a negative effect ($P_{direction}(\theta_{1,elevation} \leq 0) = 0.97\%$) on tree mortality with a decrease of 0.19 (CI95%: 0.00 to 0.41) from a tree located at 0m of elevation to a tree located at 370.84m of elevation. In contrast, solar exposure had almost no effect on tree mortality (Figure 3.5).

Trees further from roads had lower mortality than trees closer to the roads. Distance to roads had a negative effect ($P_{direction}(\theta_{1,distance\ to\ roads} \leq 0) = 0.94\%$) on tree mortality with a decrease of 0.12 (CI95%: -0.03 to 0.32) in the probability of mortality from a tree that is at 0 m from a road to a tree that is 1,653 m from a road. Larger properties had higher tree mortality than smaller properties. Property size had a positive effect ($P_{direction}(\theta_{1,property\ size} \leq 0) = 83\%$) on tree mortality with an increase of 0.11 (CI95%:-0.36 to 0.12) on the probability of tree mortality when we change from the smallest parcel (0.03 ha) to the largest parcel (309.31 ha) (Figure 3.5).

Individual tree size had weak and uncertain effects on tree mortality. Trees with bigger tree crowns had slightly lower mortality probability than trees with smaller tree crowns, including large amounts of uncertainty. Crown area had a slightly negative effect ($P_{direction}(\theta_{1,crown\ area} \leq 0) = 84\%$) with a decrease in tree mortality of 0.06 (CI95%: -0.06 to 0.20) from a tree with a tree crown area with a radius of 1.38m to a tree with a tree crown with a radius of 25m. Tree height had almost no effect on tree mortality. The difference

in the probability of mortality between a tree of 1m and 40m is near zero (CI95%:-0.08 to 0.09; Figure 3.5).

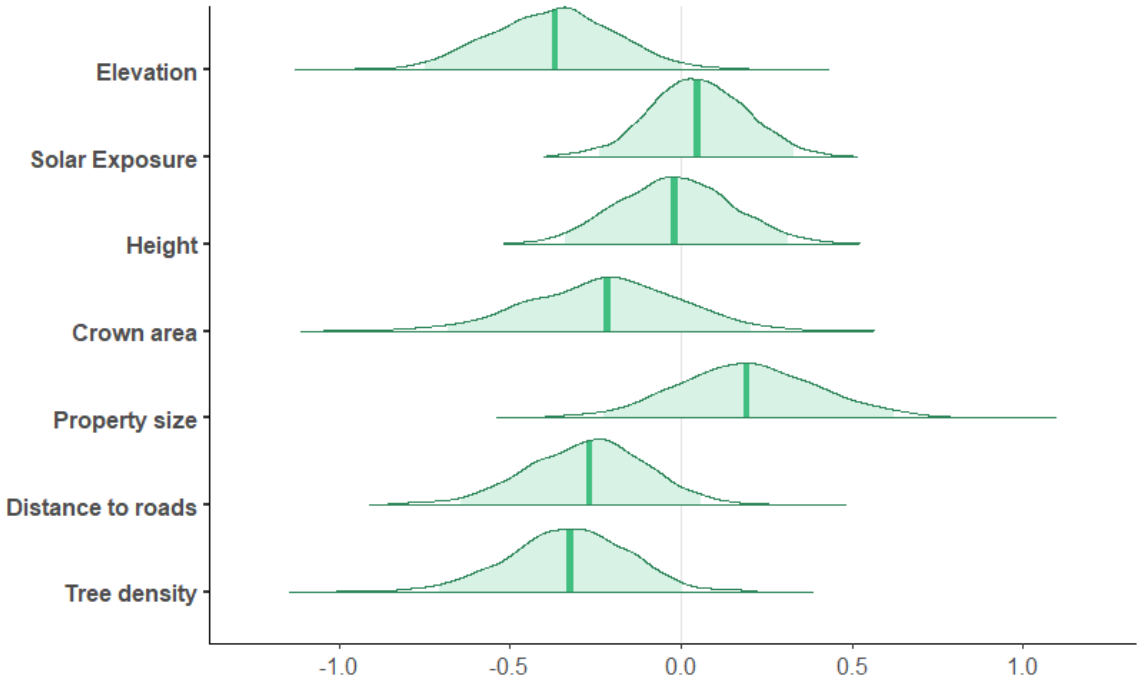

Figure 3.5 Posterior density distribution of the effect of all the variables included in the mortality model. The inner lines in the posterior distribution represent the 95%CI, and thicker lines in the posterior distribution represent the mean estimate for each parameter.

Probability of a Tree Being Truly Alive (p11)

Tree density in 2019 was the stronger predictor for the probability of a tree being truly alive, with a tree surrounded by low tree density in 2019 being more likely to be classified as alive when the tree is alive than a tree surrounded by high tree density in 2019. Tree density had a negative effect ($P_{direction}(\theta_{1,\text{tree density}} \leq 0) = 0.98\%$) on the probability of a tree being truly alive with a decrease of 0.10 (CI95%: 0.01 to 0.18) from a tree surrounded by 0% tree density in 2019 within a 30 m radius to a tree surrounded by

100% tree density in 2019 within 30 m radius. Crown area had weak and uncertain effects on the probability of a tree being truly alive (Figure 3.6).

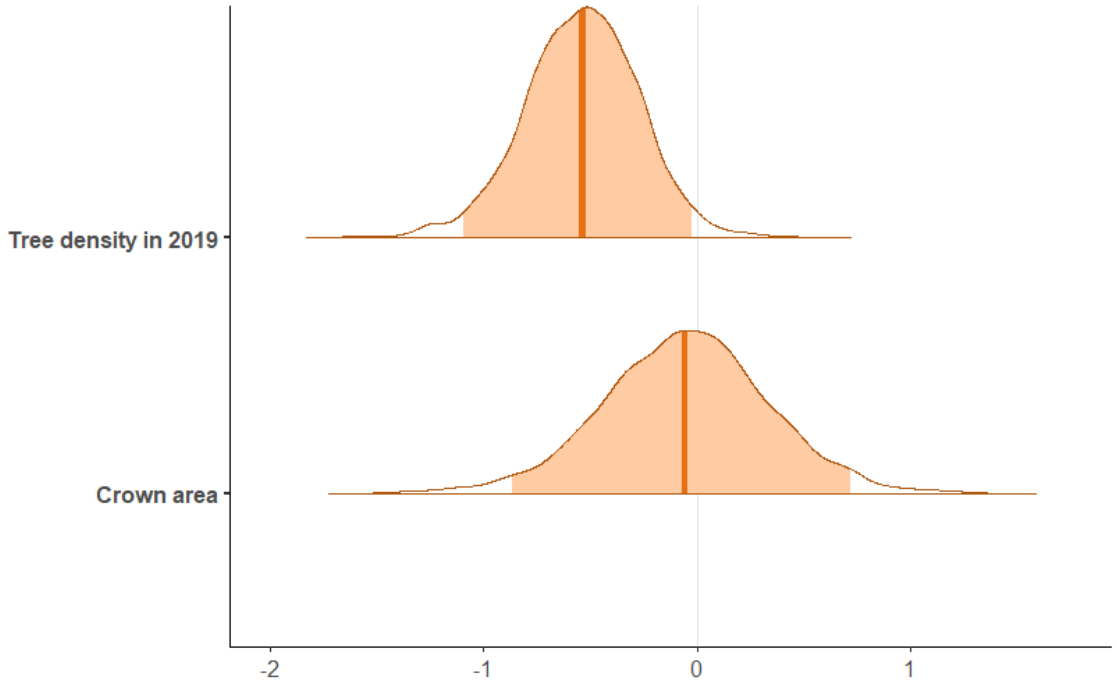

Figure 3.6 Posterior density distribution of the effect of all the variables included in the probability of a tree being truly alive (p11). The inner lines in the posterior distribution represent the 95%CI, and thicker lines in the posterior distribution represent the mean estimate for each parameter.

Probability of a Tree Being Falsely Alive (p10)

Trees surrounded by a high tree density in 2019 were more likely to be classified as dead when the tree is alive than a tree surrounded by a low tree density in 2019. Tree density had a positive effect ($P_{direction}(\theta_{1,tree\ density} \leq 0) = 0.94\%$) on the probability of a tree being falsely alive with an increase of 0.12 (CI95%: 0.00 to 0.28) from a tree surrounded by 0% tree density in 2019 within a 30 m radius to a tree surrounded by 100% tree density in 2019 within 30 m radius. Trees at higher elevations had a slightly higher probability of being detected as alive when the tree is dead than trees at lower elevations. Elevation had a slightly positive effect ($P_{direction}(\theta_{1,elevation} \leq 0) = 0.88\%$) on tree mortality

with an increase of 0.01 (CI95%: 0.00 to 0.03) from a tree located at 0m of elevation to a tree located at 370.84m of elevation. Tree height had almost no effect on tree mortality. The difference in the probability of mortality between a tree of 1m and 40m is near zero (CI95%:-0.02 to 0.01; Figure 3.7).

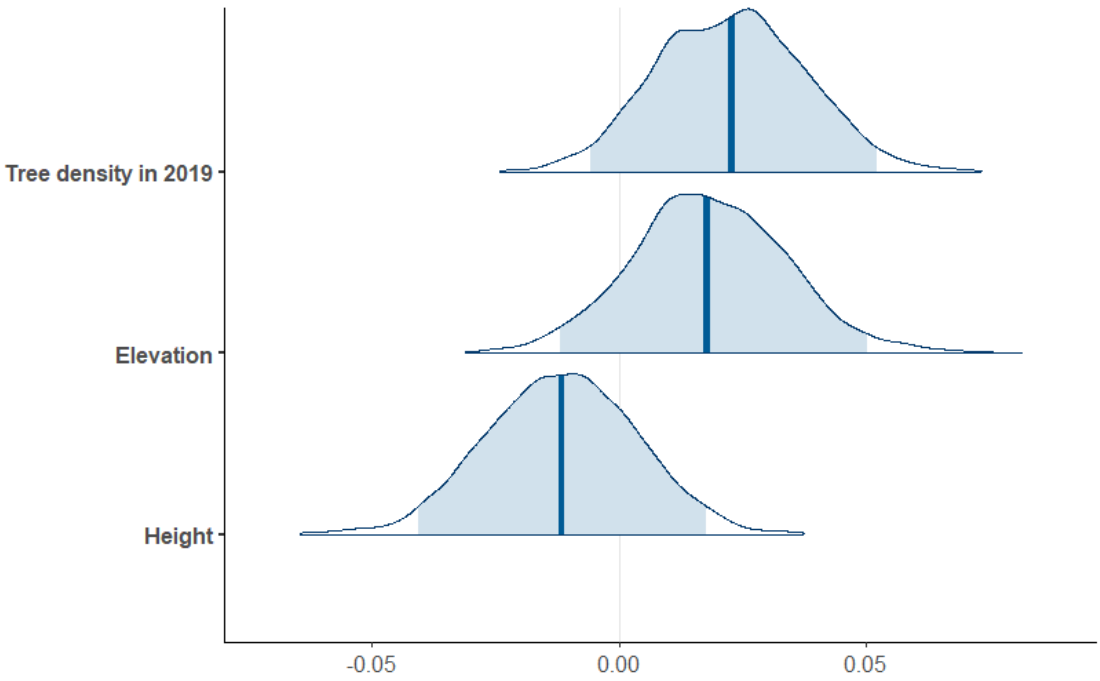

Figure 3.7 Posterior density distribution of the effect of all the variables included in the probability of a tree being falsely alive (p10). The inner lines in the posterior distribution represent the 95%CI, and thicker lines in the posterior distribution represent the mean estimate for each parameter.

Discussion

We analyzed tree mortality of 61,918 trees across 23,000 ha using field data and remote sensing imagery and modeled detection error to avoid parameter estimation bias related to the remote sensing classification. This study demonstrates the interplay between natural and human variables as drivers of tree mortality in an agricultural landscape. Proximity to roads, property size, tree isolation, and elevation showed the strongest effect on mortality from all of our variables. The mechanisms behind the effect

of these variables on mortality are likely to result from socio-ecological dynamics. The large scale of this study was essential to capturing the effects of socio-ecological dynamics on tree mortality. Novel methods in ecology that can leverage high-spatial resolution remote sensing data are likely to provide new insight into individual tree demography across scales.

We found that accessibility and socio-ecological factors associated with land-use transitions were important drivers of tree mortality in a tropical agricultural landscape. Trees closer to roads may have a higher mortality probability because they are easier to access for logging and transportation than trees further from roads (Southworth and Tucker 2001; Freitas, Hawbaker, and Metzger 2010). Another cause could be land development close to the roads, which has been observed in agricultural landscapes in Europe (Plieninger et al. 2015) and areas where the expansion of deforestation is limited to already deforested land in the tropics (Freitas, Hawbaker, and Metzger 2010). During the fieldwork, we observed a pattern in which infrastructure construction near the main road caused the death of several trees between 2012 and 2019. In this case, as in other tropical coastal areas, this resulted from the increased tourism in the area (Davenport and Davenport 2006; Potapov et al. 2017; Hoang et al. 2020). Another consequence of development could be the higher mortality of isolated trees that we observed in this study, which can occur due to the land-use change to increase profitability (Freitas, Hawbaker, and Metzger 2010; Plieninger 2012).

Our study also suggests a relationship between property size, which can indicate agricultural intensity and landowner wealth, and tree mortality. In our study region, landowners from small properties maintain a higher diversity of valuable trees that enable

them to diversify their sources of income (Garen et al. 2011; Assogbadjo et al. 2012; Metzel and Montagnini 2014; M. C. Valencia Mestre, Ferguson, and Vandermeer 2018). We found that trees on smaller properties are more likely to survive than trees on larger agricultural lands. In our study landscape, agricultural de-intensification is an ongoing process affecting smallholders that could increase tree loss. Strategies empowering smallholders to keep their land and manage it sustainably could be the key to avoiding the further loss of trees in this agricultural landscape (Camargo et al. 2005; Slusser, Calle, and Garen 2015a; Sales-Baptista and Ferraz-de-Oliveira 2021).

We expected to find a strong effect of tree size on tree mortality as there is extensive literature showing that tree size is an important driver of tree mortality (Laurance et al. 2000; Bennett et al. 2015; Nguyen et al. 2016; McDowell et al. 2018; Schwartz, Budsock, and Uriarte 2019; Gora and Esquivel-Muelbert 2021). A possible reason why we may not have detected an impact of tree crown area or tree height on mortality is the limited range of tree sizes in our sample. First, our study did not include smaller trees likely to die at higher rates than medium-to-large size trees. Second, the secondary forest and isolated trees in our study represent trees that may not have reached the critical heights where hydric failure and senescence begins to occur (Metcalf et al. 2009; Bennett et al. 2015; Zuidema 2000) or harvesting start to be profitable (Nguyen et al. 2016; Gora and Esquivel-Muelbert 2021). While smaller trees may never be detectable from remotely sensed data alone, novel methods to combine remote sensing and field data may provide insight into the full range of demographic transitions across tree size (Shriver et al. 2021; Barber et al. In review).

Trees at higher elevations are more likely to survive than trees at lower elevations. This agrees with other studies that found lower mortality rates at higher elevations; however, the biophysical mechanisms behind the higher mortality at lower elevations are still unknown (Wu et al. 2017). Other studies found increased mortality rates at higher elevations because of exposure to wind (Laurance and Curran 2008). We possibly did not find a positive effect of elevation on tree mortality because our area is an agricultural landscape where farmers' accessibility due to topography might be a stronger driver of mortality than wind. Flatter areas at low elevations are more attractive for cattle ranching and might suffer from a more intensive use than higher elevations (Camargo et al. 2005; Mon et al. 2012). Further research disentangling the mechanisms behind why lower elevations have higher mortality will require sampling at large scales to capture the heterogeneous interplay between natural and human variables on agricultural landscapes.

Collecting sufficient mortality data for this study was possible due to the use of remote sensing. Lidar and hyperspectral data allowed creating tree maps that provide ecological information in larger areas than what might be feasible with fieldwork (Hakkenberg, Peet, et al. 2018; Hakkenberg, Zhu, et al. 2018; Dalponte, Frizzera, and Gianelle 2019; Bin Zhang, Zhao, and Zhang 2020; Sankey et al. 2021). Although ecological data derived from this kind of remote sensing provides a great amount of ecological information, high-resolution hyperspectral and lidar remote sensing products are still limited in availability, particularly for the tropics (Tay, Erfmeier, and Kalwij 2018). Repeat lidar-hyperspectral flights across long time intervals are scarce, challenging the use of these data alone to quantify ecological processes that require multiple time intervals, including mortality and growth. This study presented an approach

using freely available imagery from Google Earth Pro to detect mortality of previously classified tree crowns from a single lidar and hyperspectral data collection.

A limitation of remotely measure tree mortality is the need to transfer uncertainty from the classification to the mortality model. We overcame this limitation by modeling imperfect detection. Models for imperfect detection are well-developed in the ecological literature, including capture-recapture models for wildlife (Karanth 1995; McCrea and Morgan 2014) directly transferable to tree crown measurements from the air. Another limitation of this study is that we could not differentiate between natural mortality and mortality caused by anthropogenic factors. This limited our capacity to interpret the underlying dynamics of mortality drivers in agricultural landscapes. For example, the increased mortality in isolated trees could be caused by a land-use change (Freitas, Hawbaker, and Metzger 2010; Plieninger 2012) or increased exposure to wind and drought (Williams-Linera 1990). Without the trees' death cause, we cannot discern between the anthropogenic factors and the ecological factors that influence isolated trees mortality. A solution for future research could be using airborne high-spatial resolution hyperspectral data to detect trees under stress (Zarco-Tejada et al. 2002; Meddens, Hicke, and Vierling 2011; Näsi et al. 2015) and senescent trees (Santos, Greenberg, and Ustin 2010) and assume that previously healthy trees mortality is anthropogenic and previously stressed or senescent trees mortality is ecological.

Altogether, high-resolution remote sensing data will be an increasingly powerful tool to inform the conservation of trees outside forests in agricultural landscapes. Our results point to the importance of high elevation sites as refugia for trees and suggest that accessibility, land-use change, and agricultural intensification may be driving tree

mortality. Policies and educational initiatives addressing agricultural intensification and land-use change have successfully reduced tree mortality if factors such as governability, incentives, and markets are considered (Calle et al. 2013; Alix-Garcia et al. 2018; Garrett et al. 2018; R. Fischer, Giessen, and Günter 2020). Policies and educational initiatives that target these anthropogenic factors considering the socio-economic context could reduce the mortality of agricultural trees and maintain the functionality and ecosystem services that trees provide.

REFERENCES

Adak, Alper, Seth C. Murray, Steven L. Anderson, Sorin C. Popescu, Lonesome Malambo, M. Cinta Romay, and Natalia de Leon. 2020. "Unoccupied Aerial Systems Discovered Overlooked Loci Capturing the Variation of Entire Growing Period in Maize." *The Plant Genome*, e20102. https://doi.org/10.1002/tpg2.20102.

Adler, Peter B., Stephen P. Ellner, and Jonathan M. Levine. 2010. "Coexistence of Perennial Plants: An Embarrassment of Niches." *Ecology Letters* 13 (June): 1019–29. https://doi.org/10.1111/j.1461-0248.2010.01496.x.

Alix-Garcia, Jennifer, Lisa L. Rausch, Jessica L'Roe, Holly K. Gibbs, and Jacob Munger. 2018. "Avoided Deforestation Linked to Environmental Registration of Properties in the Brazilian Amazon." *Conservation Letters* 11 (3): e12414. https://doi.org/10.1111/conl.12414.

Angelo, Sammya A. D', Ana C. S. Andrade, Susan G. Laurance, William F. Laurance, and Rita C. G. Mesquita. 2004. "Inferred Causes of Tree Mortality in Fragmented and Intact Amazonian Forests." *Journal of Tropical Ecology* 20 (2): 243–46. https://doi.org/10.1017/S0266467403001032.

Arellano, Gabriel, Daniel Zuleta, and Stuart J. Davies. 2021. "Tree Death and Damage: A Standardized Protocol for Frequent Surveys in Tropical Forests." *Journal of Vegetation Science* 32 (1): e12981. https://doi.org/10.1111/jvs.12981.

Asner, Gregory P., David E. Knapp, Joseph Boardman, Robert O. Green, Ty Kennedy-Bowdoin, Michael Eastwood, Roberta E. Martin, Christopher Anderson, and Christopher B. Field. 2012. "Carnegie Airborne Observatory-2: Increasing Science Data Dimensionality via High-Fidelity Multi-Sensor Fusion." *Remote Sensing of Environment* 124: 454–65.

Assogbadjo, A. E., R. Glèlè Kakaï, F. G. Vodouhê, C. A. M. S. Djagoun, J. T. C. Codjia, and B. Sinsin. 2012. "Biodiversity and Socioeconomic Factors Supporting Farmers' Choice of Wild Edible Trees in the Agroforestry Systems of Benin (West Africa)." *Forest Policy and Economics* 14 (1): 41–49. https://doi.org/10.1016/j.forpol.2011.07.013.

Balice, R., J. D. Miller, B. Oswald, C. Edminster, and S. Yool. 2000. "Forest Surveys and Wildfire Assessment in the Los Alamos Region; 1998-1999." Los Alamos National Laboratory. /paper/Forest-surveys-and-wildfire-assessment-in-the-Los-Balice-Miller/ef0144218ed7ba5723623cc2fc6b8d84e2fa279a.

Barber, Cristina, Sarah J. Graves, Jefferson S. Hall, Pieter A. Zuidema, Jodi Brandt, Stephanie A. Bohlman, Gregory P. Asner, Mario Bailón, and T. Trevor Caughlin. In review. "Scaling up Predictions of Tree Species Recruitment in a Tropical Landscape."

Barona, Elizabeth, Navin Ramankutty, Glenn Hyman, and Oliver T Coomes. 2010. "The Role of Pasture and Soybean in Deforestation of the Brazilian Amazon." *Environmental Research Letters* 5 (2): 024002. https://doi.org/10.1088/1748-9326/5/2/024002.

Bates, Douglas, Martin Mächler, Benjamin M. Bolker, and Steven C. Walker. 2015. "Fitting Linear Mixed-Effects Models Using Lme4." *Journal of Statistical Software* 67 (1). https://doi.org/10.18637/jss.v067.i01.

Bennett, Amy C., Nathan G. McDowell, Craig D. Allen, and Kristina J. Anderson-Teixeira. 2015. "Larger Trees Suffer Most during Drought in Forests Worldwide." *Nature Plants* 1 (10): 15139. https://doi.org/10.1038/nplants.2015.139.

Betancourt, M. J., and Mark Girolami. 2013. "Hamiltonian Monte Carlo for Hierarchical Models." https://doi.org/10.1201/b18502-5.

Binkley, Dan, Otavio Camargo Campoe, Martin Gspaltl, and David I. Forrester. 2013. "Light Absorption and Use Efficiency in Forests: Why Patterns Differ for Trees and Stands." *Forest Ecology and Management*, Light interception and growth of trees and stands, 288 (January): 5–13. https://doi.org/10.1016/j.foreco.2011.11.002.

Bolker, Ben. 2008. *Ecological Models and Data in R*. Princeton University Press. https://www.google.com/search?q=ben+bolker+ecological+models+and+data+in+r&oq=ben+bolker+e&aqs=chrome.1.69i57j0l3.13119j0j4&sourceid=chrome&ie=UTF-8.

Bonal, Damien, Benoit Burban, Clément Stahl, Fabien Wagner, and Bruno Hérault. 2016. "The Response of Tropical Rainforests to Drought—Lessons from Recent Research and Future Prospects." *Annals of Forest Science* 73 (1): 27–44. https://doi.org/10.1007/s13595-015-0522-5.

Boudreau, S., M. J. Lawes, S. E. Piper, and L. J. Phadima. 2005. "Subsistence Harvesting of Pole-Size Understorey Species from Ongoye Forest Reserve, South Africa: Species Preference, Harvest Intensity, and Social Correlates." *Forest Ecology and Management* 216 (1): 149–65. https://doi.org/10.1016/j.foreco.2005.05.029.

Boyce, Mark S, Pierre R Vernier, Scott E Nielsen, and Fiona K.A Schmiegelow. 2002. "Evaluating Resource Selection Functions." *Ecological Modelling* 157 (2–3): 281–300. https://doi.org/10.1016/S0304-3800(02)00200-4.

Bradford, John B., and David M. Bell. 2017. "A Window of Opportunity for Climate-Change Adaptation: Easing Tree Mortality by Reducing Forest Basal Area." *Frontiers in Ecology and the Environment* 15 (1): 11–17. https://doi.org/10.1002/fee.1445.

Brandt, Jodi S., Teri Allendorf, Volker Radeloff, and Jeremy Brooks. 2017. "Effects of National Forest-management Regimes on Unprotected Forests of the Himalaya." *Conservation Biology* 31 (6): 1271–82. https://doi.org/10.1111/cobi.12927.

Brandt, Jodi S., Volker Radeloff, Teri Allendorf, Van Butsic, and Anand Roopsind. 2019. "Effects of Ecotourism on Forest Loss in the Himalayan Biodiversity Hotspot Based on Counterfactual Analyses." *Conservation Biology* 33 (6): 1318–28. https://doi.org/10.1111/cobi.13341.

Breece, C. R., T. E. Kolb, B. G. Dickson, J. D. McMillin, and K. M. Clancy. 2008. "Prescribed Fire Effects on Bark Beetle Activity and Tree Mortality in Southwestern Ponderosa Pine Forests." *Forest Ecology and Management* 255 (1): 119–28. https://doi.org/10.1016/j.foreco.2007.08.026.

Breugel, Michiel van, Dylan Craven, Hao Ran Lai, Mario Baillon, Benjamin L. Turner, and Jefferson S. Hall. 2019. "Soil Nutrients and Dispersal Limitation Shape Compositional Variation in Secondary Tropical Forests across Multiple Scales." *Journal of Ecology* 107 (2): 566–81. https://doi.org/10.1111/1365-2745.13126.

Broms, Kristin M., Mevin B. Hooten, and Ryan M. Fitzpatrick. 2016. "Model Selection and Assessment for Multi-Species Occupancy Models." *Ecology* 97 (7): 1759–70. https://doi.org/10.1890/15-1471.1.

Brown, C.G., K. Sarabandi, and L.E. Pierce. 2005. "Validation of the Shuttle Radar Topography Mission Height Data." *IEEE Transactions on Geoscience and Remote Sensing* 43 (8): 1707–15. https://doi.org/10.1109/TGRS.2005.851789.

Brudvig, Lars A., Nash E. Turley, Savannah L. Bartel, Lukas Bell-Dereske, Sabrie Breland, Ellen I. Damschen, Sarah E. Evans, et al. 2021. "Large Ecosystem-Scale Effects of Restoration Fail to Mitigate Impacts of Land-Use Legacies in Longleaf Pine Savannas." *Proceedings of the National Academy of Sciences* 118 (17): e2020935118. https://doi.org/10.1073/pnas.2020935118.

Buchs, David M., Richard J. Arculus, Peter O. Baumgartner, Claudia Baumgartner-Mora, and Alexey Ulianov. 2010. "Late Cretaceous Arc Development on the SW Margin of the Caribbean Plate: Insights from the Golfito, Costa Rica, and Azuero, Panama, Complexes." *Geochemistry, Geophysics, Geosystems* 11 (7). https://doi.org/10.1029/2009GC002901.

Buckley, Yvonne M., Hariet L. Hinz, Diethart Matthies, and Mark Rees. 2001. "Interactions between Density-Dependent Processes, Population Dynamics and Control of an Invasive Plant Species, Tripleurospermum Perforatum (Scentless Chamomile)." *Ecology Letters* 4 (6): 551–58. https://doi.org/10.1046/j.1461-0248.2001.00264.x.

Bürkner, Paul-Christian. 2017. "Brms: An R Package for Bayesian Multilevel Models Using Stan." *Journal of Statistical Software* 80 (1): 1–28. https://doi.org/10.18637/jss.v080.i01.

Busck, Anne Gravsholt. 2002. "Farmers' Landscape Decisions: Relationships between Farmers' Values and Landscape Practices." *Sociologia Ruralis* 42 (3): 233–49. https://doi.org/10.1111/1467-9523.00213.

Calle, Zoraida, Enrique Murgueitio, Julián Chará, Carlos Hernando Molina, Andrés Felipe Zuluaga, and Alicia Calle. 2013. "A Strategy for Scaling-Up Intensive Silvopastoral Systems in Colombia." *Journal of Sustainable Forestry* 32 (7): 677–93. https://doi.org/10.1080/10549811.2013.817338.

Camargo, Juan, Alexander Feijoo, maria Constanza Zuñiga, Harold Cardona, and Jh Gaviria. 2005. "Silvopastoral Systems with Isolated Timber Trees within Pastures in the Coffee Region of Colombia." *Livestock Research for Rural Development* 17 (January).

Campbell, Michael J., Philip E. Dennison, Jesse W. Tune, Steven A. Kannenberg, Kelly L. Kerr, Brian F. Codding, and William R. L. Anderegg. 2020. "A Multi-Sensor, Multi-Scale Approach to Mapping Tree Mortality in Woodland Ecosystems." *Remote Sensing of Environment* 245 (August): 111853. https://doi.org/10.1016/j.rse.2020.111853.

Canham, Charles D., and María Uriarte. 2006. "Analysis Of Neighborhood Dynamics Of Forest Ecosystems Using Likelihood Methods And Modeling." *Ecological Applications* 16 (1): 62–73. https://doi.org/10.1890/04-0657.

Casas, F., and J. Viñuela. 2010. “Agricultural Practices or Game Management: Which Is the Key to Improve Red-Legged Partridge Nesting Success in Agricultural Landscapes?” *Environmental Conservation* 37 (2): 177–86. https://doi.org/10.1017/S0376892910000299.

Caughlin, T. T., J. M. Ferguson, J. W. Lichstein, P. A. Zuidema, S. Bunyavejchewin, and D. J. Levey. 2015. “Loss of Animal Seed Dispersal Increases Extinction Risk in a Tropical Tree Species Due to Pervasive Negative Density Dependence across Life Stages.” *Proceedings of the Royal Society B: Biological Sciences* 282 (1798): 20142095. https://doi.org/10.1098/rspb.2014.2095.

Caughlin, T. T., S. J. Graves, G. P. Asner, M. van Breugel, Jefferson S. Hall, R. E. Martin, M. S. Ashton, and S. A. Bohlman. 2016. “A Hyperspectral Image Can Predict Tropical Tree Growth Rates in Single-Species Stands.” *Ecological Applications* 26 (8): 2367–73.

Caughlin, T. Trevor, Cristina Barber Alvarez-Buylla, Gregory P. Asner, Nancy F. Glenn, Stephanie A. Bohlman, and Chris H. Wilson. 2020. “Monitoring Tropical Forest Succession at Landscape Scales despite Uncertainty in Landsat Time Series.” *Ecological Applications* 31 (1). https://doi.org/10.1002/eap.2208.

Caughlin, T. Trevor, Sarah J. Graves, Gregory P. Asner, Bryan C. Tarbox, and Stephanie A. Bohlman. 2019. “High-Resolution Remote Sensing Data as a Boundary Object to Facilitate Interdisciplinary Collaboration.” In *Collaboration Across Boundaries for Social-Ecological Systems Science*, edited by Stephen G. Perz, 295–326. Springer International Publishing. https://doi.org/10.1007/978-3-030-13827-1_9.

Caughlin, T. Trevor, Marinés de la Peña-Domene, and Cristina Martínez-Garza. 2019. “Demographic Costs and Benefits of Natural Regeneration during Tropical Forest Restoration.” *Ecology Letters* 22 (1): 34–44. https://doi.org/10.1111/ele.13165.

Caughlin, T. Trevor, Sami W. Rifai, Sarah J. Graves, Gregory P. Asner, and Stephanie A. Bohlman. 2016. "Integrating LiDAR-Derived Tree Height and Landsat Satellite Reflectance to Estimate Forest Regrowth in a Tropical Agricultural Landscape." Edited by Harini Nagendra and Lola Fatoyinbo. *Remote Sensing in Ecology and Conservation* 2 (4): 190–203. https://doi.org/10.1002/rse2.33.

Caughlin, Trevor T., Jessica H. Wheeler, Jill Jankowski, and Jeremy W. Lichstein. 2012. "Urbanized Landscapes Favored by Fig-Eating Birds Increase Invasive but Not Native Juvenile Strangler Fig Abundance." *Ecology* 93 (7): 1571–80. https://doi.org/10.1890/11-1694.1.

Cescatti, A., and E. Piutti. 1998. "Silvicultural Alternatives, Competition Regime and Sensitivity to Climate in a European Beech Forest." *Forest Ecology and Management* 102 (2): 213–23. https://doi.org/10.1016/S0378-1127(97)00163-1.

Chadid, Maria Alejandra, Liliana M. Dávalos, Jorge Molina, and Dolors Armenteras. 2015. "A Bayesian Spatial Model Highlights Distinct Dynamics in Deforestation from Coca and Pastures in an Andean Biodiversity Hotspot." *Forests* 6 (11): 3828–46. https://doi.org/10.3390/f6113828.

Chalauri, Giga, Vakhtang Laluashvili, and Koba Gelashvili. 2018. "Jagged Non-Zero Submatrix Data Structure." *Transactions of A. Razmadze Mathematical Institute* 172 (1): 7–14. https://doi.org/10.1016/j.trmi.2017.10.002.

Chambert, Thierry, David A. W. Miller, and James D. Nichols. 2015. "Modeling False Positive Detections in Species Occurrence Data under Different Study Designs." *Ecology* 96 (2): 332–39. https://doi.org/10.1890/14-1507.1.

Chazdon, R. L., and M. R. Guariguata. 2018. "Decision Support Tools for Forest Landscape Restoration: Current Status and Future Outlook." Ocasional paper 183. Bogor, Indonesia: CIFOR. https://www.cifor.org/knowledge/publication/6792/.

Chazdon, Robin L., and Manuel R. Guariguata. 2016. "Natural Regeneration as a Tool for Large-Scale Forest Restoration in the Tropics: Prospects and Challenges." *Biotropica* 48 (6): 716–30. https://doi.org/10.1111/btp.12381.

Chazdon, Robin L., and María Uriarte. 2016. “Natural Regeneration in the Context of Large-Scale Forest and Landscape Restoration in the Tropics.” *Biotropica* 48 (6): 709–15. https://doi.org/10.1111/btp.12409.

Cho, Moses Azong, Renaud Mathieu, Gregory P. Asner, Laven Naidoo, Jan van Aardt, Abel Ramoelo, Pravesh Debba, et al. 2012. “Mapping Tree Species Composition in South African Savannas Using an Integrated Airborne Spectral and LiDAR System.” *Remote Sensing of Environment* 125 (October): 214–26. https://doi.org/10.1016/j.rse.2012.07.010.

Comita, Liza S., Helene C. Muller-Landau, Salomón Aguilar, and Stephen P. Hubbell. 2010. “Asymmetric Density Dependence Shapes Species Abundances in a Tropical Tree Community.” *Science* 329 (5989): 330–32. https://doi.org/10.1126/science.1190772.

Comita, Liza S., and Simon M. Stump. 2020. “Natural Enemies and the Maintenance of Tropical Tree Diversity: Recent Insights and Implications for the Future of Biodiversity in a Changing World1.” *Annals of the Missouri Botanical Garden* 105 (3): 377–92.

Cook-Patton, Susan C., Sara M. Leavitt, David Gibbs, Nancy L. Harris, Kristine Lister, Kristina J. Anderson-Teixeira, Russell D. Briggs, et al. 2020. “Mapping Carbon Accumulation Potential from Global Natural Forest Regrowth.” *Nature* 585 (7826): 545–50. https://doi.org/10.1038/s41586-020-2686-x.

Cramer, Viki A., Richard J. Hobbs, and Rachel J. Standish. 2008. “What’s New about Old Fields? Land Abandonment and Ecosystem Assembly.” *Trends in Ecology & Evolution* 23 (2): 104–12. https://doi.org/10.1016/j.tree.2007.10.005.

Crk, Tanja, María Uriarte, Fabio Corsi, and Dan Flynn. 2009. “Forest Recovery in a Tropical Landscape: What Is the Relative Importance of Biophysical, Socioeconomic, and Landscape Variables?” *Landscape Ecology* 24 (5): 629–42. https://doi.org/10.1007/s10980-009-9338-8.

Crouzeilles, Renato, and Michael Curran. 2016. “Which Landscape Size Best Predicts the Influence of Forest Cover on Restoration Success? A Global Meta-Analysis on the Scale of Effect.” *Journal of Applied Ecology* 53 (2): 440–48. https://doi.org/10.1111/1365-2664.12590.

Dahlgren, Johan P. 2011. “Nonlinear Relationships between Vital Rates and State Variables in Demographic Models” 92 (5): 7.

Dalponte, Michele, and David A. Coomes. 2016. “Tree-Centric Mapping of Forest Carbon Density from Airborne Laser Scanning and Hyperspectral Data.” *Methods in Ecology and Evolution* 7 (10): 1236–45. https://doi.org/10.1111/2041-210X.12575.

Dalponte, Michele, Lorenzo Frizzera, and Damiano Gianelle. 2019. “Individual Tree Crown Delineation and Tree Species Classification with Hyperspectral and LiDAR Data.” *PeerJ* 6 (January). https://doi.org/10.7717/peerj.6227.

Davenport, John, and Julia L. Davenport. 2006. “The Impact of Tourism and Personal Leisure Transport on Coastal Environments: A Review.” *Estuarine, Coastal and Shelf Science* 67 (1): 280–92. https://doi.org/10.1016/j.ecss.2005.11.026.

Deangelis, Donald, Louis Gross, Wilfried Wolff, D. Fleming, M. Nott, and E. Comiskey. 2020. “Individual-Based Models on the Landscape: Applications to the Everglades.” In , 199–211. https://doi.org/10.1201/9780429148996-16.

Degen, B., L. Blanc, H. Caron, L. Maggia, A. Kremer, and S. Gourlet-Fleury. 2006. “Impact of Selective Logging on Genetic Composition and Demographic Structure of Four Tropical Tree Species.” *Biological Conservation* 131 (3): 386–401. https://doi.org/10.1016/j.biocon.2006.02.014.

Dokmanic, Ivan, Reza Parhizkar, Juri Ranieri, and Martin Vetterli. 2015. “Euclidean Distance Matrices: Essential Theory, Algorithms and Applications.” *IEEE Signal Processing Magazine* 32 (6): 12–30. https://doi.org/10.1109/MSP.2015.2398954.

Dumandan, Patricia Kaye T., Keith L. Bildstein, Laurie J. Goodrich, Andrii Zaiats, T. Trevor Caughlin, and Todd E. Katzner. 2021. "Shared Functional Traits Explain Synchronous Changes in Long-Term Count Trends of Migratory Raptors." *Global Ecology and Biogeography* 30 (3): 640–50. https://doi.org/10.1111/geb.13242.

Duncan, R Scot, and Virginia E Duncan. 2000. "Forest Succession and Distance from Forest Edge in an Afro-Tropical Grassland." *Biotropica* 32 (1): 33–41.

Durán, Sandra M., Roberta E. Martin, Sandra Díaz, Brian S. Maitner, Yadvinder Malhi, Norma Salinas, Alexander Shenkin, et al. 2019. "Informing Trait-Based Ecology by Assessing Remotely Sensed Functional Diversity across a Broad Tropical Temperature Gradient." *Science Advances* 5 (12): eaaw8114. https://doi.org/10.1126/sciadv.aaw8114.

Eitzel, M. V., J. Battles, R. York, and P. de Valpine. 2015. "Can't See the Trees for the Forest: Complex Factors Influence Tree Survival in a Temperate Second Growth Forest." *Ecosphere* 6 (11): art247. https://doi.org/10.1890/ES15-00105.1.

Elliott, Stephen, David Blakesley, and Kate Hardwick. 2013. *Restoring Tropical Forests: A Practical Guide*. Royal Botanic Gardens.

Esquivel, M. Jimena, Celia A. Harvey, Bryan Finegan, Fernando Casanoves, and Christina Skarpe. 2008. "Effects of Pasture Management on the Natural Regeneration of Neotropical Trees." *Journal of Applied Ecology* 45 (1): 371–80. https://doi.org/10.1111/j.1365-2664.2007.01411.x.

Esquivel, María Jimena, and Zoraida Calle Díaz. 2002. "Arboles Aislados En Potreros Como Catalizadores de La Sucesión En La Cordillera Occidental Colombiana." *Agroforestería En Las Américas* 9 (33–34): 43–47.

Esteban, Erick J. L., Carolina V. Castilho, Karina L. Melgaço, and Flávia R. C. Costa. 2021. "The Other Side of Droughts: Wet Extremes and Topography as Buffers of Negative Drought Effects in an Amazonian Forest." *New Phytologist* 229 (4): 1995–2006. https://doi.org/10.1111/nph.17005.

Fischer, Fabian Jörg, Isabelle Maréchaux, and Jérôme Chave. 2019. "Improving Plant Allometry by Fusing Forest Models and Remote Sensing." *New Phytologist* 223 (3): 1159–65. https://doi.org/10.1111/nph.15810.

Fischer, Richard, Lukas Giessen, and Sven Günter. 2020. "Governance Effects on Deforestation in the Tropics: A Review of the Evidence." *Environmental Science & Policy* 105 (March): 84–101. https://doi.org/10.1016/j.envsci.2019.12.007.

Freitas, Simone R., Todd J. Hawbaker, and Jean Paul Metzger. 2010. "Effects of Roads, Topography, and Land Use on Forest Cover Dynamics in the Brazilian Atlantic Forest." *Forest Ecology and Management* 259 (3): 410–17. https://doi.org/10.1016/j.foreco.2009.10.036.

Gardner, Toby A., Jos Barlow, Robin Chazdon, Robert M. Ewers, Celia A. Harvey, Carlos A. Peres, and Navjot S. Sodhi. 2009. "Prospects for Tropical Forest Biodiversity in a Human-Modified World." *Ecology Letters* 12 (6): 561–82. https://doi.org/10.1111/j.1461-0248.2009.01294.x.

Garen, Eva J., Kristin Saltonstall, Mark S. Ashton, Jacob L. Slusser, Shane Mathias, and Jefferson S. Hall. 2011. "The Tree Planting and Protecting Culture of Cattle Ranchers and Small-Scale Agriculturalists in Rural Panama: Opportunities for Reforestation and Land Restoration." *Forest Ecology and Management* 261 (10): 1684–95. https://doi.org/10.1016/j.foreco.2010.10.011.

Garen, Eva J., Kristin Saltonstall, Jacob L. Slusser, Shane Mathias, Mark S. Ashton, and Jefferson S. Hall. 2009. "An Evaluation of Farmers' Experiences Planting Native Trees in Rural Panama: Implications for Reforestation with Native Species in Agricultural Landscapes." *Agroforestry Systems* 76 (1): 219–36. https://doi.org/10.1007/s10457-009-9203-4.

Garrett, R. D., I. Koh, E. F. Lambin, Y. le Polain de Waroux, J. H. Kastens, and J. C. Brown. 2018. "Intensification in Agriculture-Forest Frontiers: Land Use Responses to Development and Conservation Policies in Brazil." *Global Environmental Change* 53 (November): 233–43. https://doi.org/10.1016/j.gloenvcha.2018.09.011.

Geist, Helmut J., and Eric F. Lambin. 2001. “What Drives Tropical Deforestation.” *LUCC Report Series* 4: 116.

Gelman, Andrew. 2008. “Scaling Regression Inputs by Dividing by Two Standard Deviations.” *Statistics in Medicine* 27 (15): 2865–73.

Gelman, Andrew, and Christian Hennig. 2017. “Beyond Subjective and Objective in Statistics.” *Journal of the Royal Statistical Society: Series A (Statistics in Society)* 180 (4): 967–1033. https://doi.org/10.1111/rssa.12276.

Gelman, Andrew, Aki Vehtari, Daniel Simpson, Charles C. Margossian, Bob Carpenter, Yuling Yao, Lauren Kennedy, Jonah Gabry, Paul-Christian Bürkner, and Martin Modrák. 2020. “Bayesian Workflow.” *ArXiv:2011.01808*, November. http://arxiv.org/abs/2011.01808.

Gibbons, P., D. B. Lindenmayer, J. Fischer, A. D. Manning, A. Weinberg, J. Seddon, P. Ryan, and G. Barrett. 2008. “The Future of Scattered Trees in Agricultural Landscapes.” *Conservation Biology* 22 (5): 1309–19. https://doi.org/10.1111/j.1523-1739.2008.00997.x.

Gibbons, Philip, and Miles Boak. 2000. “The Importance of Paddock Trees for Regional Conservation in Agricultural Landscapes.” *Queanbeyan: NSW National Parks and Wildlife Service*.

Gillerot, Loïc, David I. Forrester, Alessandra Bottero, Andreas Rigling, and Mathieu Lévesque. 2021. “Tree Neighbourhood Diversity Has Negligible Effects on Drought Resilience of European Beech, Silver Fir and Norway Spruce.” *Ecosystems* 24 (1): 20–36. https://doi.org/10.1007/s10021-020-00501-y.

Goldberg, Deborah E., Roy Turkington, Linda Olsvig-Whittaker, and Andrew R. Dyer. 2001. “Density Dependence in an Annual Plant Community: Variation Among Life History Stages.” *Ecological Monographs* 71 (3): 423–46. https://doi.org/10.1890/0012-9615(2001)071[0423:DDIAAP]2.0.CO;2.

Gómez-Aparicio, Lorena. 2009. "The Role of Plant Interactions in the Restoration of Degraded Ecosystems: A Meta-Analysis across Life-Forms and Ecosystems." *Journal of Ecology* 97 (6): 1202–14. https://doi.org/10.1111/j.1365-2745.2009.01573.x.

Gora, Evan M., and Adriane Esquivel-Muelbert. 2021. "Implications of Size-Dependent Tree Mortality for Tropical Forest Carbon Dynamics." *Nature Plants* 7 (4): 384–91. https://doi.org/10.1038/s41477-021-00879-0.

Gorinova, Maria I, Dave Moore, and Matthew D Hoffman. 2020. "Automatic Reparameterisation of Probabilistic Programs," 10.

Gössling, Stefan. 2002. "Global Environmental Consequences of Tourism." *Global Environmental Change* 12 (4): 283–302. https://doi.org/10.1016/S0959-3780(02)00044-4.

Grau, H. Ricardo, and Mitchell Aide. 2008. "Globalization and Land-Use Transitions in Latin America." *Ecology and Society* 13 (2). https://www.jstor.org/stable/26267952.

Graves, S.J., G.P. Asner, R.E. Martin, C.B. Anderson, M. S. Colgan, L. Kalantari, and S.A. Bohlman. 2016. "Tree Species Abundance Predictions in a Tropical Agricultural Landscape with a Supervised Classification Model and Imbalanced Data." *Remote Sensing* 8 (2): 161. https://doi.org/10.3390/rs8020161.

Griscom, H. P., and M.S. Ashton. 2011. "Restoration of Dry Tropical Forests in Central America: A Review of Pattern and Process." *Forest Ecology and Management*, The Ecology and Ecosystem Services of Native Trees: Implications for Reforestation and Land Restoration in Mesoamerica, 261 (10): 1564–79. https://doi.org/10.1016/j.foreco.2010.08.027.

Griscom, Heather P., Bronson W. Griscom, and Mark S. Ashton. 2009. "Forest Regeneration from Pasture in the Dry Tropics of Panama: Effects of Cattle, Exotic Grass, and Forested Riparia." *Restoration Ecology* 17 (1): 117–26. https://doi.org/10.1111/j.1526-100X.2007.00342.x.

Griscom, H.P., A. M. Connelly, Mark S. Ashton, M Wishnie, and J Deago. 2011. "The Structure and Composition of a Tropical Dry Forest Landscape After Land Clearance; Azuero Peninsula, Panama." *Journal of Sustainable Forestry* 30 (8): 756–74. https://doi.org/10.1080/10549811.2011.571589.

Guarín, Alejandro, and Alan H. Taylor. 2005. "Drought Triggered Tree Mortality in Mixed Conifer Forests in Yosemite National Park, California, USA." *Forest Ecology and Management* 218 (1): 229–44. https://doi.org/10.1016/j.foreco.2005.07.014.

Gustafson, J. Perry, Peter H. Raven, and Paul R. Ehrlich. 2020. *Population, Agriculture, and Biodiversity: Problems and Prospects*. University of Missouri Press.

Hakkenberg, C. R., R. K. Peet, D. L. Urban, and C. Song. 2018. "Modeling Plant Composition as Community Continua in a Forest Landscape with LiDAR and Hyperspectral Remote Sensing." *Ecological Applications* 28 (1): 177–90. https://doi.org/10.1002/eap.1638.

Hakkenberg, C. R., K. Zhu, R. K. Peet, and C. Song. 2018. "Mapping Multi-Scale Vascular Plant Richness in a Forest Landscape with Integrated LiDAR and Hyperspectral Remote-Sensing." *Ecology* 99 (2): 474–87. https://doi.org/10.1002/ecy.2109.

Hall, Jefferson S, and Mark S Ashton. 2016. *Guide to Early Growth and Survival in Plantations of 64 Tree Species Native to Panama and the Neotropics*. Smithsonian Tropical Research Institute.

Hall, Jefferson S., Brian E. Love, Eva J. Garen, Jacob L. Slusser, Kristin Saltonstall, Shane Mathias, Michiel van Breugel, et al. 2011. "Tree Plantations on Farms: Evaluating Growth and Potential for Success." *Forest Ecology and Management* 261 (10): 1675–83. https://doi.org/10.1016/j.foreco.2010.09.042.

Hardy, Olivier J. 2003. "Estimation of Pairwise Relatedness between Individuals and Characterization of Isolation-by-Distance Processes Using Dominant Genetic Markers." *Molecular Ecology* 12 (6): 1577–88. https://doi.org/10.1046/j.1365-294X.2003.01835.x.

Harvey, C A, and W A Haber. 1999. “Remnant Trees and the Conservation of Biodiversity in Costa Rican Pastures.” *Agroforestry Systems*, 32.

Harvey, C.A., N.I.J. Tucker, and A. Estrada. 2004. “Live Fences, Isolated Trees, and Windbreaks: Tools for Conserving Biodiversity in Fragmented Tropical Landscapes.” *Agroforestry and Biodiversity Conservation in Tropical Landscapes. Island Press, Washington, DC*, 261–89.

Harvey, Celia A., Carlos F. Guindon, William A. Haber, D. Hamilton DeRosier, and K. Greg Murray. 2000. “The Importance of Forest Patches, Isolated Trees and Agricultural Windbreaks for Local and Regional Biodiversity: The Case of Monteverde, Costa RicaForests and Society: The Role of Research. Sub-Plenary Sessions.” In *21. IUFRO World Congress 20007-12 Ago 2000Kuala Lumpur (Malasia)*. IUFRO, Viena (Austria).

Harvey, Celia A., Arnulfo Medina, Dalia Merlo Sánchez, Sergio Vílchez, Blas Hernández, Joel C. Saenz, Jean Michel Maes, Fernando Casanoves, and Fergus L. Sinclair. 2006. “Patterns of Animal Diversity in Different Forms of Tree Cover in Agricultural Landscapes.” *Ecological Applications* 16 (5): 1986–99. https://doi.org/10.1890/1051-0761(2006)016[1986:POADID]2.0.CO;2.

Heagney, E. C., D. S. Falster, and M. Kovač. 2021. “Land Clearing in South-Eastern Australia: Drivers, Policy Effects and Implications for the Future.” *Land Use Policy* 102 (March): 105243. https://doi.org/10.1016/j.landusepol.2020.105243.

Hoang, Thi Thu Huong, Anton Van Rompaey, Patrick Meyfroidt, Gerard Govers, Kim Chi Vu, An Thinh Nguyen, Luc Hens, and Veerle Vanacker. 2020. “Impact of Tourism Development on the Local Livelihoods and Land Cover Change in the Northern Vietnamese Highlands.” *Environment, Development and Sustainability* 22 (2): 1371–95. https://doi.org/10.1007/s10668-018-0253-5.

Holl, Karen D., Michael E. Loik, Eleanor HV Lin, and Ivan A. Samuels. 2000. “Tropical Montane Forest Restoration in Costa Rica: Overcoming Barriers to Dispersal and Establishment.” *Restoration Ecology* 8 (4): 339–49.

Holl, Karen D., John Leighton Reid, José Miguel Chaves-Fallas, Federico Oviedo-Brenes, and Rakan A. Zahawi. 2017. "Local Tropical Forest Restoration Strategies Affect Tree Recruitment More Strongly than Does Landscape Forest Cover." Edited by Lars Brudvig. *Journal of Applied Ecology* 54 (4): 1091–99. https://doi.org/10.1111/1365-2664.12814.

Houghton, R. A. 2012. "Carbon Emissions and the Drivers of Deforestation and Forest Degradation in the Tropics." *Current Opinion in Environmental Sustainability*, 4/6 Climate systems, 4 (6): 597–603. https://doi.org/10.1016/j.cosust.2012.06.006.

Iida, Yoshiko, Lourens Poorter, Frank Sterck, Abd Rahman Kassim, Matthew D. Potts, Takuya Kubo, and Takashi S. Kohyama. 2014. "Linking Size-Dependent Growth and Mortality with Architectural Traits across 145 Co-Occurring Tropical Tree Species." *Ecology* 95 (2): 353–63. https://doi.org/10.1890/11-2173.1.

Johnson, Daniel J., Wesley T. Beaulieu, James D. Bever, and Keith Clay. 2012. "Conspecific Negative Density Dependence and Forest Diversity." *Science* 336 (6083): 904–7. https://doi.org/10.1126/science.1220269.

Johnson, Dustin D., and Richard F. Miller. 2006. "Structure and Development of Expanding Western Juniper Woodlands as Influenced by Two Topographic Variables." *Forest Ecology and Management* 229 (1): 7–15. https://doi.org/10.1016/j.foreco.2006.03.008.

Kalacska, M., G.A. Sanchez-Azofeifa, J.C. Calvo-Alvarado, M. Quesada, B. Rivard, and D.H. Janzen. 2004. "Species Composition, Similarity and Diversity in Three Successional Stages of a Seasonally Dry Tropical Forest." *Forest Ecology and Management* 200 (1–3): 227–47. https://doi.org/10.1016/j.foreco.2004.07.001.

Karanth, K. Ullas. 1995. "Estimating Tiger Panthera Tigris Populations from Camera-Trap Data Using Capture—Recapture Models." *Biological Conservation* 71 (3): 333–38.

Keil, Petr, Thorsten Wiegand, Anikó B. Tóth, Daniel J. McGlinn, and Jonathan M. Chase. 2021. "Measurement and Analysis of Interspecific Spatial Associations as a Facet of Biodiversity." *Ecological Monographs*. https://doi.org/10.1002/ecm.1452.

Kellner, James R., and Stephen P. Hubbell. 2017. "Adult Mortality in a Low-Density Tree Population Using High-Resolution Remote Sensing." *Ecology* 98 (6): 1700–1709. https://doi.org/10.1002/ecy.1847.

Kellner, James R., and Stephen P. Hubbell. 2018. "Density-Dependent Adult Recruitment in a Low-Density Tropical Tree." *Proceedings of the National Academy of Sciences* 115 (44): 11268–73. https://doi.org/10.1073/pnas.1800353115.

Kemppinen, Julia, Pekka Niittynen, Henri Riihimäki, and Miska Luoto. 2018. "Modelling Soil Moisture in a High-Latitude Landscape Using LiDAR and Soil Data: Soil Moisture and LiDAR in a High-Latitude Landscape." *Earth Surface Processes and Landforms* 43 (5): 1019–31. https://doi.org/10.1002/esp.4301.

Lachlan, Charles S., John M. Dwyer, Hazel M. Chapman, Biplang G. Yadok, and Margaret M. Mayfield. 2019. "Landscape Structure Mediates Zoochorous-Dispersed Seed Rain under Isolated Pasture Trees across Distinct Tropical Regions." *Landscape Ecology* 34 (6): 1347–62. https://doi.org/10.1007/s10980-019-00846-3.

LaManna, Joseph A., Scott A. Mangan, Alfonso Alonso, Norman A. Bourg, Warren Y. Brockelman, Sarayudh Bunyavejchewin, Li-Wan Chang, et al. 2017. "Plant Diversity Increases with the Strength of Negative Density Dependence at the Global Scale." *Science* 356 (6345): 1389–92. https://doi.org/10.1126/science.aam5678.

Laurance, William F., and Timothy J. Curran. 2008. "Impacts of Wind Disturbance on Fragmented Tropical Forests: A Review and Synthesis." *Austral Ecology* 33 (4): 399–408. https://doi.org/10.1111/j.1442-9993.2008.01895.x.

Laurance, William F., Patricia Delamônica, Susan G. Laurance, Heraldo L. Vasconcelos, and Thomas E. Lovejoy. 2000. “Rainforest Fragmentation Kills Big Trees.” *Nature* 404 (6780): 836–836. https://doi.org/10.1038/35009032.

Lechuga, Victor, Vinicio Carraro, Benjamín Viñegla, José Antonio Carreira, and Juan Carlos Linares. 2017. “Managing Drought-Sensitive Forests under Global Change. Low Competition Enhances Long-Term Growth and Water Uptake in Abies Pinsapo.” *Forest Ecology and Management* 406 (December): 72–82. https://doi.org/10.1016/j.foreco.2017.10.017.

Lengkeek, Ard G. 2003. “’Diversity Makes a Difference’ : Farmers Managing Inter- and Intra-Specific Tree Species Diversity in Meru Kenya,” 181.

Lennox, Gareth D., Toby A. Gardner, James R. Thomson, Joice Ferreira, Erika Berenguer, Alexander C. Lees, Ralph Mac Nally, et al. 2018. “Second Rate or a Second Chance? Assessing Biomass and Biodiversity Recovery in Regenerating Amazonian Forests.” *Global Change Biology* 24 (12): 5680–94. https://doi.org/10.1111/gcb.14443.

Lieberman, Milton, and Diana Lieberman. 2007. “Nearest-Neighbor Tree Species Combinations in Tropical Forest: The Role of Chance, and Some Consequences of High Diversity.” *Oikos* 116 (3): 377–86. https://doi.org/10.1111/j.2006.0030-1299.15370.x.

Lopes, Clarissa Gomes Reis, Elba Maria Nogueira Ferraz, Cibele Cardoso de Castro, Elifábia Neves de Lima, Josiene Maria Falcão Fraga dos Santos, Danielle Melo dos Santos, and Elcida de Lima Araújo. 2012. “Forest Succession and Distance from Preserved Patches in the Brazilian Semiarid Region.” *Forest Ecology and Management* 271 (May): 115–23. https://doi.org/10.1016/j.foreco.2012.01.043.

Maddox, Wesley J, Pavel Izmailov, Timur Garipov, Dmitry P Vetrov, and Andrew Gordon Wilson. 2019. “A Simple Baseline for Bayesian Uncertainty in Deep Learning.” In *Advances in Neural Information Processing Systems 32*, edited by H. Wallach, H. Larochelle, A. Beygelzimer, F. d\textquotesingle Alché-Buc, E. Fox, and R. Garnett, 13153–64. Curran Associates, Inc. http://papers.nips.cc/paper/9472-a-simple-baseline-for-bayesian-uncertainty-in-deep-learning.pdf.

Madsen, Christopher, Catherine Potvin, Jefferson Hall, Katherine Sinacore, Benjamin L. Turner, and Florian Schnabel. 2020. “Coarse Root Architecture: Neighbourhood and Abiotic Environmental Effects on Five Tropical Tree Species Growing in Mixtures and Monocultures.” *Forest Ecology and Management* 460 (March): 117851. https://doi.org/10.1016/j.foreco.2019.117851.

Manning, Adrian D., Joern Fischer, and David B. Lindenmayer. 2006. “Scattered Trees Are Keystone Structures – Implications for Conservation.” *Biological Conservation* 132 (3): 311–21. https://doi.org/10.1016/j.biocon.2006.04.023.

Manning, Adrian D., Philip Gibbons, and David B. Lindenmayer. 2009. “Scattered Trees: A Complementary Strategy for Facilitating Adaptive Responses to Climate Change in Modified Landscapes?” *Journal of Applied Ecology* 46 (4): 915–19. https://doi.org/10.1111/j.1365-2664.2009.01657.x.

Matos, Fabio A. R., Luiz F. S. Magnago, Carlos Aquila Chan Miranda, Luis F. T. de Menezes, Markus Gastauer, Nathália V. H. Safar, Carlos E. G. R. Schaefer, et al. 2020. “Secondary Forest Fragments Offer Important Carbon and Biodiversity Cobenefits.” *Global Change Biology* 26 (2): 509–22. https://doi.org/10.1111/gcb.14824.

McCrea, Rachel S., and Byron J. T. Morgan. 2014. *Analysis of Capture-Recapture Data*. CRC Press.

McDowell, Nate, Craig D. Allen, Kristina Anderson-Teixeira, Paulo Brando, Roel Brienen, Jeff Chambers, Brad Christoffersen, et al. 2018. "Drivers and Mechanisms of Tree Mortality in Moist Tropical Forests." *New Phytologist* 219 (3): 851–69. https://doi.org/10.1111/nph.15027.

McElreath, Richard. 2017. "Metamorphosis and the Multilevel Model." *Elements of Evolutionary Anthropology* (blog). September 7, 2017. https://elevanth.org/blog/2017/09/07/metamorphosis-multilevel-model/.

McElreath, Richard. 2020. *Statistical Rethinking: A Bayesian Course with Examples in R and Stan*. CRC press.

McMahon, Sean M., Gabriel Arellano, and Stuart J. Davies. 2019. "The Importance and Challenges of Detecting Changes in Forest Mortality Rates." *Ecosphere* 10 (2): e02615. https://doi.org/10.1002/ecs2.2615.

Meddens, Arjan J. H., Jeffrey A. Hicke, and Lee A. Vierling. 2011. "Evaluating the Potential of Multispectral Imagery to Map Multiple Stages of Tree Mortality." *Remote Sensing of Environment* 115 (7): 1632–42. https://doi.org/10.1016/j.rse.2011.02.018.

Menge, Duncan N. L., and Robin L. Chazdon. 2016. "Higher Survival Drives the Success of Nitrogen-Fixing Trees through Succession in Costa Rican Rainforests." *The New Phytologist* 209 (3): 965–77. https://doi.org/10.1111/nph.13734.

Mesquita, Rita C. G., Patricia Delamônica, and William F. Laurance. 1999. "Effect of Surrounding Vegetation on Edge-Related Tree Mortality in Amazonian Forest Fragments." *Biological Conservation* 91 (2): 129–34. https://doi.org/10.1016/S0006-3207(99)00086-5.

Metcalf, C. Jessica E., Carol C. Horvitz, Shripad Tuljapurkar, and Deborah A. Clark. 2009. "A Time to Grow and a Time to Die: A New Way to Analyze the Dynamics of Size, Light, Age, and Death of Tropical Trees." *Ecology* 90 (10): 2766–78. https://doi.org/10.1890/08-1645.1.

Metzel, Ruth, and Florencia Montagnini. 2014. "From Farm to Forest: Factors Associated with Protecting and Planting Trees in a Panamanian Agricultural Landscape." *BOIS & FORETS DES TROPIQUES* 322 (322): 3. https://doi.org/10.19182/bft2014.322.a31225.

Miller, David A., James D. Nichols, Brett T. McClintock, Evan H. Campbell Grant, Larissa L. Bailey, and Linda A. Weir. 2011. "Improving Occupancy Estimation When Two Types of Observational Error Occur: Non-Detection and Species Misidentification." *Ecology* 92 (7): 1422–28. https://doi.org/10.1890/10-1396.1.

Milton Solano. 2011. "Panama's Road Network." https://stridata-si.opendata.arcgis.com/.

Misra, Gourav, Allan Buras, Marco Heurich, Sarah Asam, and Annette Menzel. 2018. "LiDAR Derived Topography and Forest Stand Characteristics Largely Explain the Spatial Variability Observed in MODIS Land Surface Phenology." *Remote Sensing of Environment* 218 (December): 231–44. https://doi.org/10.1016/j.rse.2018.09.027.

Mohr, Stephan, William Dawson, Michael Wagner, Damien Caliste, Takahito Nakajima, and Luigi Genovese. 2017. "Efficient Computation of Sparse Matrix Functions for Large-Scale Electronic Structure Calculations: The CheSS Library." *Journal of Chemical Theory and Computation* 13 (10): 4684–98. https://doi.org/10.1021/acs.jctc.7b00348.

Mon, Myat Su, Nobuya Mizoue, Naing Zaw Htun, Tsuyoshi Kajisa, and Shigejiro Yoshida. 2012. "Factors Affecting Deforestation and Forest Degradation in Selectively Logged Production Forest: A Case Study in Myanmar." *Forest Ecology and Management* 267 (March): 190–98. https://doi.org/10.1016/j.foreco.2011.11.036.

Monnahan, Cole C., James T. Thorson, and Trevor A. Branch. 2017. "Faster Estimation of Bayesian Models in Ecology Using Hamiltonian Monte Carlo." *Methods in Ecology and Evolution* 8 (3): 339–48. https://doi.org/10.1111/2041-210X.12681.

Muller-Landau, H C, J W Dalling, K E Harms, S J Wright, R Condit, S P Hubbell, and R B Foster. 2004. "Seed Dispersal and Density-Dependent Seed and Seedling Survival in Trichilia Tuberculata and Miconia Argentea," 42.

Murgueitio, Enrique, Zoraida Calle, Fernando Uribe, Alicia Calle, and Baldomero Solorio. 2011. "Native Trees and Shrubs for the Productive Rehabilitation of Tropical Cattle Ranching Lands." *Forest Ecology and Management*, The Ecology and Ecosystem Services of Native Trees: Implications for Reforestation and Land Restoration in Mesoamerica, 261 (10): 1654–63. https://doi.org/10.1016/j.foreco.2010.09.027.

Nakagawa, Shinichi. 2015. *Missing Data: Mechanisms, Methods, and Messages*. *Ecological Statistics*. Oxford University Press. https://oxford.universitypressscholarship.com/view/10.1093/acprof:oso/9780199672547.001.0001/acprof-9780199672547-chapter-5.

Näsi, Roope, Eija Honkavaara, Päivi Lyytikäinen-Saarenmaa, Minna Blomqvist, Paula Litkey, Teemu Hakala, Niko Viljanen, Tuula Kantola, Topi Tanhuanpää, and Markus Holopainen. 2015. "Using UAV-Based Photogrammetry and Hyperspectral Imaging for Mapping Bark Beetle Damage at Tree-Level." *Remote Sensing* 7 (11): 15467–93. https://doi.org/10.3390/rs71115467.

Nathan, Ran, and Helene C. Muller-Landau. 2000. "Spatial Patterns of Seed Dispersal, Their Determinants and Consequences for Recruitment." *Trends in Ecology & Evolution* 15 (7): 278–85. https://doi.org/10.1016/S0169-5347(00)01874-7.

Neal, Radford. 2011. "MCMC Using Hamiltonian Dynamics." In *Handbook of Markov Chain Monte Carlo*, edited by Steve Brooks, Andrew Gelman, Galin Jones, and Xiao-Li Meng. Vol. 20116022. Chapman & Hall/CRC Handbooks of Modern Statistical Methods. Chapman and Hall/CRC. https://doi.org/10.1201/b10905-6.

Nguyen, Huong, Jerome Vanclay, John Herbohn, and Jennifer Firn. 2016. "Drivers of Tree Growth, Mortality and Harvest Preferences in Species-Rich Plantations for Smallholders and Communities in the Tropics." *PLOS ONE* 11 (10): e0164957. https://doi.org/10.1371/journal.pone.0164957.

Norden, N., H.A. Angarita, F. Bongers, M. Martínez-Ramos, Iñigo Granzow-de la de la Cerda, M. van Breugel, E. Lebrija-Trejos, et al. 2015. "Successional Dynamics in Neotropical Forests Are as Uncertain as They Are Predictable." *Proceedings of the National Academy of Sciences* 112 (26): 8013–18. https://doi.org/10.1073/pnas.1500403112.

Ogle, Kiona. 2009. "Hierarchical Bayesian Statistics: Merging Experimental and Modeling Approaches in Ecology." *Ecological Applications* 19 (3): 577–81. https://doi.org/10.1890/08-0560.1.

Ogle, Kiona, and Jarrett J. Barber. 2020. "Ensuring Identifiability in Hierarchical Mixed Effects Bayesian Models." *Ecological Applications* 00 (00). https://doi.org/10.1002/eap.2159.

Oliveira Fiorini, Ana Carolina, Conner Mullally, Marilyn Swisher, and Francis E. Putz. 2020. "Forest Cover Effects of Payments for Ecosystem Services: Evidence from an Impact Evaluation in Brazil." *Ecological Economics* 169 (March): 106522. https://doi.org/10.1016/j.ecolecon.2019.106522.

Olson, Luke, Amanda Bienz, Bill Gropp, and Andrew Reisner. 2016. "The next Generation of Large-Scale Sparse Matrix Computations," 2.

Outcalt, Kenneth W., and Dale D. Wade. 2004. "Fuels Management Reduces Tree Mortality from Wildfires In Southeastern United States." *Southern Journal of Applied Forestry* 28 (1): 28–34. https://doi.org/10.1093/sjaf/28.1.28.

Ozolins, Amanda, Cris Brack, and David Freudenberger. 2001. "Abundance and Decline of Isolated Trees in the Agricultural Landscapes of Central New South Wales, Australia." *Pacific Conservation Biology* 7 (3): 195–203. https://doi.org/10.1071/pc010195.

Pacala, Stephen W., and J. A. Silander. 1985. "Neighborhood Models of Plant Population Dynamics. I. Single-Species Models of Annuals." *The American Naturalist* 125 (3): 385–411.

Pacala, Stephen W., and John A. Silander. 1987. “Neighborhood Interference among Velvet Leaf, Abutilon Theophrasti, and Pigweed, Amaranthus Retroflexus.” *Oikos* 48 (2): 217–24. https://doi.org/10.2307/3565858.

Parrotta, John A. 1993. “Secondary Forest Regeneration on Degraded Tropical Lands.” In *Restoration of Tropical Forest Ecosystems: Proceedings of the Symposium Held on October 7–10, 1991*, edited by Helmut Lieth and Martina Lohmann, 63–73. Tasks for Vegetation Science. Dordrecht: Springer Netherlands. https://doi.org/10.1007/978-94-017-2896-6_6.

Paz-Kagan, Tarin, Philip G. Brodrick, Nicholas R. Vaughn, Adrian J. Das, Nathan L. Stephenson, Koren R. Nydick, and Gregory P. Asner. 2017. “What Mediates Tree Mortality during Drought in the Southern Sierra Nevada?” *Ecological Applications* 27 (8): 2443–57. https://doi.org/10.1002/eap.1620.

Pickard, David K. 1987. “Inference for Discrete Markov Fields: The Simplest Nontrivial Case.” *Journal of the American Statistical Association* 82 (397): 90–96. https://doi.org/10.2307/2289128.

Plieninger, Tobias. 2012. “Monitoring Directions and Rates of Change in Trees Outside Forests through Multitemporal Analysis of Map Sequences.” *Applied Geography* 32 (2): 566–76. https://doi.org/10.1016/j.apgeog.2011.06.015.

Plieninger, Tobias, Christian Levers, Martin Mantel, Augusta Costa, Harald Schaich, and Tobias Kuemmerle. 2015. “Patterns and Drivers of Scattered Tree Loss in Agricultural Landscapes: Orchard Meadows in Germany (1968-2009).” *PLOS ONE* 10 (5): e0126178. https://doi.org/10.1371/journal.pone.0126178.

Potapov, Peter, Matthew C. Hansen, Lars Laestadius, Svetlana Turubanova, Alexey Yaroshenko, Christoph Thies, Wynet Smith, et al. 2017. “The Last Frontiers of Wilderness: Tracking Loss of Intact Forest Landscapes from 2000 to 2013.” *Science Advances* 3 (1): e1600821. https://doi.org/10.1126/sciadv.1600821.

Pu, Xucai, María Natalia Umaña, and Guangze Jin. 2020. “Trait-Mediated Neighbor Effects on Plant Survival Depend on Life Stages and Stage-Specific Traits in a Temperate Forest.” *Forest Ecology and Management* 472 (September): 118250. https://doi.org/10.1016/j.foreco.2020.118250.

Rawal, Arjun, Yuanwei Fang, and Andrew Chien. 2019. “Programmable Acceleration for Sparse Matrices in a Data-Movement Limited World.” In , 47–56. Rio de Janeiro, Brazil: IEEE. https://doi.org/10.1109/IPDPSW.2019.00016.

Requena-Mullor, Juan M., Kaitlin C. Maguire, Douglas J. Shinneman, and Timothy Trevor Caughlin. 2019. “Integrating Anthropogenic Factors into Regional-Scale Species Distribution Models—A Novel Application in the Imperiled Sagebrush Biome.” *Global Change Biology* 25 (11): 3844–58. https://doi.org/10.1111/gcb.14728.

Ribbens, Eric, John A. Silander, and Stephen W. Pacala. 1994. “Seedling Recruitment in Forests: Calibrating Models to Predict Patterns of Tree Seedling Dispersion.” *Ecology* 75 (6): 1794–1806. https://doi.org/10.2307/1939638.

Robiglio, Valentina, and Fergus Sinclair. 2011. “Maintaining the Conservation Value of Shifting Cultivation Landscapes Requires Spatially Explicit Interventions.” *Environmental Management* 48 (2): 289–306. https://doi.org/10.1007/s00267-010-9611-2.

Romero-Mujalli, Daniel, Florian Jeltsch, and Ralph Tiedemann. 2019. “Individual-Based Modeling of Eco-Evolutionary Dynamics: State of the Art and Future Directions.” *Regional Environmental Change* 19 (1): 1–12. https://doi.org/10.1007/s10113-018-1406-7.

Royle, J. Andrew, and William A. Link. 2006. “Generalized Site Occupancy Models Allowing for False Positive and False Negative Errors.” *Ecology* 87 (4): 835–41. https://doi.org/10.1890/0012-9658(2006)87[835:GSOMAF]2.0.CO;2.

Rudel, Thomas K., Ruth Defries, Gregory P. Asner, and William F. Laurance. 2009. "Changing Drivers of Deforestation and New Opportunities for Conservation." *Conservation Biology* 23 (6): 1396–1405. https://doi.org/10.1111/j.1523-1739.2009.01332.x.

Rudel, Thomas K., and Bruce Horowitz. 1996. *Tropical Deforestation: The Human Dimension*. Columbia University Press.

Sales-Baptista, Elvira, and Maria Isabel Ferraz-de-Oliveira. 2021. "Grazing in Silvopastoral Systems: Multiple Solutions for Diversified Benefits." *Agroforestry Systems* 95 (1): 1–6. https://doi.org/10.1007/s10457-020-00581-8.

Sánchez-Romero, Rosa, Patricia Balvanera, Alicia Castillo, Francisco Mora, Luis E. García-Barrios, and Carlos E. González-Esquivel. 2021. "Management Strategies, Silvopastoral Practices and Socioecological Drivers in Traditional Livestock Systems in Tropical Dry Forests: An Integrated Analysis." *Forest Ecology and Management* 479 (January): 118506. https://doi.org/10.1016/j.foreco.2020.118506.

Sankey, Joel B., Temuulen T. Sankey, Junran Li, Sujith Ravi, Guan Wang, Joshua Caster, and Alan Kasprak. 2021. "Quantifying Plant-Soil-Nutrient Dynamics in Rangelands: Fusion of UAV Hyperspectral-LiDAR, UAV Multispectral-Photogrammetry, and Ground-Based LiDAR-Digital Photography in a Shrub-Encroached Desert Grassland." *Remote Sensing of Environment* 253 (February): 112223. https://doi.org/10.1016/j.rse.2020.112223.

Santos, Maria J., Jonathan A. Greenberg, and Susan L. Ustin. 2010. "Using Hyperspectral Remote Sensing to Detect and Quantify Southeastern Pine Senescence Effects in Red-Cockaded Woodpecker (Picoides Borealis) Habitat." *Remote Sensing of Environment* 114 (6): 1242–50. https://doi.org/10.1016/j.rse.2010.01.009.

Schimel, David, Ryan Pavlick, Joshua B. Fisher, Gregory P. Asner, Sassan Saatchi, Philip Townsend, Charles Miller, Christian Frankenberg, Kathy Hibbard, and Peter Cox. 2015. "Observing Terrestrial Ecosystems and the Carbon Cycle from Space." *Global Change Biology* 21 (5): 1762–76. https://doi.org/10.1111/gcb.12822.

Schmidt, K. S., and A. K. Skidmore. 2001. "Exploring Spectral Discrimination of Grass Species in African Rangelands." *International Journal of Remote Sensing* 22 (17): 3421–34. https://doi.org/10.1080/01431160152609245.

Schneider, Manuel K., Richard Law, and Janine B. Illian. 2006. "Quantification of Neighbourhood-Dependent Plant Growth by Bayesian Hierarchical Modelling." *Journal of Ecology* 94 (2): 310–21.

Schwartz, Naomi B., Andrew M. Budsock, and María Uriarte. 2019. "Fragmentation, Forest Structure, and Topography Modulate Impacts of Drought in a Tropical Forest Landscape." *Ecology* 100 (6): e02677. https://doi.org/10.1002/ecy.2677.

Seidl, Rupert, Werner Rammer, Robert M. Scheller, and Thomas A. Spies. 2012. "An Individual-Based Process Model to Simulate Landscape-Scale Forest Ecosystem Dynamics." *Ecological Modelling* 231 (April): 87–100. https://doi.org/10.1016/j.ecolmodel.2012.02.015.

Shen, Lingyun, Mingjing Yan, Gang Wu, and Xiyou Su. 2020. "Individual Tree Location Detection by High-Resolution RGB Satellite Imagery in Urban Area." In *Proceedings of the 2020 International Conference on Computing, Networks and Internet of Things*, 139–43. Sanya China: ACM. https://doi.org/10.1145/3398329.3398351.

Shriver, Robert K., Charles B. Yackulic, David M. Bell, and John B. Bradford. 2021. "Quantifying the Demographic Vulnerabilities of Dry Woodlands to Climate and Competition Using Range-Wide Monitoring Data." *Ecology* n/a (n/a): e03425. https://doi.org/10.1002/ecy.3425.

Silva, Wg., Jp. Metzger, S. Simões, and C Simonetti. 2007. "Relief Influence on the Spatial Distribution of the Atlantic Forest Cover on the Ibiúna Plateau, SP." *Brazilian Journal of Biology* 67 (3): 403–11. https://doi.org/10.1590/S1519-69842007000300004.

Sloan, Sean. 2015. "The Development-Driven Forest Transition and Its Utility for REDD+." *Ecological Economics* 116 (August): 1–11. https://doi.org/10.1016/j.ecolecon.2015.04.010.

Sluiter, Raymond, and Steven M. de Jong. 2007. "Spatial Patterns of Mediterranean Land Abandonment and Related Land Cover Transitions." *Landscape Ecology* 22 (4): 559–76. https://doi.org/10.1007/s10980-006-9049-3.

Slusser, Jacob L, Alicia Calle, and Eva Garen. 2015a. "1.2 Sustainable Ranching and Restoring Forests in Agricultural Landscapes, Panama," 8.

Slusser, Jacob L, Alicia Calle, and Eva Garen. 2015b. "Sustainable Ranching and Restoring Forests in Agricultural Landscapes, Panama," 8.

Soranno, Patricia A., Edward G. Bissell, Kendra S. Cheruvelil, Samuel T. Christel, Sarah M. Collins, C. Emi Fergus, Christopher T. Filstrup, et al. 2015. "Building a Multi-Scaled Geospatial Temporal Ecology Database from Disparate Data Sources: Fostering Open Science and Data Reuse." *GigaScience* 4 (1): s13742-015. https://doi.org/10.1186/s13742-015-0067-4.

Sortibrán, Lugui, Miguel Verdú, and Alfonso Valiente-Banuet. 2014. "Nurses Experience Reciprocal Fitness Benefits from Their Distantly Related Facilitated Plants." *Perspectives in Plant Ecology, Evolution and Systematics* 16 (5): 228–35. https://doi.org/10.1016/j.ppees.2014.07.001.

Southworth, Jane, and Catherine Tucker. 2001. "The Influence of Accessibility, Local Institutions, and Socioeconomic Factors on Forest Cover Change in the Mountains of Western Honduras." *Mountain Research and Development* 21 (3): 276–83. https://doi.org/10.1659/0276-4741(2001)021[0276:TIOALI]2.0.CO;2.

Stan Development Team. 2019a. *Stan Modeling Language Users Guide and Reference Manual, 2.26*. https://mc-stan.org.

Stan Development Team. 2019b. *Stan Reference Manual*. Version 2.23. https://mc-stan.org/docs/2_23/reference-manual/index.html.

Stoll, Peter, and Jacob Weiner. 2000. "A Neighborhood View of Interactions among Individual Plants." In *The Geometry of Ecological Interactions*, edited by Ulf Dieckmann, Richard Law, and Johan A. J. Metz, 1st ed., 11–27. Cambridge University Press. https://doi.org/10.1017/CBO9780511525537.003.

Sy, V. De, M. Herold, F. Achard, R. Beuchle, J. G. P. W. Clevers, E. Lindquist, and L. Verchot. 2015. "Land Use Patterns and Related Carbon Losses Following Deforestation in South America." *Environmental Research Letters* 10 (12): 124004. https://doi.org/10.1088/1748-9326/10/12/124004.

Tarbox, Bryan C., Carlita Fiestas, and T. Trevor Caughlin. 2018. "Divergent Rates of Change between Tree Cover Types in a Tropical Pastoral Region." *Landscape Ecology* 33 (12): 2153–67. https://doi.org/10.1007/s10980-018-0730-0.

Tay, Jessica Y. L., Alexandra Erfmeier, and Jesse M. Kalwij. 2018. "Reaching New Heights: Can Drones Replace Current Methods to Study Plant Population Dynamics?" *Plant Ecology* 219 (10): 1139–50. https://doi.org/10.1007/s11258-018-0865-8.

Thomas, R. Q., J. R. Kellner, D. B. Clark, and D. R. Peart. 2013. "Low Mortality in Tall Tropical Trees." *Ecology* 94 (4): 920–29. https://doi.org/10.1890/12-0939.1.

Torres-Romero, Erik Joaquín, and Miguel Á Olalla-Tárraga. 2015. "Untangling Human and Environmental Effects on Geographical Gradients of Mammal Species Richness: A Global and Regional Evaluation." *Journal of Animal Ecology* 84 (3): 851–60. https://doi.org/10.1111/1365-2656.12313.

Turek, Javier S., and Alexander G. Huth. 2018. "Efficient, Sparse Representation of Manifold Distance Matrices for Classical Scaling." In *Proceedings of the IEEE Conference on Computer Vision and Pattern Recognition*, 2850–58. Salt Lake City, UT: IEEE. https://doi.org/10.1109/CVPR.2018.00301.

Urban, Dean, and Timothy Keitt. 2001. "Landscape Connectivity: A Graph-Theoretic Perspective." *Ecology* 82 (5): 1205–18. https://doi.org/10.2307/2679983.

Uriarte, María, Richard Condit, Charles D. Canham, and Stephen P. Hubbell. 2004. "A Spatially Explicit Model of Sapling Growth in a Tropical Forest: Does the Identity of Neighbours Matter?" *Journal of Ecology* 92 (2): 348–60. https://doi.org/10.1111/j.0022-0477.2004.00867.x.

Uriarte, María, Robert Muscarella, and Jess K. Zimmerman. 2018. "Environmental Heterogeneity and Biotic Interactions Mediate Climate Impacts on Tropical Forest Regeneration." *Global Change Biology* 24 (2): e692–704. https://doi.org/10.1111/gcb.14000.

Vahidi, Hossein, Brian Klinkenberg, Brian A. Johnson, L. Monika Moskal, and Wanglin Yan. 2018. "Mapping the Individual Trees in Urban Orchards by Incorporating Volunteered Geographic Information and Very High Resolution Optical Remotely Sensed Data: A Template Matching-Based Approach." *Remote Sensing* 10 (7): 1134. https://doi.org/10.3390/rs10071134.

Valencia Mestre, Maria. 2017. "From Treeless Pastures to Silvo-Pastoral Systems: The Extent and Drivers of Tree Management Styles." University of Michigan, Horace H. Rackham School of Graduate Studies. https://deepblue.lib.umich.edu/handle/2027.42/138751.

Valencia Mestre, Mariana. 2017. "From Treeless Pastures to Silvo-Pastoral Systems: The Extent and Drivers of Tree Management Styles." PhD Thesis.

Valencia Mestre, Mariana C., Bruce G. Ferguson, and John Vandermeer. 2018. "Syndromes of Production and Tree-Cover Dynamics of Neotropical Grazing Land." *Agroecology and Sustainable Food Systems* 0 (0): 1–24. https://doi.org/10.1080/21683565.2018.1483994.

Valenta, Magalí D., Rodolfo A. Golluscio, Ana L. Frey, Lucas A. Garibaldi, and Pablo A. Cipriotti. 2020. "Short-Term Responses to Sheep Grazing in a Patagonian Steppe." *The Rangeland Journal* 42 (1): 1. https://doi.org/10.1071/RJ19012.

Vehtari, Aki, Jonah Gabry, Mans Magnusson, Yuling Yao, Paul-Christian Bürkner, Topi Paananen, and Andrew Gelman. 2020. *Loo: Efficient Leave-One-out Cross-Validation and WAIC for Bayesian Models*. https://mc-stan.org/loo/.

Vehtari, Aki, Andrew Gelman, Daniel Simpson, Bob Carpenter, and Paul-Christian Bürkner. 2020. "Rank-Normalization, Folding, and Localization: An Improved $\widehat{R}$ for Assessing Convergence of MCMC." *Bayesian Analysis*, July. https://doi.org/10.1214/20-BA1221.

Vignola, Raffaele, Celia Alice Harvey, Pavel Bautista-Solis, Jacques Avelino, Bruno Rapidel, Camila Donatti, and Ruth Martinez. 2015. "Ecosystem-Based Adaptation for Smallholder Farmers: Definitions, Opportunities and Constraints." *Agriculture, Ecosystems & Environment* 211 (December): 126–32. https://doi.org/10.1016/j.agee.2015.05.013.

Waser, Lars T., Christian Ginzler, and Nataliia Rehush. 2017. "Wall-to-Wall Tree Type Mapping from Countrywide Airborne Remote Sensing Surveys." *Remote Sensing* 9 (8): 766. https://doi.org/10.3390/rs9080766.

Williams-Linera, Guadalupe. 1990. "Vegetation Structure and Environmental Conditions of Forest Edges in Panama." *Journal of Ecology* 78 (2): 356–73. https://doi.org/10.2307/2261117.

Wu, Hao, Scott B. Franklin, Jianming Liu, and Zhijun Lu. 2017. "Relative Importance of Density Dependence and Topography on Tree Mortality in a Subtropical Mountain Forest." *Forest Ecology and Management* 384 (January): 169–79. https://doi.org/10.1016/j.foreco.2016.10.049.

Zahawi, Rakan A., Karen D. Holl, Rebecca J. Cole, and J. Leighton Reid. 2013. "Testing Applied Nucleation as a Strategy to Facilitate Tropical Forest Recovery." Edited by Cristina Banks-Leite. *Journal of Applied Ecology* 50 (1): 88–96. https://doi.org/10.1111/1365-2664.12014.

Zaiats, Andrii, Brynne E. Lazarus, Matthew J. Germino, Marcelo D. Serpe, Bryce A. Richardson, Sven Buerki, and T. Trevor Caughlin. 2020. "Intraspecific Variation in Surface Water Uptake in a Perennial Desert Shrub." *Functional Ecology* 34 (6): 1170–79. https://doi.org/10.1111/1365-2435.13546.

Zambrano, Jenny, Noelle G. Beckman, Philippe Marchand, Jill Thompson, María Uriarte, Jess K. Zimmerman, María N. Umaña, and Nathan G. Swenson. 2020. "The Scale Dependency of Trait-Based Tree Neighborhood Models." *Journal of Vegetation Science* 31 (4): 581–93. https://doi.org/10.1111/jvs.12880.

Zambrano, Jenny, Yoshiko Iida, Robert Howe, Luxiang Lin, Maria Natalia Umana, Amy Wolf, Samantha J. Worthy, and Nathan G. Swenson. 2017. "Neighbourhood Defence Gene Similarity Effects on Tree Performance: A Community Transcriptomic Approach." *Journal of Ecology* 105 (3): 616–26. https://doi.org/10.1111/1365-2745.12765.

Zarco-Tejada, P. J., J. R. Miller, G. H. Mohammed, T. L. Noland, and P. H. Sampson. 2002. "Vegetation Stress Detection through Chlorophyll a + b Estimation and Fluorescence Effects on Hyperspectral Imagery." *Journal of Environmental Quality* 31 (5): 1433–41. https://doi.org/10.2134/jeq2002.1433.

Zhang, Bin, Lin Zhao, and Xiaoli Zhang. 2020. "Three-Dimensional Convolutional Neural Network Model for Tree Species Classification Using Airborne Hyperspectral Images." *Remote Sensing of Environment* 247 (September): 111938. https://doi.org/10.1016/j.rse.2020.111938.

Zhang, Bo, and Donald L DeAngelis. 2020. "An Overview of Agent-Based Models in Plant Biology and Ecology." *Annals of Botany* 126 (4): 539–57. https://doi.org/10.1093/aob/mcaa043.

Zomer, Robert J., Henry Neufeldt, Jianchu Xu, Antje Ahrends, Deborah Bossio, Antonio Trabucco, Meine van Noordwijk, and Mingcheng Wang. 2016. "Global Tree Cover and Biomass Carbon on Agricultural Land: The Contribution of Agroforestry to Global and National Carbon Budgets." *Scientific Reports* 6 (1): 29987. https://doi.org/10.1038/srep29987.

Zuidema, Pieter A. 2000. "Demography of Exploited Tree Species in the Bolivian Amazon," 240.

Zuleta, Daniel, Alvaro Duque, Dairon Cardenas, Helene C. Muller-Landau, and Stuart J. Davies. 2017. “Drought-Induced Mortality Patterns and Rapid Biomass Recovery in a Terra Firme Forest in the Colombian Amazon.” *Ecology* 98 (10): 2538–46. https://doi.org/10.1002/ecy.1950.

APPENDIX A

Zero-Inflated Model

$$P(Y=y|\alpha,\delta,\lambda)=\begin{cases}\alpha+(1-\alpha)\left(\frac{1}{1+\lambda\delta}\right)^{\frac{1}{\delta}}, y=0\\ (1-\alpha)\frac{(1-\alpha)\Gamma\left(y+\frac{1}{\delta}\right)}{\Gamma\left(\frac{1}{\delta}\right)\Gamma(y+1)}\left(\frac{1}{1+\lambda\delta}\right)^{\frac{1}{\delta}}\left(\frac{1}{1+\lambda\delta}\right)^{y}, y>0\end{cases}$$

Equation A1

Where $E(Y)=\lambda(1-\alpha)=\mu$ and $Var(Y)=\mu+(\frac{\alpha}{1-\alpha}+\frac{\delta}{1-\alpha})\mu^2$ and $0\leq\alpha\leq1$, $\delta>0$, and $\lambda>0$ are the mean and over-dispersion parameters. The full model describes the negative binomial phase as in equation A3 and the binomial phase as in equation.A4.

$P\sim Bernoulli(\rho)$

$\text{logit}(\rho)=X\beta+X\alpha_{sp}+X\alpha_{p}$

$\alpha_{sp}\sim normal(\mu_{sp},\sigma_{sp})$

$\mu_{sp}\sim normal(0,1)$

σ_{sp} *~student_t(3,0,10)*

$\alpha_{p}\sim normal(\mu_{d},\sigma_{p})$

$\mu_{p}\sim normal(0,1)$

σ_{p} *~ student_t(3,0,10)*

Equation A2

$R\sim Negative\ binomial(\mu,\Phi)$

$\log(\mu)=X\beta+X\alpha_{sp}+X\alpha_{p}$

$\Phi\sim gamma(0.01,0.01)$

$\alpha_{sp}\sim normal(\mu_{sp},\sigma_{sp})$

$$\mu_{sp} \sim normal(0,1)$$

$$\sigma_{sp} \sim normal(0,1)$$

$$\alpha_p \sim normal(\mu_d, \sigma_p)$$

$$\mu_p \sim normal(0,1)$$

$$\sigma_p \sim normal(0,1)$$

Equation A3

Where P is the presence or absence of recruits on a plot, R is the recruitment abundance, and X is a matrix containing the fixed effects. The fixed effects included in equation 3 are the conspecific tree crown area, the heterospecific tree crown area, and elevation. The fixed effects included in equation 4 are the conspecific tree crown area, the squared conspecific tree crown area, and the heterospecific tree crown area. **β** are the fixed effects parameters, and **α** are the random effects; α_{sp} are species random effects, and α_p are property identity random effects. For the shape of the negative binomial distribution, we used a non-informative prior ($gamma(0.01, 0.01)$) to allow the shape to adjust for the over-dispersion of the data.

Model Predictive Capacity per Species

Tree species recruit abundance for two out of five species (*Byrsonima crassifolia* and *Guazuma ulmifolia*) was best predicted when the fixed effects and intercepts varied by property and recruits species (Appendix A, Table A2 the models named: Species & Property, and Individual tree crowns, Species & Property). One species' recruit abundance (*Calycophyllum candidissimum*) was best predicted when the fixed effects and intercepts varied by property (Appendix A, Table A2 the models named: Property, and Individual tree crowns & Property). Another species' recruit abundance (*Enterolobium cyclocarpum*)

was best predicted when the fixed effects and intercepts varied by recruits' species (Appendix A, Table A3 the models named: Species, and Individual tree crowns & Species).

Tables Chapter 1

Table A1 Main species characteristics included in this study. Family and successional stage was obtained from Kalacska et al. (2004). Human use of tree species by local framers was obtained from Metzel and Montagnini 2014. Uses: W =Wood, FR = Fruit/Food for humans, T = Traditional Use, FW = Firewood, PA = Physical Attributes, LF = Living Fence Posts, M = Medicinal, E = Environmental purpose, FL = Food for livestock. Dispersal syndromes were obtained from Griscom and Ashton (2011).

Species	Family	Dispersal syndrome	Successional stages	Human use
Byrsonima crassifolia	Malpighiaceae	Animal	Early to mid-succession	W, PA, FW, LF, FR, E
Calycophyllum candissium	Rubiaceae	Wind	Mid to late-succession	W, PA, FW, LF
Cedrela orodata	Meliaceae	Wind	Early to mid-succession	W, LF, FW, FL
Guazuma ulmifolia	Sterculiaceae	Cattle	Early to mid-succession	PA, FW, LF, FR, FL, T
Enterolobium cyclocarpum	Fabaceae	Cattle & gravity	Early and late succession	W, PA, LF, FL, T

Table A2 Summary of the characteristics of the adult tree crowns included in this study.

	Number	Average area (m^2)	Maximum area (m^2)	Minimum area (m^2)
Tree crowns	23875	93	349	1
Five focal species tree crowns	3847	114	348	5
Non focal species tree crowns	20028	92	349	1

Table A3 **Median of the out of sample MAE (95% CI) of the 9 models fitted using different combinations of our fixed effects (elevation, conspecific tree crown area, and heterospecific tree crown area), and random effects (property boundaries and species identity). In the model name "Species" refers to recruit species. The "All recruits species" column shows the MAE of the model for all recruits species, while "byrscr", "calyca", "cedrod", "guazul" and "entecy" columns show the MAE of the model for each species, calculated using a subset of predictions from the full model. In bold, the lowest errors (best prediction capacity) and underlined the highest errors (worst prediction capacity). The recruits species are byrscr= *Byrsonima crassifolia*, calyca= *Calycophyllum candidissimum*, cedrod= *Cedrela odorata*, guazul= *Guazuma ulmifolia* and entecy= *Enterolobium cyclocarpum***

Model name	Model			Median of the out of sample MAE (95%CI)					
	Structure	Binomial	Negative binomial	All species	byrscr	calyca	cedrod	guazul	entecy
Intercept	Fixed Effects	___	___	0.176 (0.112/0.255)	0.137 (0.104/0.175)	0.188 (0.153/0.224)	0.344 (0.305/0.388)	0.170 (0.134/0.205)	0.111 (0.076/0.149)
	Random effects (varying intercept)	___	___						
Elevation	Fixed Effects	Elevation	___	0.176 (0.112/0.255)	0.136 (0.102/0.173)	0.188 (0.153/0.224)	0.344 (0.305/0.388)	0.169 (0.134/0.205)	0.111 (0.077/0.149)
	Random effects (varying intercept)	___	___						
Species	Fixed Effects	Elevation	___	0.185 (0.120/0.264)	0.136 (0.102/0.173)	0.338 (0.265/0.412)	0.349 (0.305/0.404)	0.160 (0.131/0.192)	0.042 (0.028/0.056)
	Random effects (varying intercept and slope)	Species	Species						

Model name	Model			Median of the out of sample MAE (95%CI)					
	Structure	Binomial	Negative binomial	All species	byrscr	calyca	cedrod	guazul	entecy
Property	Fixed Effects	Elevation	___	0.174 (0.104/0.257)	0.134 (0.095/0.175)	0.183 (0.147/0.224)	0.344 (0.298/0.397)	0.166 (0.130/0.209)	0.109 (0.072/0.151)
	Random effects (varying intercept and slope)	Property	Property						
Species & Property	Fixed Effects	Elevation	___	0.183 (0.110/0.278)	0.100 (0.075/0.132)	0.324 (0.247/0.413)	0.374 (0.306/0.464)	**0.149 (0.121/0.185)**	0.040 (0.031/0.054)
	Random effects (varying intercept and slope)	Property & Species	Property & Species						
Tree crown area	Fixed Effects	Elevation, Conspecific & Heterospecific	Conspecific & Heterospecific	0.176 (0.112/0.259)	0.107 (0.080 /0.136)	0.164 (0.136 /0.197)	**0.341 (0.295 /0.390)**	0.215 (0.169 /0.270)	0.120 (0.080 0.166)
	Random effects	_	___						

Model name	Model			Median of the out of sample MAE (95%CI)					
	Structure	Binomial	Negative binomial	All species	byrscr	calyca	cedrod	guazul	entecy
Individual tree crowns & Species	Fixed Effects	Elevation, Conspecific & Heterospecific	Conspecific & Heterospecific	0.176 (0.104/0.286)	0.094 (0.073/0.115)	0.292 (0.205/0.410)	0.388 (0.312/0.515)	0.161 (0.133/0.192)	**0.038 (0.026/0.052)**
	Random effects (varying intercept and slope)	Species	Species						
Individual tree crowns & property	Fixed Effects	Elevation, Conspecific & Heterospecific	Conspecific & Heterospecific	**0.169 (0.102/ 0.264)**	0.104 (0.080/0.136)	**0.160 (0.133/0.194)**	0.365 (0.296/0.455)	0.202 (0.148/0.272)	0.097 (0.061/0.144)
	Random effects (varying intercept and slope)	Property	Property						

Model name	Model			Median of the out of sample MAE (95%CI)					
	Structure	Binomial	Negative binomial	All species	byrscr	calyca	cedrod	guazul	entecy
Individual tree crowns, Species & Property	Fixed Effects	Elevation, Conspecific & Heterospecific	Conspecific & Heterospecific	0.173 (0.096/0.326)	**0.093 (0.073/0.112)**	0.233 (0.178/0.301)	0.491 (0.320/0.963)	**0.149 (0.119/0.191)**	0.041 (0.026/0.072)
	Random effects (varying intercept and slope)	Property & Species	Property & Species						

Figures Chapter 1

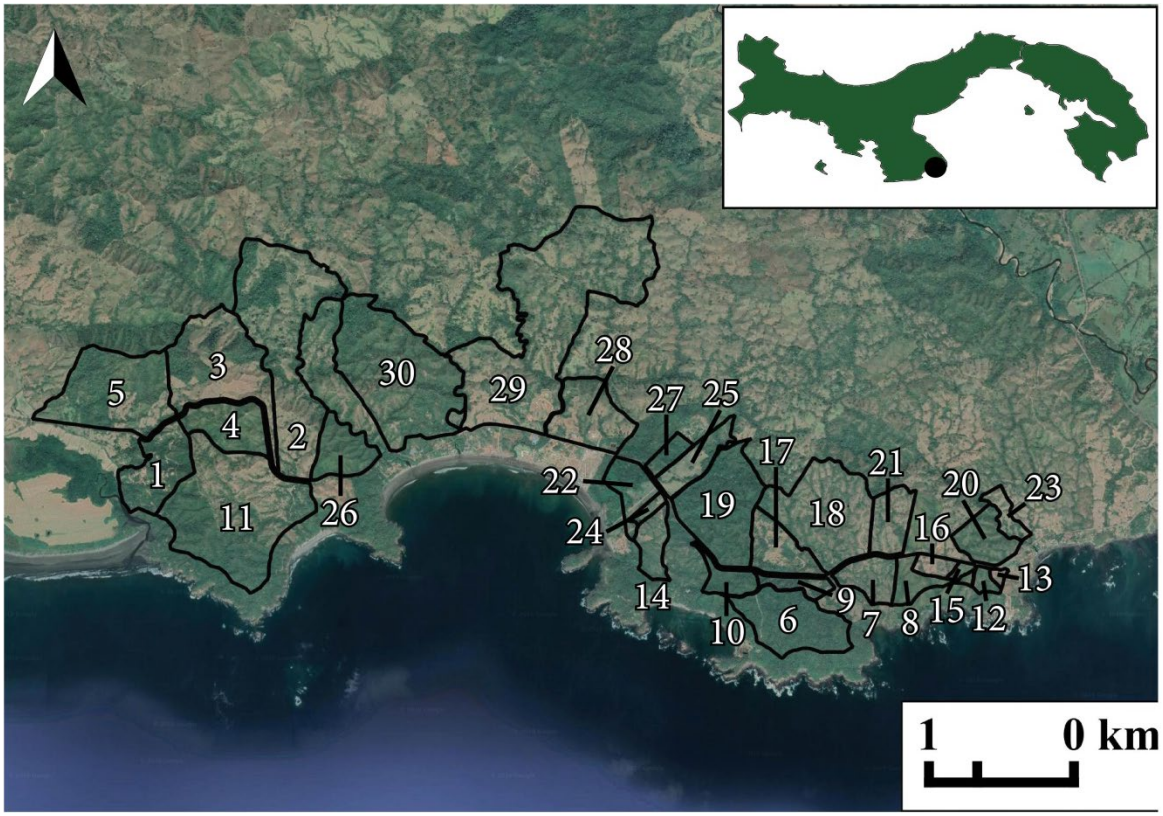

Figure A1 Study area in Southwestern Panama. The black lines represent the properties included in this study. Green colors indicate mostly tree and other woody vegetation covers, and tan colors indicate dry grass cover associated with pastures and other non-forested land covers. The numbers indicate the 30 properties we sampled from in this paper. The black dot in the upper-right corner displays the location of the study site in Panama. Map data: Google, Airbus, Maxar Technologies.

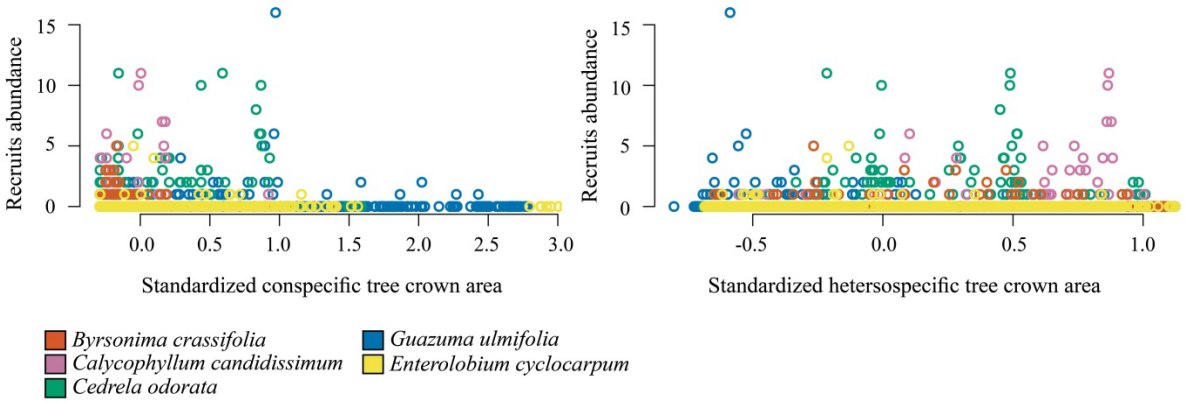

Figure A2 Raw data on recruit abundance plotted against conspecific and heterospecific tree crown area.

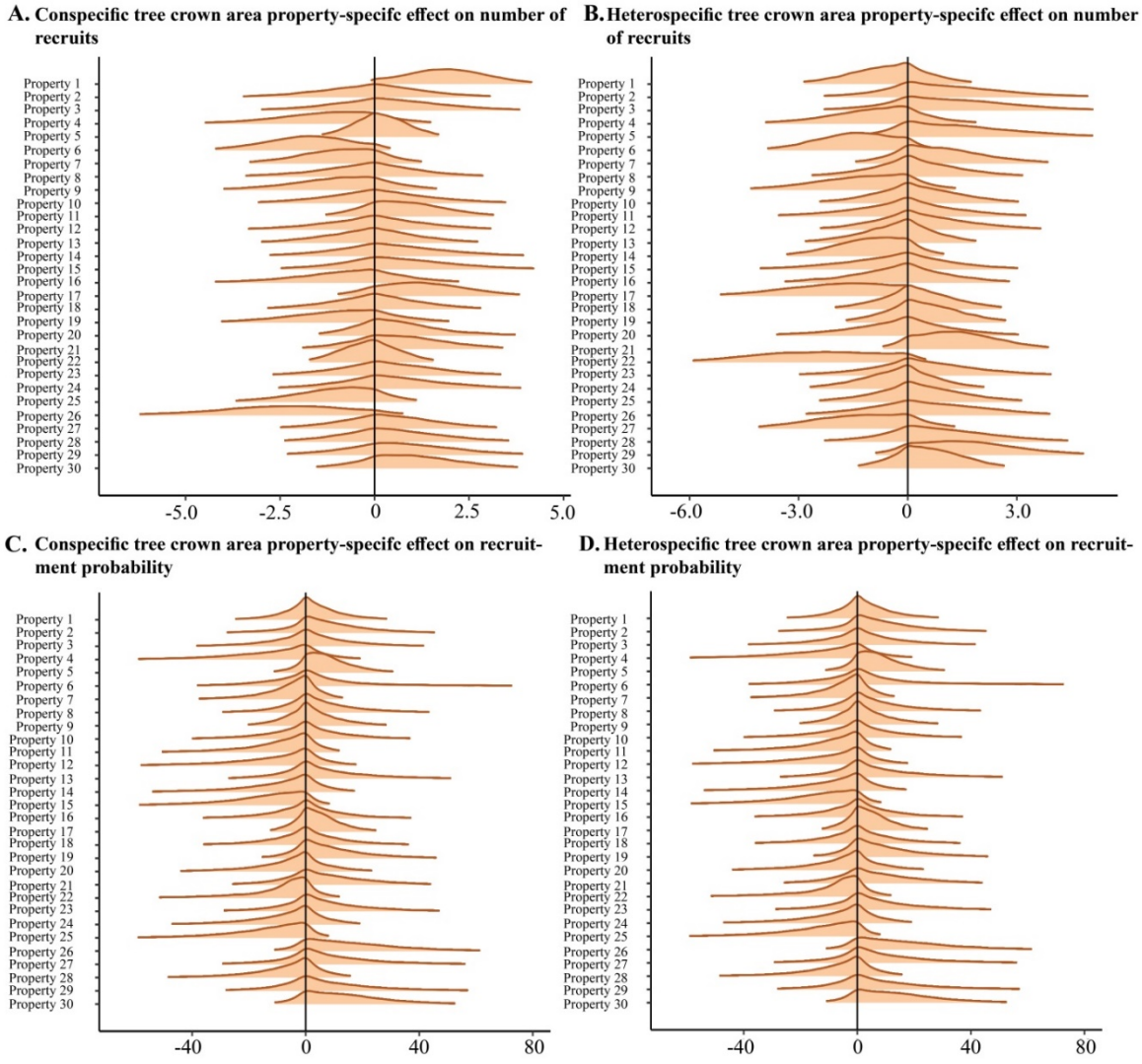

Figure A3 Posterior distribution of the conspecific and heterospecific tree crown area effects on the number of recruits and the probability of recruitment by property identity. Panel A shows the conspecific total tree crown area effect on the number of recruits at each of the 30 properties included in this study. Panel B shows the heterospecific total tree crown area effect on the number of recruits at each of the 30 properties included in this study. Panel C shows the conspecific total tree crown area effect on the probability of recruitment at each of the 30 properties included in this study. Panel C shows the heterospecific total tree crown area effect on the probability of recruitment at each of the 30 properties included in this study. The CI displayed for these posterior distributions is 95%.

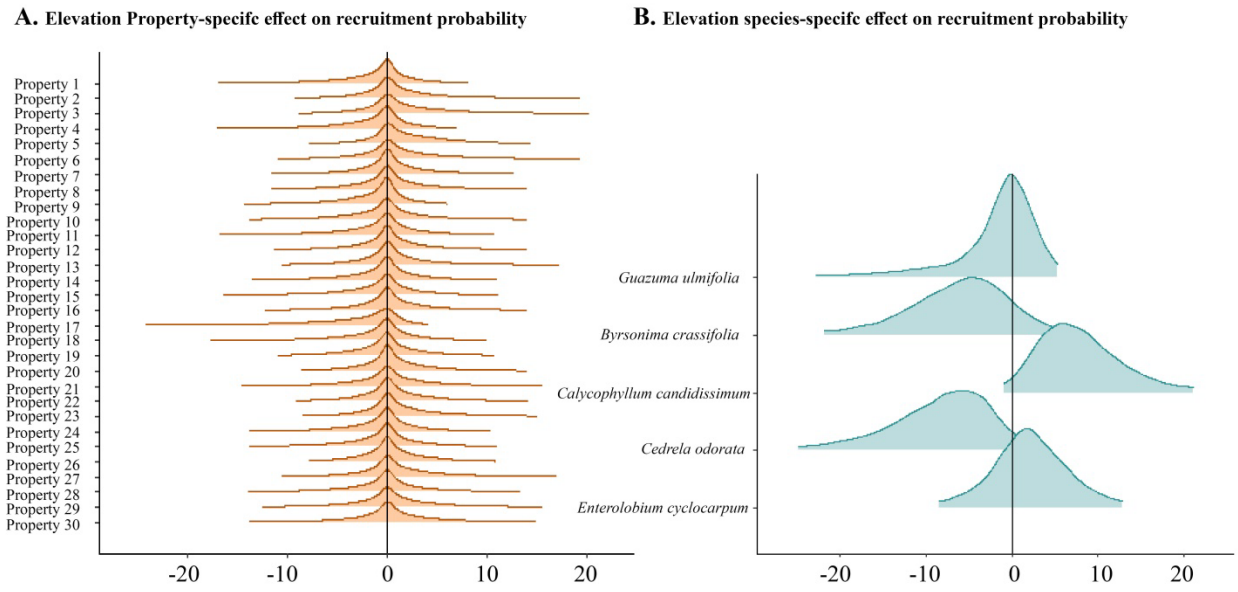

Figure A4 Posterior distribution of elevation effect on the probability of recruitment by property identity and species. Panel A shows the effect of elevation on each of the 30 properties included in this study. Panel B shows the effect of elevation for each of the 5 species included in this study. The CI displayed for these posterior distributions is 95%.

APPENDIX B

Code For Chapter 2

Simulation Sparse Matrix Code

```
data{
 int N;      // number of individuals
 vector [N] size_t0;   // size of focal plants
 vector [N] growth;   // growth of focal plants, response
 vector [N] sizemat[N];  // full size matrix
 vector [N] distmat[N];  // full distance matrix
}
parameters{
 real alpha;
 real beta;
 real sigma;
 real<lower=0> a1;
 real a3;
 real<lower=0> a2;
 }
transformed parameters{
 vector[N] kernel;
 vector[N] mu;
 vector[N] smat[N];
 vector[N] dmat[N];
```

```
 for(i in 1:N){
 for(j in 1:N){
  smat[i,j]=sizemat[i,j]^a1;
  dmat[i,j]=distmat[i,j]^2*a2;
 }}
 for(n in 1:N)
  kernel[n]=sum(smat[n]./exp(dmat[n]));
 for(n in 1:N)
  mu[n]=alpha+size_t0[n]*beta+a3*kernel[n];
}
model{
 alpha~normal(0,5);
 beta~normal(0,5);
 a1~normal(0,5);
 a2~normal(0,5);
 a3~normal(0,5);
 sigma~exponential(1);


 growth ~ normal(mu,sigma);
}
```

Simulation Ragged Matrix Code

```
      data{
       int N;      // number of individuals
       vector [N] size_t0;   // size of focal plants
       vector [N] growth;   // growth of focal plants, response
       vector [obs] size_vector;  //vector of non-zero size observation
s
       vector [obs] dist_vector;  //vector of non-zero distance observa
tions
       int pos[N];     // order of the first non-zero values
       int n_nb[N];     //number of non-zero values per row
      }
      parameters{
       real alpha;
       real beta;
       real sigma;
       real<lower=0> a1;
       real a3;
       real<lower=0> a2;
       }
      transformed parameters{
       vector[N] kernel;
```

```
 vector[N] mu;
 vector[obs] size_vec;
 vector[obs] dist_vec;
 for (i in 1:obs){
  dist_vec[i]=dist_observations[i]^2;
  size_vec[i]=size_observations[i]^a1;
 }
 for(n in 1:N)
  kernel[n]=sum(segment(size_vec, pos[n], n_nb[n]))/
        exp(segment(dist_vec, pos[n], n_nb[n])*a2));
 for(n in 1:N)
  mu[n]=alpha+size_t0[n]*beta+a3*kernel[n];
}
model{
 alpha~normal(0,5);
 beta~normal(0,5);
 a1~normal(0,5);
 a2~normal(0,5);
 a3~normal(0,5);
 sigma~exponential(1);

 growth ~ normal(mu,sigma);
```

```
}
```

Real Data Sparse Matrix Code

```
data {
 int N;      //number of available places for recruitment
 int K;      //number of parent trees
 vector [K] dist[N];   //array containing N vectors with K distan
ces
 int x[N];      //count of seedlings
 int CP[N];     //count of cabbage palms
 vector [N] one;    //vector of ones for the division
}
parameters {
 real<lower=0> a;
 real<lower=0> b;
 real<lower=0> c;
 real<lower=0> phy;
}
transformed parameters{
 real mu[N];
 real aa[N];
```

```
 for(i in 1:N) {
 aa[i] = sum(ones[i] ./(c+dist[i]));
 }
 for (n in 1:N){
  mu[n]=(a+b*aa[n])*CP[n];
 }
}
model{
 a~normal(0,100);
 b~normal(0,100);
 c~normal(0,100);
 phy~exponential(0.5);

 x~neg_binomial_2(mu,phy);
 }

 }
```

Real Data Ragged Matrix Code

```
      data {
       int N;      //number of available places for recruitment
       int K;      //number of non-zero parent trees
       vector [K] distrag;   //vector containing all the non-zero dista
nces
       int x[N];      //count of seedlings
       int CP[N];     //count of cabbage palms
       int n_nb[N];     //vector giving the amount of non-zero values
       int pos [N];    //vector giving the position of non-zero values
       vector [N] one;    //vector of ones for the division
      }
      parameters {
      real<lower=0> a;
       real<lower=0> b;
       real<lower=0> c;
       real<lower=0> phy;
       }
      transformed parameters{
       real mu[N];
       real aa[N];
```

```
 for(i in 1:N) {
 aa[i] = sum(one[i] ./(c +segment(distrag,pos[i],n_nb[i])));
 }

 for (n in 1:N){
 if (n_nb[n]==0){mu[n]=a;}
 else{
  mu[n]=(a+b*aa[n])*CP[n];
 }
 }
}
model{
 a~normal(0,100);
 b~normal(0,100);
 c~normal(0,100);
 phy~exponential(0.5);

 x~neg_binomial_2(mu,phy);

 }
}
```

Real Data Centered Parametrization Code

```
data {
 int N;      //number of plots
 int K;      //number of non-zero parent trees
 int M;      //number of random levels
 vector [K] sizeN;    //matrix of neighbor size
 vector [K] distN;    //matrix of neighbor distances
 int x[N];      //number of seedlings
 int seeds[N];     //number of seeds
 int am[N];     //vector giving the number of non-zero values
 int pos [N];    //vector giving the position of non-zero values
 int Cseedlings [N];   //number of conspecific seedlings
 int plots[N];     //random effect of plots
 }


parameters {
 real a;
 real b;
 real<lower=0> ger;
 real mu;
 real e [M];
```

```
        real sigma_plot;



      }

      transformed parameters{

       real<lower=0, upper=1> s[N];

       real g[N];



       for (n in 1:N){

       if (am[n]==0){g[n]=mu+ b*Cseedlings[n]+omega[plots[n]];}

       else{

        g[n] = mu + b*Cseedlings[n] + a* sum(segment(sizeN,pos[n],am[n]
) ./

          exp(ger*log(segment(distN,pos[n],am[n])))) + e[plots[n]];

        }

       }



      }

      model{

       a~normal(0,1);

       b~normal(0,1);

       ger~normal(0,1);

       mu~nomal(0,1);
```

```
 e~normal(0,sigma_plot);

 sigma_plot~normal(0,1);



 x~binomial_logit(seeds,g);

 }

}
```

Real Data Non-Centered Parametrization Code

```
data{

 int N;      //number of plots

 int K;      //number of non-zero parent trees

 int M;      //number of random levels

 vector [K] sizeN;    //matrix of neighbor size

 vector [K] distN;    //matrix of neighbor distances

 int x[N];      //number of seedlings

 int seeds[N];     //number of seeds

 int am[N];     //vector giving the number of non-zero values

 int pos [N];    //vector giving the position of non-zero values

 int Cseedlings [N];   //number of conspecific seedlings

 int plots[N];     //random effect of plots

}

parameters {
```

```
 real a;

 real b;

 real<lower=0> ger;

 real mu;

 real mu_omega;

 real slope_omega[M];

 real scale_omega;




}

transformed parameters{

 real<lower=0, upper=1> s[N];

 real g[N];

 real e [M];


 for (n in 1:M){

 omega[n]= mu_omega +slope_omega[n]*scale_omega+;

 }

 for (n in 1:N){

 if (am[n]==0){g[n]=mu+ b*Cseedlings[n]+omega[plots[n]];}

 else{
```

```
        g[n] = mu + b*Cseedlings[n] + a* sum(segment(sizeN,pos[n],am[n]
) ./
          exp(ger*log(segment(distN,pos[n],am[n]))))  + e[plots[n]];
        }
       }
      }
      model{
       a~normal(0,1);
       b~normal(0,1);
       ger~normal(0,1);
       mu~nomal(0,1);
       el~normal(0,1);
       mu_plot~normal(0,1);
       gamma_el~normal(0,1);

       for (n in 1:N){
       x~binomial_logit(seeds,g);
       }
      }
```

Tables Chapter 2

Table B1 Parameters estimations and convergence metrics for the simulation at an effective neighborhood radius of 10m using the sparse matrix

	mean	se_mean	sd	2.5%	25%	50%	75%	97.5%	n_eff	Rhat
alpha	0.802	0.000	0.005	0.792	0.798	0.802	0.805	0.811	589.177	1.002
beta	0.200	0.000	0.000	0.199	0.199	0.200	0.200	0.201	682.105	1.001
sigma	0.010	0.000	0.000	0.009	0.010	0.010	0.010	0.011	9991.240	1.000
a1	0.083	0.001	0.020	0.045	0.070	0.083	0.096	0.122	476.237	1.007
a3	0.036	0.000	0.002	0.033	0.035	0.036	0.037	0.040	470.260	1.007
a2	0.050	0.000	0.000	0.050	0.050	0.050	0.050	0.050	1547.105	1.002

Table B2 Parameters estimations and convergence metrics for the simulation at an effective neighborhood radius of 10m using the ragged matrix

	mean	se_mean	sd	2.5%	25%	50%	75%	97.5%	n_eff	Rhat
alpha	0.801	0.000	0.005	0.792	0.798	0.801	0.805	0.811	719.437	1.002
beta	0.200	0.000	0.000	0.199	0.199	0.200	0.200	0.201	886.849	1.001
sigma	0.010	0.000	0.000	0.009	0.010	0.010	0.010	0.011	7256.505	1.000
a1	0.085	0.001	0.019	0.048	0.073	0.085	0.097	0.121	414.132	1.004
a3	0.036	0.000	0.002	0.033	0.035	0.036	0.037	0.039	411.221	1.004
a2	0.050	0.000	0.000	0.050	0.050	0.050	0.050	0.050	1915.463	1.001

Table B3. Parameters estimations and convergence metrics for the simulation at an effective neighborhood radius of 15m using the ragged matrix

	mean	se_mean	sd	2.5%	25%	50%	75%	97.5%	n_eff	Rhat
alpha	0.779	0.000	0.005	0.770	0.776	0.779	0.783	0.789	594.089	1.006
beta	0.200	0.000	0.000	0.199	0.200	0.200	0.200	0.201	717.067	1.005
sigma	0.010	0.000	0.000	0.009	0.010	0.010	0.010	0.011	10171.718	1.000
a1	0.083	0.001	0.019	0.046	0.070	0.083	0.096	0.119	374.962	1.006
a3	0.036	0.000	0.002	0.033	0.035	0.036	0.037	0.040	366.440	1.006
a2	0.050	0.000	0.000	0.049	0.050	0.050	0.050	0.050	1402.778	1.000

Table B4 Parameters estimations and convergence metrics for the simulation at an effective neighborhood radius of 5m using the sparse matrix

	mean	se_mean	sd	2.5%	25%	50%	75%	97.5%	n_eff	Rhat
alpha	1.261	0.163	0.290	0.996	1.091	1.153	1.235	1.893	3.176	4.305
beta	-0.001	0.250	0.434	-1.007	0.184	0.192	0.197	0.207	3.005	50.028
sigma	0.439	0.362	0.626	0.150	0.156	0.160	0.165	1.845	3.002	140.750
a1	0.779	0.833	1.447	0.006	0.054	0.135	0.295	4.024	3.016	14.803
a3	0.025	0.007	0.013	0.000	0.020	0.029	0.035	0.040	3.920	2.162
a2	0.075	0.067	0.117	0.019	0.022	0.023	0.025	0.337	3.002	66.883

Table B5 Parameters estimations and convergence metrics for the simulation at an effective neighborhood radius of 15m using the sparse matrix

	mean	se_mean	sd	2.5%	25%	50%	75%	97.5%	n_eff	Rhat
alpha	0.557	0.301	0.737	-1.901	0.775	0.779	0.782	0.788	6.005	57.134
beta	0.221	0.029	0.071	0.199	0.200	0.200	0.200	0.466	6.014	48.657
sigma	0.152	0.192	0.472	0.009	0.010	0.010	0.010	1.763	6.017	44.446
a1	0.378	0.399	0.977	0.044	0.071	0.086	0.102	3.632	6.007	51.499
a3	0.033	0.004	0.010	0.000	0.035	0.036	0.037	0.040	6.151	7.314
a2	0.068	0.024	0.060	0.050	0.050	0.050	0.050	0.268	6.005	93.599

Table B6 Parameters estimations and convergence metrics for the simulation at an effective neighborhood radius of 20 m using the sparse matrix

	mean	se_mean	sd	2.5%	25%	50%	75%	97.5%	n_eff	Rhat
alpha	0.715	0.387	0.951	-1.753	1.034	1.114	1.180	1.270	6.032	14.753
beta	0.257	0.230	0.564	-0.758	0.187	0.193	0.200	1.913	6.004	93.621
sigma	0.320	0.197	0.483	0.150	0.156	0.160	0.165	1.913	6.004	108.395
a1	0.746	0.741	1.818	0.003	0.054	0.135	0.326	6.730	6.018	20.566
a3	0.143	0.156	0.383	0.000	0.022	0.032	0.037	1.412	6.004	69.271
a2	0.190	0.212	0.518	0.019	0.022	0.024	0.026	1.905	6.003	301.199

Table B7 Parameters estimations and convergence metrics for the simulation at an effective neighborhood radius of 5 m using the ragged matrix

	mean	se_mean	sd	2.5%	25%	50%	75%	97.5%	n_eff	Rhat
alpha	1.010	0.149	0.382	-0.201	1.053	1.119	1.179	1.291	6.557	4.212
beta	0.204	0.012	0.033	0.179	0.189	0.195	0.201	0.319	7.330	3.488
sigma	0.186	0.035	0.096	0.149	0.155	0.159	0.163	0.554	7.282	6.040
a1	0.419	0.323	0.806	0.005	0.049	0.114	0.258	2.998	6.208	7.364
a3	0.027	0.004	0.012	0.000	0.022	0.031	0.036	0.040	7.818	2.160
a2	0.032	0.012	0.033	0.019	0.022	0.023	0.025	0.160	7.343	5.720

Table B8 Parameters estimations and convergence metrics for the simulation at an effective neighborhood radius of 20 m using the ragged matrix

	mean	se_mean	sd	2.5%	25%	50%	75%	97.5%	n_eff	Rhat
alpha	1.024	0.143	0.357	-0.142	1.059	1.119	1.175	1.279	6.267	4.984
beta	0.203	0.013	0.032	0.180	0.190	0.195	0.200	0.313	6.359	4.516
sigma	0.194	0.047	0.118	0.149	0.156	0.159	0.163	0.617	6.171	12.826
a1	0.376	0.335	0.828	0.005	0.047	0.110	0.222	3.112	6.104	7.949
a3	0.028	0.003	0.011	0.000	0.024	0.031	0.036	0.040	9.731	1.667
a2	0.024	0.001	0.006	0.019	0.022	0.023	0.025	0.038	21.075	1.648

Table B9 Parameters estimations and convergence metrics for the model using the strangle fig tree recruitment data using the sparse matrix

	mean	se_mean	sd	2.5%	25%	50%	75%	97.5%	n_eff	Rhat
a	0.025	0.000	0.012	0.007	0.015	0.023	0.032	0.055	1563.654	1.001
b	11.678	0.135	4.361	5.408	8.426	10.853	14.279	22.010	1051.286	1.003
j	101.016	1.820	60.904	18.804	52.914	89.764	137.913	242.091	1119.526	1.004
phy	1.847	0.021	0.760	0.787	1.309	1.679	2.235	3.688	1293.255	1.001

Table B10 Parameters estimations and convergence metrics for the model using the strangle fig tree recruitment data using the ragged matrix

	mean	se_mean	sd	2.5%	25%	50%	75%	97.5%	n_eff	Rhat
a	0.025	0.000	0.012	0.007	0.017	0.023	0.031	0.055	1258.888	0.999
b	11.740	0.145	4.281	5.582	8.644	11.066	14.124	22.143	870.239	1.002
j	102.137	1.938	61.069	16.779	56.247	91.220	138.665	243.538	993.227	1.002
phy	1.860	0.020	0.695	0.843	1.380	1.742	2.243	3.549	1213.048	1.001

Table B11 Parameters estimations and convergence metrics for the model using the seedling recruitment data using the ragged matrix and a centered parametrization of the random effects

	mean	se_mean	sd	2.5%	25%	50%	75%	97.5%	n_eff	Rhat
a	-0.029	0.000	0.008	-0.048	-0.034	-0.028	-0.024	-0.018	1671.536	1.002
b	-0.778	0.005	0.224	-1.242	-0.924	-0.769	-0.615	-0.381	1821.962	1.001
mu	-2.491	0.004	0.174	-2.862	-2.599	-2.482	-2.370	-2.166	1644.832	1.001
ger	0.217	0.003	0.138	0.010	0.106	0.202	0.307	0.516	1982.572	1.001

Table B12 Parameters estimations and convergence metrics for the model using the seedling recruitment data using the ragged matrix and a non-centered parametrization of the random effects

	mean	se_mean	sd	2.5%	25%	50%	75%	97.5%	n_eff	Rhat
a	-0.030	0.000	0.008	-0.049	-0.035	-0.028	-0.023	-0.018	1550.833	1
b	-0.764	0.005	0.226	-1.216	-0.911	-0.756	-0.605	-0.354	1782.110	1
mu	-2.499	0.025	1.006	-4.406	-3.174	-2.514	-1.804	-0.540	1584.808	1
ger	0.221	0.003	0.143	0.012	0.104	0.205	0.320	0.527	1732.220	1

Figures Chapter 2

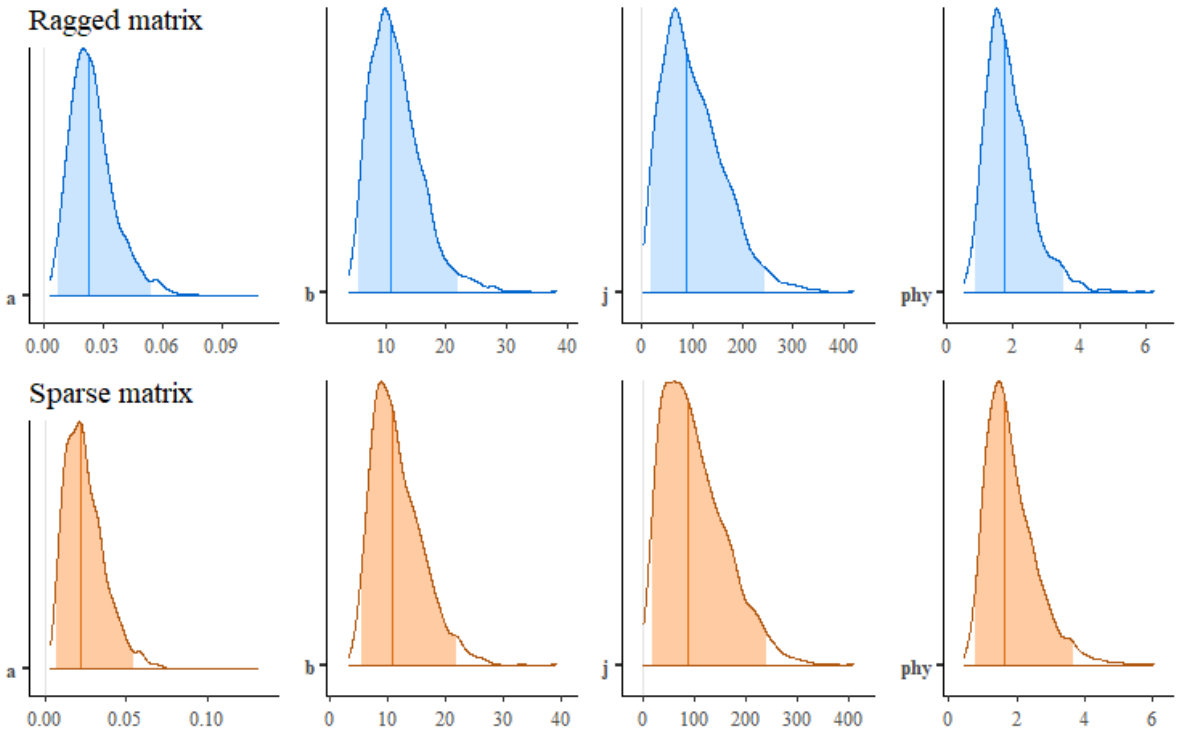

Figure B1 Parameters posterior density of the model describing seed dispersal of invasive strangler fig trees parametrized using the ragged matrix and the sparse matrix. Both parametrizations provided similar estimates and 95%CI. The 95% CI are the shaded areas in the posterior distribution.

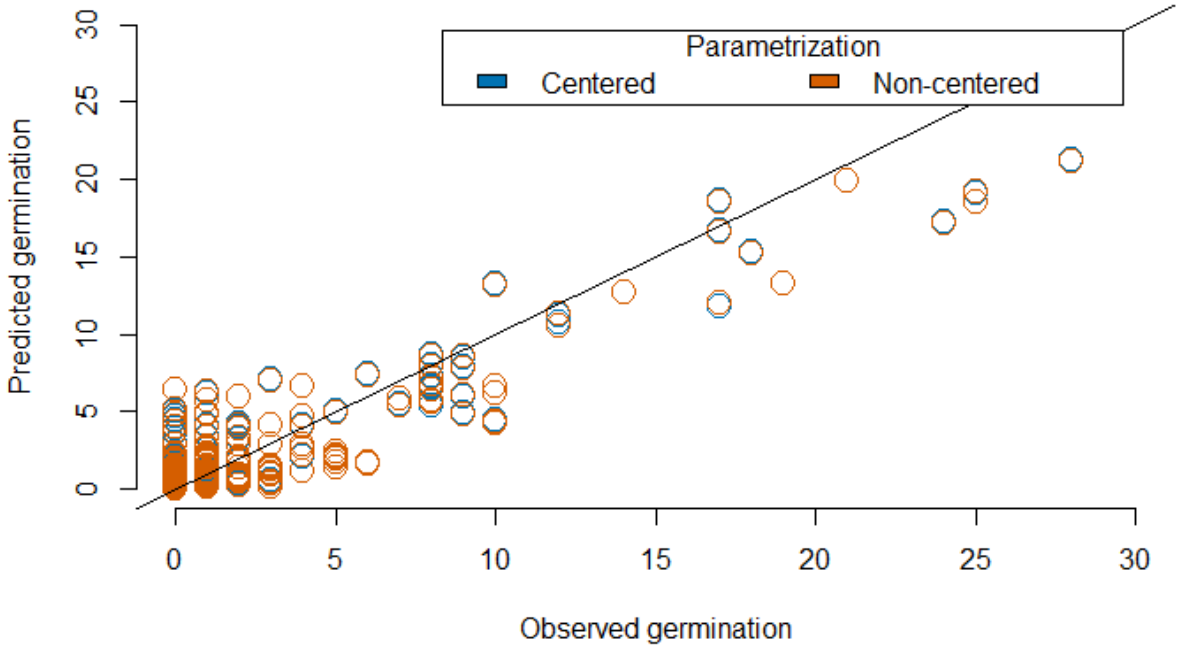

Figure B2 Predicted germination against observed germination for the centered and non-centered parametrizations. Both parametrization present similar differences between the predicted and observed germination and slightly underestimate germination.

APPENDIX C

Detection Probability Model Selection

We tested different combinations of variables that could influence detection probability in high-resolution imagery from Google Earth Pro, such as NDVI in 2019, crown area, tree height, elevation, and slope (Table C1). We evaluated the model's predictive capacity using the looic approximation from the package loo(Vehtari, Gabry, et al. 2020). The package's output provides the difference between the expected log pointwise predictive density for a new dataset (elpd_diff). We consider models different in more than one elpd_diff to have a significant difference in a predictive capacity. We choose models for p_{11} and p_{10} that had as few variables as possible in common but that had lower elpd_diff than1 to avoid identifiability problems while using the best predictive model (Table S2 and S3).

Table C1 Combination of variables and models tested using the looic approximation to select the models with the best prediction capacity of detectability

Model name	Variables
Model I	Intercept
Model 1	NDVI in 2019, crown area
Model 2	NDVI in 2019, tree height
Model 3	NDVI in 2019, crown area, elevation
Model 4	NDVI in 2019, crown area, slope
Model 5	NDVI in 2019, tree height, elevation
Model 6	Crown area
Model 7	Crown area, slope
Model 8	Crown area, elevation
Model 9	Tree height
Model 10	Tree height, slope
Model 11	Tree height, elevation
Model 12	Slope, aspect, elevation
Model 13	Slope
Model 14	Elevation

Table C2 Result of the looic approximation for p10. elpd_diff = the difference between the expected log pointwise predictive density for a new dataset

	elpd_diff
Model 3	0.0
Model 2	-0.4
Model 1	-0.5
Model 5	-0.8
Model 8	-0.9
Model 4	-1.2
Model 12	-1.6
Model 6	-2.4
Model 7	-3.0
Model I	-5.7
Model 11	-5.7
Model 10	-6.0
Model 9	-6.9

Table C3 Result of the looic approximation for p11. elpd_diff = the difference between the expected log pointwise predictive density for a new dataset

	elpd_diff
Model 1	0.0
Model 3	-0.7
Model 4	-1.2
Model 6	-2.4
Model 2	-2.5
Model 8	-3.0
Model 5	-3.1
Model 7	-3.4
Model I	-4.3
Model 13	-5.1
Model 12	-5.5
Model 9	-5.6
Model 14	-5.6
Model 11	-6.5
Model 10	-6.8